

Quantum computing enhanced computational catalysis

Vera von Burg,¹ Guang Hao Low,² Thomas Häner,³ Damian S. Steiger,³
Markus Reiher,^{1,*} Martin Roetteler,² and Matthias Troyer^{2,†}

¹*Laboratorium für Physikalische Chemie, ETH Zürich,
Vladimir-Prelog-Weg 2, 8093 Zürich, Switzerland*

²*Microsoft Quantum, Redmond, Washington 98052, USA*

³*Microsoft Quantum, 8038 Zürich, Switzerland*

(Dated: February 2, 2022)

The quantum computation of electronic energies can break the curse of dimensionality that plagues many-particle quantum mechanics. It is for this reason that a universal quantum computer has the potential to fundamentally change computational chemistry and materials science, areas in which strong electron correlations present severe hurdles for traditional electronic structure methods. Here, we present a state-of-the-art analysis of accurate energy measurements on a quantum computer for computational catalysis, using improved quantum algorithms with more than an order of magnitude improvement over the best previous algorithms. As a prototypical example of local catalytic chemical reactivity we consider the case of a ruthenium catalyst that can bind, activate, and transform carbon dioxide to the high-value chemical methanol. We aim at accurate resource estimates for the quantum computing steps required for assessing the electronic energy of key intermediates and transition states of its catalytic cycle. In particular, we present new quantum algorithms for double-factorized representations of the four-index integrals that can significantly reduce the computational cost over previous algorithms, and we discuss the challenges of increasing active space sizes to accurately deal with dynamical correlations. We address the requirements for future quantum hardware in order to make a universal quantum computer a successful and reliable tool for quantum computing enhanced computational materials science and chemistry, and identify open questions for further research.

I. INTRODUCTION

Quantum computing [1–4] has the potential to efficiently solve some computational problems that are exponentially hard to solve on classical computers. Among these problems, one of the most prominent cases is the calculation of quantum electronic energies in molecular systems [5–9]. Due to its many applications in chemistry and materials science, this problem is widely regarded as the “killer application” of future quantum computers [10], a view that was supported by our first rigorous resource estimate study for the accurate calculation of electronic energies of a challenging chemical problem [11].

At the heart of chemistry is predicting the outcome of chemical processes in order to produce chemicals, drugs, or functional molecular assemblies and materials. A prerequisite for this ability to predict chemical processes is an understanding of the underlying reaction mechanisms. Quantum mechanics allows one to assign energies to molecular structures so that a comparison of these energies in a sequence of molecular transformations can be taken as a measure to rate the viability of such a chemical reaction. Relative energies are a direct means

to predict reaction heats and activation barriers for chemical processes. However, the reliability of such predictions depends crucially on the accuracy of the underlying energies, of which the electronic energy is often the most important ingredient. This energetic contribution of the dynamics of the electrons in a molecule can be calculated by solving the electronic Schrödinger equation, typically done in a so-called one-particle basis, the set of molecular orbitals.

The computational complexity of an exact solution of the electronic Schrödinger equation on classical computers is prohibitive as the many-electron basis expansion of the quantum state of interest grows exponentially with the number of molecular orbitals (often called the “curse of dimensionality”). An exact diagonalization of the electronic Hamiltonian in the full many-electron representation is therefore hard and limited to small molecules that can be described by comparatively few (on the order of twenty) orbitals. Once accomplished, it is said that a full configuration interaction (full-CI) solution in this finite orbital basis has been found. Since typical molecular systems will require on the order of 1000 molecular orbitals for their reliable description, exact-diagonalization methods need to restrict the orbital space to about twenty orbitals chosen from the valence orbital space (called complete active space (CAS) CI). Accordingly, approximate methods have been developed in quantum chemistry for large orbital spaces. By contrast, quantum com-

* To whom correspondence should be addressed. Electronic mail: markus.reiher@phys.chem.ethz.ch

† To whom correspondence should be addressed. Electronic mail: mtroyer@microsoft.com

puting allows for an encoding of a quantum state in a number of qubits that scales only linearly with the number of molecular orbitals and has therefore the potential to deliver full-CI solutions for large orbital spaces that are inaccessible to traditional computing because of the exponential scaling.

In our previous case study on the feasibility of quantum computing for chemical reactivity [11], we chose to investigate electronic structures of a biocatalyst with still unknown mode of action, i.e., the active site of nitrogenase which is a polynuclear iron-sulfur cluster. This choice was motivated by the fact that such polynuclear $3d$ transition metal clusters are known to exhibit strongly correlated electronic structures that are hard to describe reliably with approximate electronic structure methods on classical computers (electronically excited states of molecules in photophysical and photochemical applications represent another example of this class of problems). In Ref. [11], which relied on a structure model of the active site of nitrogenase in its resting state, we avoided biasing toward the electronic ground state of that particular structure by optimizing arbitrary electronic states for that structure for spin and charge states. These did not coincide with the electronic ground state of the resting state as emphasized in the supporting information of Ref. [11]. Although the resource estimates provided in Ref. [11] supported the view that quantum computing is a true competitor of state-of-the-art CAS-CI-type electronic structure methods such as the density matrix renormalization group (DMRG) [12, 13] or full configuration interaction quantum Monte Carlo (FCIQMC) [14] for studies of chemical reaction mechanisms, we did not consider an actual reaction mechanism.

In this work, we therefore revisit the problem of quantum computing enhanced reaction mechanism elucidation by considering the latest algorithmic advances, but now with a focus on a specific chemical reaction that is prototypical for homogeneous catalysis and equally well relevant for heterogeneous catalysis. The example that we chose is the catalytic functionalization of carbon dioxide, i.e., the capture of the small green-house gas carbon dioxide by a catalyst that activates and eventually transforms it to a useful chemical such as methanol. Hence, we continue to focus on small-molecule activation catalysis, but emphasize that, despite the obvious interest into this specific system in the context of carbon capture technologies, our analysis is of general value to a huge body of chemical reactivity studies. Moreover, we re-examine some of our initial assumptions that are a moving target in the fast developing field of quantum computing. These are the gate counts for the quantum algorithm that performs the

energy measurement and assumptions on the error corrected gate times on a future quantum computer, which are heavily dependent on the underlying technology of its hardware. Furthermore, we extend our previous work with respect to the steps that need to be carried out by a quantum computer, specifically regarding the resources of the state preparation step.

Since our previous work [11], there has been significant progress in quantum algorithms, but also a better understanding of what it takes to build a scalable quantum computer has been reached. On the algorithmic side, Hamiltonians represented by a linear combination of unitaries in a so-called black-box query model can now be simulated with optimal cost using techniques called “qubitization” [15] and “quantum signal processing” [16]. In addition, structure in broad families of Hamiltonians can be exploited to reduce the cost of simulation even more. This includes Hamiltonians with geometrically local interactions [17] and large separations in energy scales [18]. Even more recently, very promising tight theoretical bounds on the performance of traditional Lie-Trotter-Suzuki formulas on average-case Hamiltonians have been obtained [19].

Here, we introduce further refinements to the technique of qubitization applied to molecular systems, which has already been noted [20] to be particularly promising in terms of the dominant quantum Toffoli-gate complexity [21]. We assume that the two-electron tensor describing interactions between N molecular orbitals has a low-rank approximation in a so-called double-factorized representation. This leads to Toffoli gate cost estimates that are orders of magnitude better. For instance, we previously estimated that obtaining an energy level of a Nitrogen fixation problem to 1mHartree [11] cost the equivalent of 1.5×10^{14} Toffoli gates. This was reduced to 2.3×10^{11} Toffoli gates by Berry et al. [22] using a so-called single-factorized representation in the qubitization approach. Under similar assumptions on the rank as Berry et al., we achieve 1.2×10^{10} Toffoli gates, a further improvement of more than an order of magnitude.

We have also taken into account realistic assumptions for mid-term quantum hardware. While our previous work [11] focused on optimistic future devices with logical gate times of 100ns and all-to-all connectivity between qubits, we here employ gate times of 10 μ s for fault tolerant gates with nearest neighbor connectivity – realistic assumptions for mid-term quantum computer architectures. We therefore also discuss the overhead due to mapping the quantum algorithm to a two-dimensional planar layout, which further increases the overall runtime but makes the estimates more realistic.

II. A HOMOGENEOUS CARBON DIOXIDE FIXATION CATALYST

The catalytic process that we selected for our present work is the binding and transformation of carbon dioxide. The infrared absorption properties of carbon dioxide make it a green-house gas that is a major contributor to climate change. Naturally, limiting or even inverting rising carbon dioxide levels in the atmosphere is a truly important goal and all possible ways to accomplish it must be considered. One option, although currently not the most relevant one [23], is carbon dioxide utilization by chemical transformation. In basic research, options have been explored to fix and react inert carbon dioxide to yield chemicals of higher value (see Refs. [24, 25] for two recent examples). Also, homogeneous transition metal catalysts have been designed in the past decade, many of them based on ruthenium as the central metal atom. Despite the fact that eventually heterogeneous catalysis may be preferred over homogeneous catalysis, understanding the basics of carbon dioxide fixation chemistry is facilitated by well-defined homogeneous systems. While formate is often the product of such a fixation process, methanol is a chemical of higher value. Not many catalysts have been reported so far that can transform carbon dioxide directly into methanol [26] and all of these are plagued by a comparatively low turnover number. To find synthetic catalysts that robustly produce high-value chemicals from carbon dioxide with high turnover number is therefore an important design challenge and computational catalysis can provide decisive insights as well as virtual screening to meet this challenge.

For our assessment of quantum computing resource estimates, we chose a catalyst reported by the Leitner group [27] as extensive density functional theory (DFT) calculations on its mechanism have already been reported by this group. Hence, key molecular structures have already been identified based on DFT. A detailed mechanistic picture has emerged, from which we took intermediates and transition state structures for our resource estimate analysis. Lewis structures of the eight structures selected for our work are shown in Fig. 1.

In this work, we focus on the electronic structure of isolated complex structures and therefore neglect any surrounding such as a solvent as well as energy contributions from nuclear dynamics that would be required for the calculation of free energies (cf. [11] on how to include them). The heavy element ruthenium is known to form complexes that are often low-spin, i.e., singlet or doublet, and do not feature strong multi-configurational character (by contrast to its lighter homolog iron). It is therefore

not surprising that we found no pronounced multi-configurational character as highlighted by the orbital entanglement diagrams provided in the supplementary material. Hence, the Ru complexes selected for our resource estimate study feature mostly dynamic electron correlation indicated by small weights of all but one electronic configurations (Slater determinants) that contribute to the exact wave function in a full configuration interaction expansion. For our resource analysis, this is of little importance but highlights the importance of a larger and faster universal quantum computer with a few thousand logical qubits for complete state representation, to accurately capture all relevant dynamical correlations.

The presentation of the CO₂-fixating ruthenium catalyst of the Leitner group [27] was accompanied by extensive DFT calculations of the potentially relevant molecular structures, which is a routine procedure in chemistry. However, DFT electronic energies are plagued by approximations made to the exchange-correlation functional [28, 29] and can therefore be of unknown reliability (cf., e.g., Refs. [30–32]). The authors of Ref. [27] selected the Minnesota functional M06-L [33] because they found good overall agreement with their experimental results. In order to demonstrate the uncertainty that generally can affect DFT results, which can be very cumbersome if experimental data are not available for comparison, we supplemented the DFT data of Ref. [27] with results obtained with the standard generalized-gradient-approximation functional PBE [34] and its hybrid variant PBE0 [35] for the eight structures of the reaction mechanism considered in this work (data shown in Fig. 2).

As can be seen in Fig. 2, whereas structure optimization (compare results for structures optimized with the same functional with the single-point data denoted by the double slash notation) has a small effect on the relative electronic energies, the difference between the functionals can amount to more than 50 kJ/mol (i.e., 19 mHartree per molecule) and can even reverse the qualitative ordering of the compounds (compare structures ‘V’ and ‘VIII’). Obviously, in the absence of any additional information (such as experimental data or more accurate calculations), it is virtually impossible to settle on reliable energetics with potentially dramatic consequences for the elucidation of a reaction mechanism.

III. QUANTUM COMPUTING ENHANCED COMPUTATIONAL CATALYSIS

The elucidation of chemical reaction mechanisms is routinely accomplished with approximate quan-

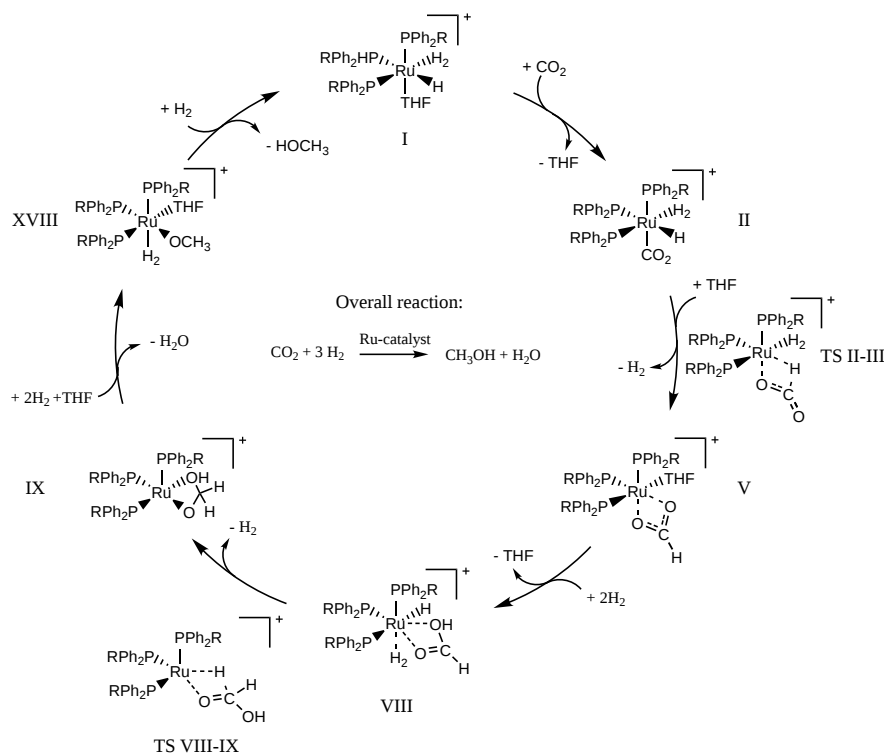


Figure 1. Selected steps of the catalytic cycle elucidated in Ref. [27] on the basis of DFT calculations: intermediates and transition state structures considered for the present work are shown (Roman numerals are according to the original publication).

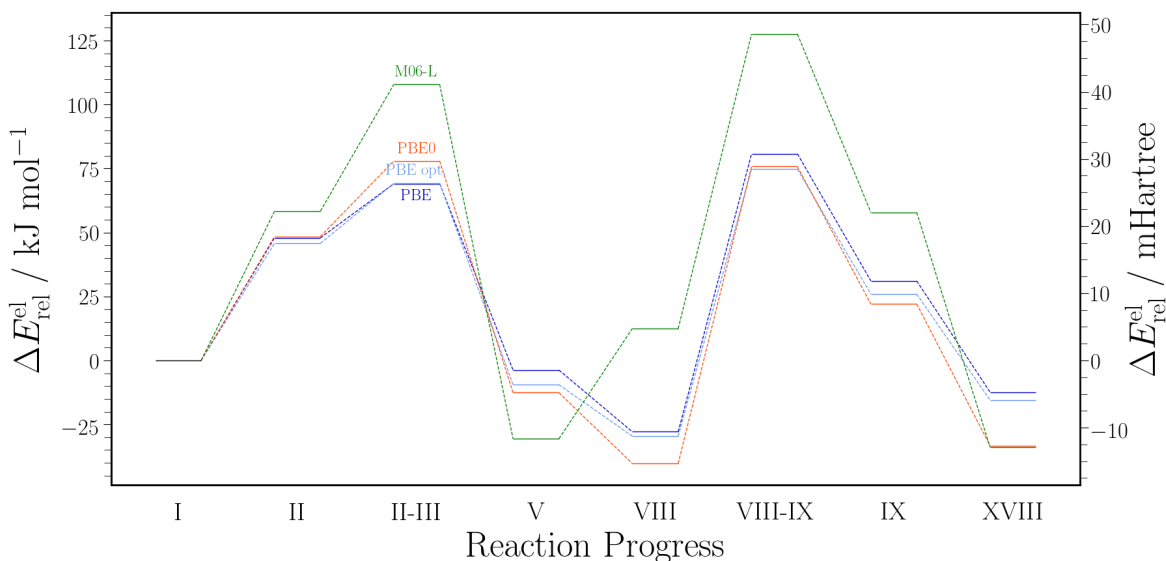


Figure 2. Relative DFT electronic reaction energies for the catalytic cycle obtained with a def2-TZVP basis set and three different approximate density functionals: M06-L [27], PBE, and PBE0 on M06-L/def2-SVP-optimized structures taken from Ref. [27]. For comparison, we provide relative electronic reaction energies from PBE/def2-TZVP//PBE/def2-TZVP calculations (in Pople’s double slash notation, where the density functional behind the double slash is the one for which the structure was obtained) labeled as “PBE opt.”.

tum chemical methods [36, 37], for which usually stationary structures on Born-Oppenheimer potential energy surfaces are optimized, yielding stable reactants, products, and intermediates of a chemical process. More importantly, optimized first-order saddle points on such a surface represent transition state structures, which are key for detailed kinetic studies and hence for the prediction of concentration fluxes.

In the following, we discuss where in the mechanism elucidation process quantum computing can be efficient, useful, and decisive, and hence, how quantum computing can efficiently enhance and reinforce computational catalysis to make a difference. As there are many steps involved that require a deep understanding of various branches of theoretical chemistry, we provide an overview of the essential steps in Fig. 3. Understanding chemical catalysis, and chemical reactions in general, requires an exploration of relevant molecular structures (*structure exploration* in Fig. 3), which is usually done manually and with DFT approaches (as in Ref. [27] for our example here), but which can now also be done in a fully automated and even autonomous way [38]. These structures need to be assigned an energy which may be conveniently separated into an electronic contribution (steps 1-7 in Fig. 3) and a remaining part (*additional free energy calculations* in Fig. 3) containing nuclear and other effects (calculated in a standard rigid-rotor-harmonic-oscillator model accompanied by dielectric continuum embedding or by explicit molecular dynamics) to eventually yield a free energy calculated from all related microstates. Relative free-energy differences will eventually be used as barrier heights in expressions for absolute rate constants (*kinetic modeling* in Fig. 3) that can then be used in kinetic modeling for predicting concentration fluxes through the chemical web of relevant molecular structures. Ultimately, such knowledge can be exploited to improve on existing or to design new catalysts with enhanced catalytic properties.

Accuracy matters: A reaction rate depends exponentially on the energy difference between a transition state structure and its corresponding stable reactants, which are connected by an elementary reaction step. Because of this exponential dependence, highly accurate energy differences are decisive. While many contributions enter these free energy differences, the electronic energy difference is the most crucial one in bond breaking and bond making processes.

Electronic energies are key components (steps 1-7 in Fig. 3): Electronic energies are notoriously difficult to calculate and standard approximations are affected by unknown errors that

can be large. Only for electronically simple structures, so-called closed-shell single-determinant electronic structures, well-established methods exist that run efficiently on a classical computer (such as explicitly correlated local coupled cluster schemes with, at least, perturbatively treated triple excitations [39]). For general electronic structures, however, no method of comparable accuracy exists that is at the same time feasible for moderately sized molecules. In particular for strong correlation cases, which require more than one Slater determinant for a qualitatively correct description of the electronic wave function, it can be hard to obtain an accurate total electronic energy, which then enters the calculation of relative energies.

In our previous work [11], we considered a quantum computer of moderate size within reach in the not too distant future. Moreover, we assumed that such a machine might have 100 to 200 logical qubits available for the representation of a quantum state. Such a state would be constructed from single-particle states, i.e., molecular orbitals for molecular structures. For decades, it has been the goal of quantum chemistry to devise methods that efficiently construct approximations to a many-electron state represented in terms of orbitals. If the full many-electron Hamiltonian is expressed and diagonalized in a complete many-electron (determinantal) basis constructed from such a one-electron basis, then a full-CI calculation may be carried out. Such an exact diagonalization is, however, routinely only feasible for about 18 orbitals [40] (a record calculation was recently carried out for 24 orbitals [41]) due to the exponentially growing number of many-electron states with the number of orbitals.

Required accuracy: A reasonable target accuracy for relative energies (and therefore also for total electronic energies of individual molecular species) is about 1 mHartree, if not 0.1 mHartree. This corresponds to about 2.6 and 0.26 kJ/mol, respectively. Note that thermal energy RT (T being temperature and R the gas constant) at room temperature is on the order of 2.6 kJ/mol, which may be related to the kinetic energy of a reactant molecule at average velocity (compare this to the spread observed for different DFT functionals in our example in the last section).

It is important to understand that this target accuracy is important for relative energies, i.e., for the energy differences that eventually enter the rate constant expressions. For total electronic energies, however, this accuracy does not match the precision with which these energies are actually known. In fact, the true total energies are typically off by a huge energy offset because one does not make an effort to describe core electrons, which contribute significantly

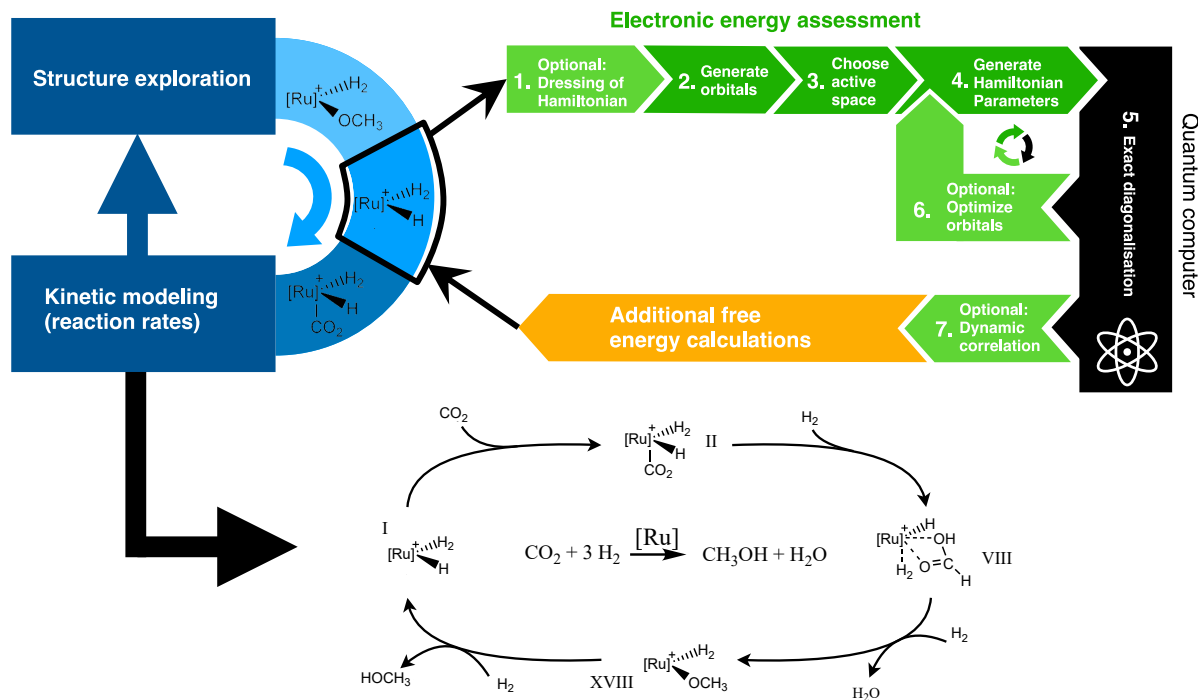


Figure 3. Protocol of computational catalysis with the key step of quantum computing embedded in black, which is usually accomplished with traditional methods such as CASSCF, DMRG, or FCIQMC (see text for further explanation).

to the total electronic energy, but not to reaction chemistry as they are atomically conserved. Hence, such calculations rely on significant error cancellation effects that occur when atomic contributions to the total electronic energy drop out in the calculation of reaction energies (which are relative energies) as they are conserved during a reaction (consider, e.g., a molecular orbital that is mostly of $1s$ -atomic orbital character and remains unaffected by a chemical reaction, but contributes significantly to the total electronic energy).

Challenges of electronic structure (steps 1-7 in Fig. 3): It is therefore most important to get the electronic (valence) structure of each relevant molecular structure right. Here, quantum computing offers an opportunity [11]. It is important to realize that a typical chemical catalysis problem does not involve very many valence orbitals in every elementary reaction step. As a consequence, the size of the active orbital space, from which the electronic wave function is constructed, does usually not need to be very large and can be easily handled with methods such as Complete Active Space Self Consistent Field (CASSCF), DMRG, or FCIQMC. The latter two are capable of handling active orbital spaces of up to about 100 spatial orbitals owing to efficient

approximations. However, sometimes there may be a price to pay for these approximations and that is a residual uncertainty regarding convergence of the electronic energy. For instance, a DMRG result will critically depend on – apart from a fixed finite value of the bond dimension – proper convergence of the sweeping algorithm, which, at times, might be difficult to determine. In the case of the more recent FCIQMC approach, which is under continuous development and offers extraordinarily efficient scaling on large traditional parallel computers, convergence with respect to the number of walkers or extrapolation to an infinite number of walkers may be hard to achieve for certain molecules. We also note that it is generally hard for any quantum chemical approach (hence, also for DMRG and FCIQMC) to deliver rigorous yet useful information about the error associated with a specific result. Moreover, any active-space approach is plagued by a severe drawback discussed below, namely the neglect of dynamic electronic correlation arising from the majority of virtual orbitals neglected.

Importance of dynamic electron correlation (steps 1 and 7 in Fig. 3): As noted already above, moderately sized molecules, such as the ones studied in this work, may easily require on the order of 1000

or more spatial molecular orbitals for a description that may be considered accurate within the chemically relevant accuracy of about 1 mHartree or even 0.1 mHartree for relative energies. However, the restriction to the valence orbital space from which the active space of the most strongly correlated orbitals is chosen [42, 43] compromises this accuracy (note that these active orbitals may be identified based on natural-orbital occupation numbers [44] or on orbital entanglement measures [45, 46], even in a completely automated fashion [45, 47]). The vast majority of orbitals that are weakly entangled and neglected in this procedure give rise to dynamic electron correlations, which are neglected in a small-CAS calculation. However, the dynamic electron correlation contribution to the total electronic energy is decisive and so standard recipes exist to approximate it. The most prominent one is the a posteriori correction (step 7 in Fig. 3) provided by multi-reference perturbation theory [48], which, however, requires elements of the three- and four-body reduced density matrices (3-RDMs and 4-RDMs, respectively) that would be extremely hard to obtain by quantum computing. Not even approximate approaches that rely on at most some 3-RDM elements will be accessible by quantum computing for interesting molecules. To evade such a computational bottleneck, perturb-then-diagonalize approaches (step 1 in Fig. 3) such as range-separation DFT for CAS-type methods [49–51] or transcorrelation approaches [52] were proposed for quantum computing [11].

Quantum computing is supposed to be a valuable and, in the long run, ultimately superior competitor to the aforementioned traditional methods (i) because rigorous error estimates are available and (ii) because systems may be accessible that are traditionally not feasible because of the curse of dimensionality when a total state is to be represented in a large set of orbitals. Its true benefits will fully unfold if energy measurements in the full orbital basis become feasible (on this, see the discussion in the Conclusions section).

Four-index transformation (step 4 in Fig. 3): A cumbersome technical step, to be carried out by traditional computing on classical computers, is the four-index transformation of the two-electron interaction integrals in the Hamiltonian, which scales with the fifth power of the number of basis functions. In this transformation, the final parameters for the electronic Coulomb Hamiltonian in the molecular orbital basis are produced from the four-index integrals defined in the atomic orbital basis, i.e., in the basis which is provided for the representation of all molecular orbitals (typically a set of Gaussian-type functions such as the def2-TZVP basis set used in the DFT

calculations presented above). Note, however, that this transformation, while being expensive but feasible for a small CAS, becomes a threat to the whole calculation when the active space grows to eventually incorporate the complete one-electron (atomic orbital) basis (of say, more than 1000 basis functions). Hence, the sheer number of two-electron parameters in the electronic Hamiltonian will require us to rethink how to deal with these terms growing to the fourth power in the number of orbitals, such as in recent work [53] that generate sparse low-rank approximations to the two-electron integrals. Naturally, this issue has also been discussed in modern traditional approaches [54].

IV. QUANTUM ALGORITHMS FOR CHEMISTRY

For the catalysis problem we require quantum algorithms that provide reliable results with controlled errors on the electronic energy in a given orbital basis. Uncontrolled approximations in quantum algorithms would negate the advantages offered by quantum computers, which will require tremendous effort to build and operate even at a moderately sized error-corrected scale.

Though it is without doubt that the popular variational quantum eigensolver (VQE) [55] can obtain parameters of a unitary coupled cluster (UCC) parametrization of the electronic wavefunction that is likely to be accurate (especially when higher than double excitations are considered [56]), this scheme unavoidably generates a residual unknown uncertainty in the true electronic energy. Reducing these errors by improving the ansatz will require significantly more gate operations than are expected to be possible on non-error corrected noisy intermediate scale quantum devices [57, 58]. Moreover, the number of repetitions required to estimate energies with sufficient accuracy of 1 mHartree or better is enormous [59].

We also note that knowledge of reliable and controllable errors in quantum algorithms is a decisive advantage over classical methods such as DMRG and FCIQMC, for which convergence control with respect to their parameters is not necessarily easy or even feasible.

Therefore, we turn to one of the most promising applications of quantum computers, which is a bounded-error simulation of quantum systems using quantum phase estimation. The main idea is to synthesize a quantum circuit that implements the real time-evolution operator $W = e^{-iH/\alpha}$ by a given Hamiltonian H for some normalizing factor α , which henceforth are always in atomic units of Hartree.

When applied n times to an eigenstate $H|\psi_k\rangle = E_k|\psi_k\rangle$, a phase nE_k/α is accumulated. Quantum phase estimation then estimates the energy E_k with a standard deviation $\Delta_E = \mathcal{O}(\alpha/n)$ [60]. If one prepares an arbitrary trial state $|\psi_{\text{trial}}\rangle$ rather than an eigenstate, phase estimation collapses the trial state to the k -th eigenstate with probability $p_k = |\langle\psi_k|\psi_{\text{trial}}\rangle|^2$ and it returns an estimate to the corresponding energy E_k [61].

The phase estimation procedure is executed on a quantum computer by applying a sequence of quantum gates. If the unitary W is implemented using a number c_W of quantum gates, the overall quantum gate cost of obtaining a single estimate \hat{E}_k is then

$$c_W \times \frac{\pi\alpha}{2\Delta_E}, \quad (1)$$

where the factor $\frac{\pi\alpha}{2\Delta_E}$ arises from previous analyses on the performance of phase estimation [20, 62] (combined with a so-called phase-doubling trick [20, 63]). In general, the quantum circuit only approximates W to some bounded error Δ_W in spectral norm. This adds a systematic bias of $\alpha\Delta_W$ to the estimate \hat{E}_k . Thus, we budget for this error by making the somewhat arbitrary choice of performing phase estimation to an error of $0.9\Delta_E$, and compiling W so that $\Delta_W \leq 0.1\Delta_E/\alpha$. To date, there are several prominent quantum algorithms for approximating real time-evolution, such as Lie-Trotter-Suzuki product formulas [64], sparse Hamiltonian simulation [65], linear-combination of unitaries [66], qubitization [15], and quantum signal processing [16]. In this work, we consider the electronic Hamiltonian in its non-relativistic form with Coulomb interactions (in Hartree atomic units),

$$H = \sum_{ij,\sigma} h_{ij} a_{(i,\sigma)}^\dagger a_{(j,\sigma)} \quad (2)$$

$$+ \frac{1}{2} \sum_{ijkl,\sigma\rho} h_{ijkl} a_{(i,\sigma)}^\dagger a_{(k,\rho)}^\dagger a_{(l,\rho)} a_{(j,\sigma)},$$

which is parametrized through the one- and two electron integrals h_{ij} and h_{ijkl} of the molecular orbitals $\{\psi_i\}$,

$$h_{ij} = \int \psi_i^*(x_1) \left(-\frac{\nabla^2}{2} - \sum_m \frac{Z_m}{|x_1 - r_m|} \right) \psi_j(x_1) d^3x_1, \quad (3)$$

$$h_{ijkl} = \int \psi_i^*(x_1) \psi_j(x_1) \left(\frac{1}{|x_1 - x_2|} \right) \psi_k^*(x_2) \psi_l(x_2) d^3x_1 d^3x_2, \quad (4)$$

where x_i denote electronic coordinates and Z_m is the charge number of nucleus m at position r_m

(note that a relativistic generalization is straightforward [67]). We explicitly separate the fermion indices $p \equiv (i, \sigma)$ into an index where $i \in \{1, \dots, N\}$ enumerates the N spatial molecular orbitals, and $\sigma \in \{0, 1\}$ indexes spin-up and spin-down. Hence, the fermion operators satisfy the usual anti-commutation relations

$$\{a_p, a_q\} = 0, \quad \{a_p^\dagger, a_q^\dagger\} = 0, \quad \{a_p, a_q^\dagger\} = \delta_{pq} \mathcal{I}, \quad (5)$$

and the coefficients h_{ij} , h_{ijkl} are real and satisfy the symmetries

$$h_{ij} = h_{ji}, \quad (6)$$

$$h_{ijkl} = h_{jikl} = h_{ijlk} = h_{jilk} = h_{lkij}$$

$$= h_{lkji} = h_{klji} = h_{klji}.$$

For the purposes of phase estimation through the so-called *qubitization* approach, it is not necessary to simulate time-evolution e^{-iHt} . Whereas our previous work [11] approximated the time-evolution operation using Lie-Trotter-Suzuki product formulas, it can be advantageous in some cases to implement the unitary walk operator $W = e^{i \sin^{-1}(H/\alpha)}$ [15, 68, 69] instead, which has some normalizing constant $\alpha \geq \|H\|$ that ensures the arcsine is real. This walk operator can be implemented exactly, assuming access to arbitrary single-qubit rotations, in contrast to all known quantum algorithms where time-evolution e^{-iHt} can only be approximated. After estimating the phase $\hat{\theta} = \sin^{-1}(E_k/\alpha)$ with phase estimation, we may obtain \hat{E}_k by applying $\sin(\hat{\theta})$ in a classical postprocessing step.

We focus on the qubitization technique applied to electronic structure Eq. (2), with the goal of minimizing the quantum gate costs in Eq. (1). In fault-tolerant architectures, quantum gate costs reduce to the number of so-called primitive Clifford gates (e.g. Hadamard = $\frac{1}{\sqrt{2}} \begin{bmatrix} 1 & -1 \\ 1 & 1 \end{bmatrix}$, phase = $\begin{bmatrix} 1 & 0 \\ 0 & i \end{bmatrix}$, and controlled-NOT) and non-Clifford gates (e.g. $T = \begin{bmatrix} 1 & 0 \\ 0 & \sqrt{i} \end{bmatrix}$ and Toffoli, which applies a NOT gate controlled on two input bits being in the ‘one’ state). As the physical resources needed to implement a single error-corrected primitive non-Clifford gate, such as the T gate is on the order of 100 to 10000 times more costly than a single two-qubit Clifford gate [70, 71] – and one Toffoli gate may be implemented by four T gates – much recent work has focused on optimizing the non-Clifford-gate cost of W . Within an atom-centered basis set (such as the ones employed in this work), this focus has reduced the T gate cost of obtaining a single estimate \hat{E}_k from $\tilde{\mathcal{O}}(N^5/\Delta_E^{3/2})$ using Trotter methods to $\tilde{\mathcal{O}}(\alpha_{\text{CD}} N^{3/2}/\Delta_E)$ Toffoli gates and $\mathcal{O}(N^{3/2} \log N/\Delta_E)$ qubits using qubitization combined with a so-called single-factorized Hamiltonian

representation, where $\alpha_{\text{CD}} = \mathcal{O}(N^3)$ [22] is a certain norm of the Hamiltonian. Our main technical contribution is a further reduction of the gate cost of W and the normalizing factor to $\alpha_{\text{DF}} = \mathcal{O}(N^{3/2})$ as described in the next Section.

V. EFFICIENT ENCODING OF DOUBLE-FACTORIZED ELECTRONIC STRUCTURE

Our main algorithmic advance is based on a quantum algorithm to ‘qubitize’ the so-called double-factorized representation H_{DF} of the electronic Hamiltonian H . On the one hand, the double-factorized representation is sparse, and therefore minimizes the cost c_W of qubitization, which generally scales with the number of terms needed to represent the Hamiltonian. On the other hand, the double-factorized representation is a partial diagonalization of the original Hamiltonian, and hence has a small normalizing constant α_{DF} . Despite these favorable properties, previous quantum simulations using this representation are based on Trotter methods [72, 73].

The double-factorized form builds upon the single-factorized representation H_{CD} of the Hamiltonian H where

$$H_{\text{CD}} \doteq \sum_{ij,\sigma} \tilde{h}_{ij} a_{(i,\sigma)}^\dagger a_{(j,\sigma)} \quad (7)$$

$$+ \frac{1}{2} \sum_{r \in [R]} \left(\sum_{ij,\sigma} L_{ij}^{(r)} a_{(i,\sigma)}^\dagger a_{(j,\sigma)} \right)^2, \quad (8)$$

$$\tilde{h}_{ij} \doteq h_{ij} - \frac{1}{2} \sum_l h_{illj}.$$

Note that the rank- R factorization of the two-electron tensor $h_{ijkl} = \sum_{r \in [R]} L_{ij}^{(r)} L_{kl}^{(r)\top}$ Eq. (2) into the $N \times N$ symmetric matrices $L^{(r)}$ always exists due the symmetry constraints Eq. (6), and may be computed using either a singular-value decomposition or a Cholesky decomposition. This representation also facilitates a low-rank approximation by truncating the rank R . In the worst-case, $R \leq N^2$. However, it was noted by Peng et al. [53] that rank $R \sim N \log N$ for typical molecular systems when N is proportional to the number of atoms, which is a provable statement for 1D systems [74]. This reduces the number of terms needed to describe the second-quantized Hamiltonian from $\mathcal{O}(N^4)$ in Eq. (2) to $\mathcal{O}(RN^2)$ in Eq. (7). This representation was first exploited by Berry et al. [22] to qubitize H_{CD} with a normalizing constant $\alpha_{\text{CD}} \doteq 2\|\tilde{h}\|_{\text{EW}} + 2 \sum_{r \in [R]} \|L^{(r)}\|_{\text{EW}}^2$ expressed using

the entry-wise norm $\|L^{(r)}\|_{\text{EW}} \doteq \sum_{ij \in [N]} |L_{ij}^{(r)}|$.

The technical innovation in our approach is a quantum circuit, detailed in the supplementary material, for qubitizing the double-factorized Hamiltonian

$$H_{\text{DF}} = \sum_{ij,\sigma} \tilde{h}_{ij} a_{(i,\sigma)}^\dagger a_{(j,\sigma)} \quad (9)$$

$$+ \frac{1}{2} \sum_{r \in [R]} \left(\sum_{ij,\sigma} \sum_{m \in [M^{(r)}]} \lambda_m^{(r)} \vec{R}_{m,i}^{(r)} \vec{R}_{m,j}^{(r)} a_{(i,\sigma)}^\dagger a_{(j,\sigma)} \right)^2.$$

This is obtained by a rank- $M^{(r)}$ eigendecomposition of the symmetric matrices $L^{(r)} = \sum_{m \in [M^{(r)}]} \lambda_m^{(r)} \vec{R}_m^{(r)} \cdot (\vec{R}_m^{(r)})^\top$ into a total of $M \doteq \sum_{r \in [R]} M^{(r)}$, each normalized to be of unit length $\|\vec{R}_m^{(r)}\|_2 = 1$. The number of terms in Eq. (9) is even further reduced to $\mathcal{O}(MN)$ as Peng et al. [53] also noted that for typical molecular systems where $N \gg 10^3$ scales with the number of atoms, one may retain $M \sim N \log N$ eigenvectors and truncate the rest. A key technical step in our approach is to work in the Majorana representation of fermion operators

$$\gamma_{p,0} = a_p + a_p^\dagger, \quad (10)$$

$$\gamma_{p,1} = -i(a_p - a_p^\dagger), \quad (11)$$

$$\{\gamma_{p,x}, \gamma_{q,y}\} = 2\delta_{pq}\delta_{xy}\mathcal{I}. \quad (12)$$

As we show in the supplementary material, this representation maps

$$H_{\text{DF}} \rightarrow \left(\sum_i h_{ii} - \frac{1}{2} \sum_{il} h_{ill} + \frac{1}{2} \sum_{il} h_{lil} \right) \mathcal{I} \quad (13)$$

$$+ \text{One}_{L^{(-1)}} + \frac{1}{2} \sum_{r \in [R]} \text{One}_{L^{(r)}}^2,$$

which is expressed as a sum of squares of one-body Hamiltonians

$$\text{One}_L \doteq \frac{i}{2} \sum_{ij} \sum_{\sigma} L_{ij} \gamma_{i,\sigma,0} \gamma_{j,\sigma,1}, \quad (14)$$

$$L_{ij}^{(-1)} \doteq h_{ij} - \frac{1}{2} \sum_l h_{ill} + \sum_l h_{lil}. \quad (15)$$

This leads to a normalizing constant

$$\alpha_{\text{DF}} = \|L^{(-1)}\|_{\text{SC}} + \frac{1}{4} \sum_{r \in [R]} \|L^{(r)}\|_{\text{SC}}^2. \quad (16)$$

Note that the difference between $L^{(-1)}$ and \tilde{h} is the mean-field Coulomb repulsion contribution term $\sum_l h_{lil}$. Note that α_{DF} is also significantly smaller

than α_{CD} from previous approaches [22]. In addition to the factor of eight reduction in the prefactor of the two-electron norms, the dependence of α_{DF} on Schatten norms $\|L^{(r)}\|_{\text{SC}}$ is beneficial as they can be up to a factor of N smaller than the entry-wise norms $\|L^{(r)}\|_{\text{EW}}$ that α_{CD} depends on, as follows from the following tight inequalities for any Hermitian $N \times N$ matrix h ,

$$\|h\|_{\text{SC}} \doteq \sum_{k \in [N]} |\text{Eigenvalues}[h]_k|, \quad (17)$$

$$\frac{1}{N} \|h\|_{\text{EW}} \leq \|h\|_{\text{SC}} \leq \|h\|_{\text{EW}}, \quad (18)$$

which we prove in the supplementary material and may be of independent interest.

The Toffoli gate complexity of synthesizing the walk operator to an error $\Delta_W = 0.1\Delta_E/\alpha_{\text{DF}}$, as detailed in the supplementary material, is then

$$c_W \leq \frac{2M}{1+\lambda} + 2\lambda N\beta + 8N\beta + 4N + \mathcal{O}(\sqrt{R \log M} + \sqrt{M \log(1/\Delta_W)}), \quad (19)$$

for any choice of integer $\lambda \geq 0$, and where the parameter $\beta = \left\lceil 5.652 + \log_2 \left(\frac{N}{\Delta_W} \right) \right\rceil$. This also uses the following number of qubits

$$N\beta(1+\lambda) + 2N + \mathcal{O}(\log(N/\Delta_W)). \quad (20)$$

Note that λ controls the number of ancillary qubits. By choosing $\lambda = \mathcal{O}(\sqrt{\frac{M}{N\beta}})$, the Toffoli cost is $c_W = \mathcal{O}(\sqrt{MN\beta} + N\beta)$, which is advantageous when $M \gg N\beta$, using $\mathcal{O}(\sqrt{MN\beta} + N + \beta)$ qubits. Assuming the empirical scaling of M and R by Peng et al., our algorithm encodes electronic spectra for atom-centered basis sets into the walk operator using only $c_W = \tilde{\mathcal{O}}(N)$ Toffoli gates, and with a normalizing constant α_{DF} , which improves upon the $\tilde{\mathcal{O}}(N^{3/2})$ Toffoli gates and larger normalizing constant α_{CD} required by the single-factorized approach [22].

In the following examples we consider, typical values of λ that minimize the Toffoli costs are between 1 and 5, and the Toffoli gate counts and qubit counts we quote exclude the sub-dominant big- $\mathcal{O}(\cdot)$ component of Eqs. (19) and (20).

A. Truncation

We now describe our procedure for obtaining, by truncating eigenvalues, low-rank approximations \tilde{H}_{DF} of the double-factorized Hamiltonian Eq. (13) from an initial numerically-exact representation H_{DF} . We focus on truncating the two-electron terms as those tend to dominate the cost of block-encoding.

Given a target approximation error ϵ , we consider two truncations schemes, which we call *coherent* and *incoherent*. The coherent scheme upper bounds the actual error

$$\|\tilde{H}_{\text{DF}} - H_{\text{DF}}\| \leq \epsilon_{\text{co}}, \quad (21)$$

in spectral norm for any given choice of ϵ_{co} . This upper bound is obtained by a triangle inequality, which assumes that all truncated terms have an error that adds linearly. That is, if the difference $\tilde{H}_{\text{DF}} - H_{\text{DF}} = \sum_j H_j$ is a sum of terms, then we truncate so that

$$\sum_j \|H_j\| \leq \epsilon_{\text{co}}. \quad (22)$$

We find that this bound is often quite loose, and the gap between the actual error and ϵ grows with system size. This motivates the *incoherent* scheme, which assumes that the error of truncated terms add incoherently by a sum-of-squares. Thus, we truncate so that

$$\sqrt{\sum_j \|H_j\|^2} \leq \epsilon_{\text{in}}. \quad (23)$$

Suppose we remove a single eigenvalue $\lambda_m^{(r)}$ from Eq. (13) during truncation. Using the identity $A^2 - (A - B)^2 = AB + BA - B^2$, the difference

$$H_{\text{DF}} - \tilde{H}_{\text{DF}} = \frac{1}{2} \left(\left\{ \text{One}_{L^{(r)}}, \frac{\lambda_m^{(r)}}{2} \sum_{\sigma} \gamma_{\tilde{R}_m^{(r)}, \sigma, 0} \gamma_{\tilde{R}_m^{(r)}, \sigma, 1} \right\} - \left(\frac{\lambda_m^{(r)}}{2} \sum_{\sigma} \gamma_{\tilde{R}_m^{(r)}, \sigma, 0} \gamma_{\tilde{R}_m^{(r)}, \sigma, 1} \right)^2 \right), \quad (24)$$

can be bounded in $\|\cdot\|$ as follows:

$$\begin{aligned} \|H_{\text{DF}} - \tilde{H}_{\text{DF}}\| &\leq |\lambda_m^{(r)}| \sum_{n \neq m} |\lambda_n^{(r)}| + \frac{1}{2} |\lambda_m^{(r)}|^2 \\ &= |\lambda_m^{(r)}| \left(\|L^{(r)}\|_{\text{SC}} - \frac{1}{2} |\lambda_m^{(r)}| \right) \\ &\leq \|L^{(r)}\|_{\text{SC}} |\lambda_m^{(r)}|. \end{aligned} \quad (25)$$

In the coherent scheme, we truncate eigenvalues in the index set \mathcal{T} such that $\sum_{(r,m) \in \mathcal{T}} \|L^{(r)}\|_{\text{SC}} |\lambda_m^{(r)}| \leq \epsilon_{\text{co}}$. In the incoherent scheme, we truncate such that $\sqrt{\sum_{(r,m) \in \mathcal{T}} (\|L^{(r)}\|_{\text{SC}} |\lambda_m^{(r)}|)^2} \leq \epsilon_{\text{in}}$. In both cases we may maximize the number of truncated eigenvalues by deleting those with the smallest value of $\|L^{(r)}\|_{\text{SC}} |\lambda_m^{(r)}|$ first.

In the following, we truncate according to the sum-of-square procedure. While this approach does

not rigorously bound the total error, we find that it better matches the error we observed for our benchmark systems, see Fig. 4, but still tends to significantly overestimate the actual error.

VI. RESULTS

For the intermediates depicted in the catalytic cycle in Fig. 1, we carried out density functional calculations that delivered the data presented in Fig. 2 and wave function calculations with various active orbital spaces for the analyses discussed below. For the sake of brevity, we refer the reader to the supplementary material for all technical details on these standard quantum chemical calculations.

For each of these key intermediates and transition states we then evaluate the cost of performing quantum phase estimation to chemical accuracy, both for small active spaces of 52–65 orbitals and larger ones, and then discuss runtimes and qubit requirements.

A. Selection of active orbitals

As mentioned in Section IV, the electronic Hamiltonian in Eq. (2) is parametrized by one- and two-electron integrals, h_{ij} and h_{ijkl} , respectively, over the molecular orbitals of a restricted orbital subspace, the active space. For the selection of the active space (cf. Fig. 3), all strongly correlated orbitals must be identified (see the detailed discussion for our carbon dioxide fixation process in the supporting information). For this, we relied on orbital entanglement measures which we applied in an automated procedure [45, 47], but we emphasize that the importance of this choice for selecting the different orbital space sizes for this work is not crucial at all. Analysis of the resulting states in terms of these orbital entanglement measures, pair-orbital mutual information, and occupation numbers shows that the electronic ground states of the catalyst structures selected for our study are not dominated by static correlation. For such cases, the traditional quantum chemistry toolbox offers efficient and very accurate coupled cluster methods at the basis set limit, which represent a true challenge for quantum algorithms to compete with. Still, we seek to analyze a general approach in quantum computation that can deal with strong (static) correlation (and possibly with any correlation problem in the not too distant future). It is therefore not decisive for our resource analysis that the active space sizes chosen (see supporting information) do neither obey nor exploit typical patterns of electron correlation. It was, however, still possible to select a small active space of strongly correlated

orbitals on the size of five to sixteen orbitals. The main purpose of this work is understanding the performance of quantum algorithms on an actual chemical problem of varying size. The varying size is the growing size of the orbital space in which the exact wave function is constructed. In order to construct a proper test bed, we are therefore forced to choose active-space sizes that are arbitrary with respect to the proper balance of static and dynamic correlation. In other words, to grow the active space sizes beyond the classical limit, we had to add weakly correlated orbitals. Naturally, it then became increasingly difficult to select the active spaces based on orbital entanglement alone (because all such orbitals show similarly weak entanglement entropy measures). In this study, we therefore resorted to criteria which ensure a reproducible selection that is, at the same time, reasonable from a chemical point of view. We chose three different active space sizes (small, intermediate, and large) for each molecular structure of the catalytic cycle. The first active space comprises those orbitals selected based on orbital entanglement criteria. Note that this small active space is identical to the one employed in the CASSCF calculations that produced the molecular orbitals from which the Hamiltonian parameters h_{ij} and h_{ijkl} were calculated. The intermediate active space includes all the orbitals of the small active space and then in addition the valence orbitals of ruthenium and the ligands (excluding the triphos ligand and, if present, solvent molecules), as well as the orbitals involved in ligand-metal bonding. For the largest active space, we further supplemented these orbitals with the π and π^* orbitals on the triphos ligand, as they form a well-defined and easily identifiable set of orbitals. Apart from these three active spaces per catalyst structure, we created even larger active spaces for structure XVIII, for which we additionally selected three active spaces of size $n=100$, 150, and 250 spatial molecular orbitals. Since a manual selection is pointless for such large active spaces of mostly dynamically correlated orbitals, we selected the $n/2$ occupied and $n/2$ virtual orbitals around the Fermi level. For each of these active spaces, we obtained the one- and two-electron integrals h_{ij} and h_{ijkl} via a four-index transformation (see also Fig. 3). These integrals then served as input to the quantum algorithms.

B. Resource estimates

We now evaluate the cost of phase estimation to chemical accuracy for various structures in the carbon capture catalytic cycle of Section II. The active spaces of the molecules considered in this section are

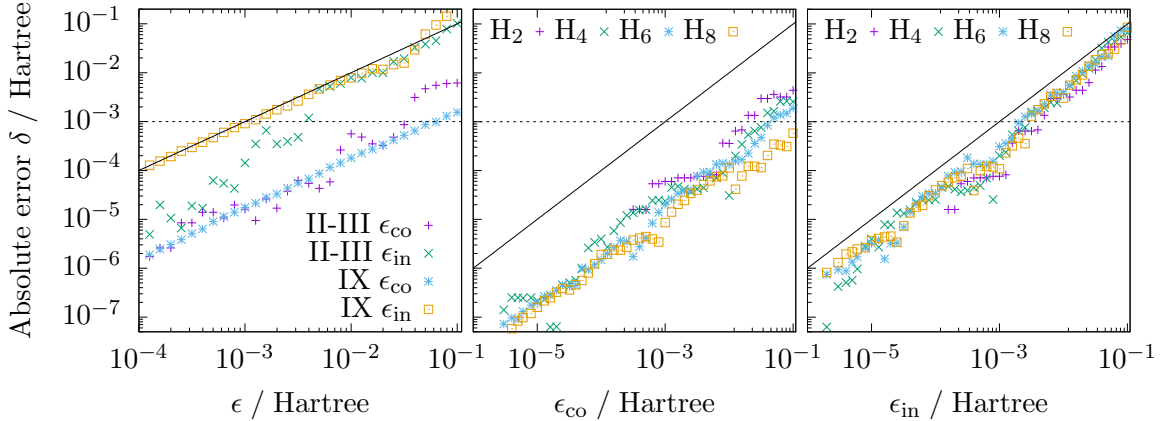


Figure 4. Empirical absolute error δ (in Hartree) of the ground-state electronic energy resulting from applying the two truncation schemes to the two-electron integrals of the Hamiltonian at various thresholds ϵ_{co} , ϵ_{in} , evaluated from DMRG-CI calculations. The lines $\delta = \epsilon$ and $\delta = 1\text{mHartree}$ are meant to guide the eye. (Left) Absolute error of the ground-state electronic DMRG-CI energy for the two truncation schemes for complex II-III with 6 active orbitals and complex IX with 16 active orbitals. (Middle) Absolute error in the ground-state electronic DMRG-CI energy of linear Hydrogen chains of length 2, 4, 6, and 8 at different truncation thresholds ϵ_{co} for the coherent truncation scheme and (Right) ϵ_{in} for the incoherent truncation.

in the range of 52–65 orbitals, although we tabulate more results for 2–250 orbitals in the supplementary material. In addition, we also evaluate the scaling of cost with respect to the active space size N while keeping the number of atoms fixed, and find a different scaling law of $M \sim N^{2.5}$ for the number of eigenvectors compared to that of $M \sim N \log N$ [53] when increasing the number of atoms. We find, as shown in Table I, that the gate cost for systems in the 52-orbital to 65-orbital range is on the order of 10^{10} Toffoli gates, using about 4000 qubits.

The cost depends on the truncation threshold ϵ_{in} as plotted in Fig. 5. At the highly aggressive threshold of $\epsilon_{\text{in}} = 100\text{mHartree}$, the rank of these examples roughly matches the parameters fit by Peng et al. [53] to three-dimensional hydrocarbons for 54 orbitals. However, the numerically computed shift in energy at that threshold can exceed chemical accuracy, following Fig. 4, and should be interpreted as a most optimistic cost estimate. Therefore, we choose $\epsilon_{\text{in}} = 1\text{mHartree}$, which our numerical simulations indicate closely reflect chemical accuracy. Irrespective of the truncation scheme, we note that the logarithmic scaling with $1/\epsilon_{\text{in}}$ means that the Toffoli costs vary by at most factor of five between these extremes. By varying the active space size between 2 and 250 orbitals for the different catalyst structures, we find in Fig. 6 that the Toffoli cost of phase estimation scales with $\sim N^{3.25}$. The exponent is a combination of two factors: Across all configurations of the catalytic cycle, the number of eigenvectors scales with $M \sim N^{2.5}$, hence $c_W \sim \sqrt{MN} \sim N^{1.75}$,

and the normalizing constant $\alpha_{\text{DF}} \sim N^{1.5}$ Hartree.

We next demonstrate the extent of our algorithmic improvements by applying our techniques to the 54-orbital representation of the FeMoco active site of nitrogenase that we considered previously [11], and comparing costs with prior art based on Trotterization and qubitization of the single-factorized representation. As seen in Table II, our Toffoli cost following Eq. (19) is on the order of 1.22×10^{10} using 3600 qubits. Assuming that the number of logical qubits is not a limiting factor, this is a dramatic improvement over the 6.0×10^{14} T gates and 142 qubits in our original estimate [11], and a significant improvement over the 1.2×10^{12} Toffoli gates of the single-factorized approach [75], where $\alpha_{\text{CD}} = 3.6 \times 10^4$ Hartree with 3.0×10^5 unique non-zero terms, and a rank of $R \sim 200$ was claimed to be sufficient to achieve chemical accuracy with respect to a CCSD ansatz. This is seen in Table III where, for the sake of comparison, we choose a truncation threshold of $\epsilon_{\text{in}} = 73\text{mHartree}$ to normalize the rank between our results and the single-factorized approach. Moreover, our double-factorized approach also improves upon the 2.3×10^{11} Toffoli gates of highly-optimized implementations [75] based on the unfactorized Hamiltonian Eq. (2), which has $\alpha = 9.9 \times 10^3$ Hartree with 4.4×10^5 unique non-zero terms. Our improvement largely stems from a normalizing factor α_{DF} that is 33 to 120 times smaller as the number of terms in all approaches at this threshold are roughly equal. This trend also applies to the various carbon fixation catalyst structures that we consider

Table I. Number of Toffoli gates for estimating an energy level to an error of 1 mHartree using a truncation threshold of $\epsilon_{\text{in}} = 1\text{mHartree}$ for the largest active spaces of structures in the catalytic cycle considered here. Our approach allows for a trade-off between the number of logical qubits required and the Toffoli count.

Structure	Orbitals	Electrons	R	M	α_{DF} /Hartree	Using fewer qubits		Using fewer Toffolis	
						Qubits	Toffolis/ 10^{10}	Qubits	Toffolis/ 10^{10}
I	52	48	613	23566	177.3	3400	1.3	6900	1.1
II	62	70	734	33629	374.4	4200	3.6	8400	3.1
II-III	65	74	783	38122	416.0	4400	4.5	8900	3.7
V	60	68	670	29319	371.1	4100	3.3	8200	2.9
VIII	65	76	794	39088	425.7	4400	4.6	8900	3.8
VIII-IX	59	72	666	29286	384.4	4000	3.4	8000	2.9
IX	62	68	638	28945	396.6	4200	3.5	8400	3.1
XVIII	56	64	705	29594	293.5	3700	2.5	7400	2.1

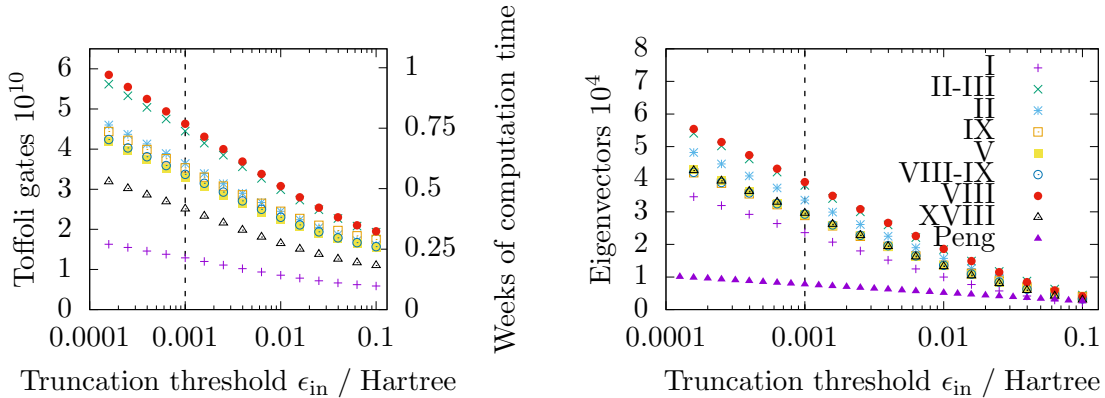


Figure 5. (Left) Toffoli cost versus truncation threshold for phase estimation to a precision of 1mHartree in the double-factorized representation of the catalytic cycle in Fig. 1 with a number of orbitals listed in Table I. Computation time is assumed to be $10\mu\text{s}$ between each Toffoli, or 100kHz. (Right) Number of eigenvector in the double-factorized representation. The data points by Peng et al. are for three-dimensional hydrocarbons [53] with 54 orbitals.

when we perform a similar comparison but instead use the same incoherent truncation scheme for all examples at a more conservative error threshold of $\epsilon_{\text{in}} = 1\text{mHartree}$.

C. Runtimes and qubit counts

We finally relate these gate count estimates to expected runtimes on future quantum computers. Exact runtime will, of course, depend on details of the system and error correction schemes. In our previous analysis [11], we optimistically assumed gate times of 100ns for fault tolerant logical gate operations, which may be a long-term achievable goal. As a more realistic assumption for mid-term fault tolerant quantum computers we now expect that the physical gate times in current quantum computer architectures range from tens of nanoseconds for solid state qubits to tens of microseconds for ion traps. Realizing fault tolerance by using quantum error correction with the surface code [76], will lead to logical

gate times for a Toffoli gate of about $10\mu\text{s}$ to 10ms depending on the architecture. The lower estimate of $10\mu\text{s}$ means that 10^{10} Toffoli gates correspond to a runtime of 28 hours or about a day, while the upper estimate of 10ms would correspond to several years. These considerations show that fast gate times will be essential for realistic quantum computation for chemical catalysis.

The above estimates do not explicitly consider the cost of layout, i.e. the mapping onto a nearest neighbor planar square lattice topology of error corrected logical qubits. We argue that this overhead is negligible, since the subroutine with dominant cost, the table lookup discussed in the supplementary material is based on FANOUT operators [77] and maps well to this topology. Moreover, we here assume that any overhead of layout as well as Clifford gates are included in the assumed gate time for a Toffoli gate, as these dominant FANOUT operations may be implemented in a constant Clifford depth of 4 in parallel with the sequentially applied Toffolis. Fault tolerant gates also have an overhead in the

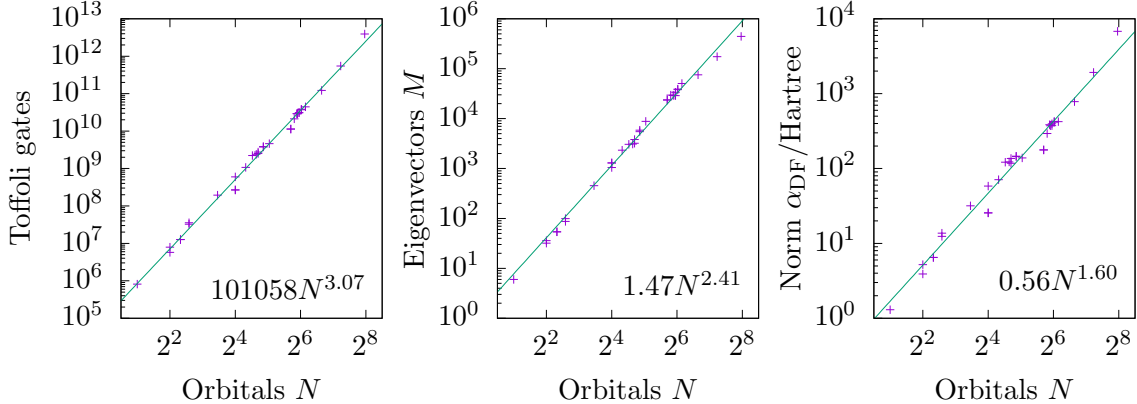


Figure 6. (Left) Scaling of minimized Toffoli cost across all configurations of the catalytic cycle with respect to active space size, for performing phase estimation to a precision of 1mHartree in the double-factorized representation. The fitted power-law curve has an exponent arising from the product $\alpha_{DFCW} \sim \alpha_{DF}\sqrt{MN}/\Delta_E$ in Eqs. (1) and (19) (middle) where M is the number of eigenvectors and (right) the normalizing constant is α_{DF} .

Table II. Comparison of our new double-factorization approach for H_{DF} applied to the FeMoco active site of nitro- genase ($N = 54$) with prior approaches based on Trotterization [11] or qubitization [22] using the unfactorized H or single-factorized H_{CD} Hamiltonian, and also for the VIII structure in the catalytic cycle ($N = 65$) where all examples apply the incoherent truncation scheme with the same threshold of $\epsilon_{in} = 1\text{mHartree}$.

Structure	Approach	α / Hartree	Terms	Qubits	Toffoli gates	Comments
FeMoco	Qubitization H_{DF}	300.5	1.3×10^6	3600	2.3×10^{10}	$\epsilon_{in} = 1\text{mHartree}$.
	Qubitization H_{DF}	296.9	2.8×10^5	3600	1.22×10^{10}	Optimistic $\epsilon_{in} = 73\text{mHartree}$.
	Trotterization H [11]	-	-	142	1.5×10^{14}	Optimistic Trotter number.
	Qubitization H [22]	9.9×10^3	4.4×10^5	5100	2.3×10^{11}	Truncation evaluated by CCSD.
	Qubitization H_{CD} [22]	3.6×10^4	4.0×10^5	3000	1.2×10^{12}	Truncation evaluated by CCSD.
VIII	Qubitization H_{DF}	425.7	2.5×10^6	4600	4.6×10^{10}	$\epsilon_{in} = 1\text{mHartree}$.
	Qubitization H	1.1×10^4	2.2×10^6	11000	9.3×10^{11}	$\epsilon_{in} = 1\text{mHartree}$.
	Qubitization H_{CD}	4.2×10^4	1.3×10^6	5800	2.1×10^{12}	$\epsilon_{in} = 1\text{mHartree}$.

Table III. Scaling of cost in our double-factorization approach with truncation threshold for the FeMoco active site of nitro- genase ($N = 54$). For comparison, the last line has $R = 200$ which matches that used Berry et al. [22].

ϵ_{in} / mHartree	Rank R	Eigenvectors M	Terms $M \times N$	α_{DF} / Hartree	Qubits	#Toffoli gates
1	567	2.4×10^4	1.30×10^6	300.5	3600	2.3×10^{10}
10	371	1.33×10^4	7.2×10^5	300.0	3600	1.67×10^{10}
100	178	4.2×10^3	2.3×10^5	295.8	3600	1.16×10^{10}
73	200	5.2×10^3	2.8×10^5	296.9	3600	1.22×10^{10}

number of qubits, with hundreds to thousands of physical qubits needed per logical qubit [11, 76], depending on the quality of the qubits. 4000 logical qubits will thus correspond to millions of physical qubits. This implies the need for a scalable quantum computer architecture, scaling to millions of qubits.

D. State preparation

To determine the ground state energy using phase estimation, it is required to prepare a trial state $|\psi_{\text{trial}}\rangle$ which has a high overlap with the true ground state $|\psi_0\rangle$ of the Hamiltonian H as discussed in Section IV. While the exact ground state is unknown, we used state-of-the-art DMRG calculations to obtain an approximate ground state $|\tilde{\psi}_0\rangle$ for each of

our systems (see supplementary material for further details). An approximate configuration interaction wave function obtained by reconstruction [78] from the corresponding matrix product state wave function optimized with DMRG served to provide an overlap with the trial state prepared on the quantum computer. Since the trial state is chosen to be HF determinant for this case, the overlap is given by the square of the coefficient in front of the Hartree-Fock determinant in the configuration interaction expansion, i.e., the one with the first $N/2$ orbitals occupied where N is the number of electrons. We found that there is a large overlap for all of our systems, see Table IV. We expect this overlap to not shrink substantially with increasing precision of the approximate ground state obtained by DMRG and hence preparing the dominant single-determinant state is sufficient for the molecular structures considered in this work. Recall that the Ru complexes selected for our study do not exhibit strong multi-reference character. If this overlap had turned out to be small, we would defer to Ref. [79] for options on how to prepare a multi-determinant initial state in order to boost the success probability of phase estimation.

VII. CONCLUSIONS

In this work, we considered computational catalysis leveraged by quantum computing. We rely on accurate error bounds on the electronic energy accessible in quantum algorithms to obtain sufficiently accurate data for intermediate and transition state structures of a catalytic cycle. In particular, i) we considered decisive steps of a synthetic catalyst that is known to convert carbon dioxide to methanol (and for which traditional work based on density functional theory had already been reported alongside the experimental results [27]), ii) we presented a new quantum algorithm in the qubitization framework that exploits a double-factorized electronic structure representation, which significantly reduces the runtime, iii) we validated the truncation schemes by comparison with density matrix renormalization group calculations, iv) we confirmed that starting the quantum algorithm from a single determinant initial state has high success probability for the carbon dioxide functionalization process studied in this work, and v) we calculated realistic resource estimates for mid-term scalable quantum computers and related them to expected runtimes.

A pressing challenge in the cost of quantum simulation for large molecular systems is the rapid growth in the number of four-index two-electron integrals. By using integral decomposition techniques in the double-factorized representation [54, 80], we simul-

taneously minimize two key parameters governing the cost of qubitization: the number of coefficients that must be loaded into the quantum computer and a certain bound α_{DF} on the spectral norm of the Hamiltonian. Compared to other simulation techniques such as Trotterization, qubitization also enables a large trade-off in non-Clifford gate count by using additional qubits. In the case of estimating an energy level to chemical accuracy, we found that our approach has a Toffoli gate cost with respect to active space size N , while keeping the number of atoms fixed, that scales like $\sim N^{3.25}$. When the number of atoms also grows with N , our technique promises a Toffoli cost scaling like $\sim \alpha_{\text{DF}} N \log(N)$, assuming the empirically fitted sparsity of double-factorization by other authors [53], and where $\alpha_{\text{DF}} \sim N^{1.5}$ based on Hydrogen chain benchmarks. When applied to structures in the catalytic cycle with 52–65 orbitals, our approach requires roughly 10^{10} – 10^{11} Toffoli gates and ~ 4000 logical qubits. Note that the benefit of our reduced Toffoli count can far outweigh the cost of using more logical qubits – the physical qubit count of the overall algorithm is typically dominated by that required for the fault-tolerant distillation of non-Clifford gates. Under realistic assumptions on the performance of mid-term quantum hardware, this corresponds to a runtime of a few weeks for a single calculation. While this seems similar to the results of our previous paper [11], we here use much more conservative and realistic estimates for the clock speeds of mid-term quantum computers, while Ref. [11] assumed ambitious specifications for the long term.

From our results it is evident that a future universal quantum computer can only lead the range of electronic structure methods if further developments provide faster algorithms that can treat much larger active spaces in order to be competitive. We emphasize that, although no logical qubit has been realized experimentally so far, a universal quantum computer that can represent a state on a few thousand logical qubits would revolutionize electronic structure theory as it bears the potential to provide an accurate exact-diagonalization energy for a moderately sized molecular system of on the order of 100 atoms in the full single-particle basis set. As a consequence, any necessarily approximate a-priori or a-posteriori correction for the nagging dynamic correlation problem (that arises solely from the choice of a reduced-dimensional active space) would no longer be needed. It is clear that such a calculation would be an ultimate goal, but also that it would present new technical challenges.

Going to an order of magnitude larger active space sizes as considered here would increase the quantum computational requirements by three orders of mag-

Table IV. Overlap $|\langle \tilde{\psi}_0 | \psi_{\text{trial}} \rangle|^2$ of the dominant single-determinant state $|\psi_{\text{trial}}\rangle$ with the approximate ground state $|\tilde{\psi}_0\rangle$ obtained with DMRG for the complexes considered in this work. The type of molecular orbital (MO) basis is given as well as the size of active space of the DMRG calculation in terms of orbitals and electrons.

Complex	MO basis	Orbitals	Electrons	$ \langle \tilde{\psi}_0 \psi_{\text{trial}} \rangle ^2$
I	CAS(4,5)SCF	52	48	0.847
II	CAS(8,6)SCF	62	70	0.848
II-III	CAS(8,6)SCF	65	74	0.848
V	CAS(12,11)SCF	60	68	0.841
VIII	CAS(2,2)SCF	65	76	0.869
VIII-IX	CAS(4,4)SCF	59	72	0.863
IX	CAS(16,16)SCF	62	68	0.807
XVIII	CAS(4,4)SCF	56	64	0.889

nitude. Hence, despite the advances reported in this work, it is obvious that further algorithmic improvements of quantum algorithms are urgently needed in order to get timings down so that a quantum computer can become superior to traditional approaches, i.e., to eventually demonstrate a quantum advantage in real-world chemistry applications. Given the innovation rate in quantum algorithms for chemistry of many orders of magnitude over the past years, we are confident for this to happen. One direction is exploring novel sparse representations. Another promising avenue is exploiting the fact that the number of electrons may grow much smaller than the size of the single-particle basis set when expanding the latter to incorporate dynamical correlations. That can lead to significant savings compared to the algorithms presented here.

VIII. COMMENTS ON THE INTEGRAL FILES

The integral files used in this work are available upon request from the corresponding author and will

be made publicly available upon publication.

ACKNOWLEDGMENTS

We are grateful to Markus Hölscher for valuable discussions on the catalyst synthesized in the Leitner lab and for providing us with the correct structure of complex I and to Ali Alavi for sharing his insights into the FCIQMC algorithm with us. VvB and MR gratefully acknowledge financial support by the Swiss National Science Foundation (project no. 200021 182400). We also thank Dominic Berry, Garnet Chan, Joonho Lee, Hongbin Liu, and Mathias Soeken for comments on the manuscript.

-
- [1] Richard P. Feynman, “Simulating physics with computers”, *Int. J. Theor. Phys.* **21**, 467–488 (1982).
- [2] Krysta M. Svore and Matthias Troyer, “The quantum future of computation”, *IEEE Computer* **49**, 21–30 (2016).
- [3] Yudong Cao, Jonathan Romero, Jonathan P. Olson, Matthias Degroote, Peter D. Johnson, Mária Kieferová, Ian D. Kivlichan, Tim Menke, Borja Peropadre, Nicolas P. D. Sawaya, Sukin Sim, Libor Veis, and Alán Aspuru-Guzik, “Quantum Chemistry in the Age of Quantum Computing”, *Chem. Rev.* **119**, 10856–10915 (2019).
- [4] Sam McArdle, Suguru Endo, Alán Aspuru-Guzik, Simon C. Benjamin, and Xiao Yuan, “Quantum computational chemistry”, *Rev. Mod. Phys.* **92**, 015003 (2020).
- [5] Daniel S. Abrams and Seth Lloyd, “Simulation of Many-Body Fermi Systems on a Universal Quantum Computer”, *Phys. Rev. Lett.* **79**, 2586–2589 (1997).
- [6] Alán Aspuru-Guzik, Anthony D. Dutoi, Peter J. Love, and Martin Head-Gordon, “Simulated Quantum Computation of Molecular Energies”, *Science* **309**, 1704–1707 (2005).

- [7] Libor Veis and Jiří Pittner, “Quantum computing applied to calculations of molecular energies: CH2 benchmark”, *J. Chem. Phys.* **133**, 194106 (2010).
- [8] Libor Veis, Jakub Višňák, Timo Fleig, Stefan Knecht, Trond Saue, Lucas Visscher, and Jiří Pittner, “Relativistic quantum chemistry on quantum computers”, *Phys. Rev. A* **85**, 030304 (2012).
- [9] Libor Veis and Jiří Pittner, “Quantum Computing Approach to Nonrelativistic and Relativistic Molecular Energy Calculations”, in *Quantum Information and Computation for Chemistry* (John Wiley & Sons, Ltd, 2014) pp. 107–136.
- [10] Katherine Bourzac, “Chemistry is quantum computing’s killer app”, *C&EN* **95**, 27–31 (2017).
- [11] Markus Reiher, Nathan Wiebe, Krysta M. Svore, Dave Wecker, and Matthias Troyer, “Elucidating reaction mechanisms on quantum computers”, *PNAS* **114**, 7555–7560 (2017).
- [12] Steven R. White, “Density matrix formulation for quantum renormalization groups”, *Phys. Rev. Lett.* **69**, 2863–2866 (1992).
- [13] Alberto Baiardi and Markus Reiher, “The Density Matrix Renormalization Group in Chemistry and Molecular Physics: Recent Developments and New Challenges”, *J. Chem. Phys.* **152**, 040903 (2020).
- [14] George H. Booth, Alex J. W. Thom, and Ali Alavi, “Fermion Monte Carlo without fixed nodes: A game of life, death, and annihilation in Slater determinant space”, *J. Chem. Phys.* **131**, 054106 (2009).
- [15] Guang Hao Low and Isaac L. Chuang, “Hamiltonian simulation by qubitization”, *Quantum* **3**, 163 (2019).
- [16] Guang Hao Low and Isaac L. Chuang, “Optimal Hamiltonian Simulation by Quantum Signal Processing”, *Phys. Rev. Lett.* **118**, 010501 (2017).
- [17] Jeongwan Haah, Matthew Hastings, Robin Kothari, and Guang Hao Low, “Quantum Algorithm for Simulating Real Time Evolution of Lattice Hamiltonians”, in *2018 IEEE 59th Annual Symposium on Foundations of Computer Science (FOCS)*, FOCS ’18 (IEEE, Washington, DC, USA, 2018) pp. 350–360.
- [18] Guang Hao Low and Nathan Wiebe, “Hamiltonian Simulation in the Interaction Picture”, [arXiv preprint arXiv:1805.00675](https://arxiv.org/abs/1805.00675) (2018).
- [19] Andrew M Childs, Yuan Su, Minh C Tran, Nathan Wiebe, and Shuchen Zhu, “A theory of trotter error”, [arXiv preprint arXiv:1913.08854](https://arxiv.org/abs/1913.08854) (2020).
- [20] Ryan Babbush, Craig Gidney, Dominic W. Berry, Nathan Wiebe, Jarrod McClean, Alexandru Paler, Austin Fowler, and Hartmut Neven, “Encoding electronic spectra in quantum circuits with linear T complexity”, *Phys. Rev. X* **8**, 041015 (2018).
- [21] Guang Hao Low, Vadym Kliuchnikov, and Luke Schaeffer, “Trading T-gates for dirty qubits in state preparation and unitary synthesis”, [arXiv preprint arXiv:1812.00954](https://arxiv.org/abs/1812.00954) (2018).
- [22] Dominic W. Berry, Craig Gidney, Mario Motta, Jarrod R. McClean, and Ryan Babbush, “Qubitization of Arbitrary Basis Quantum Chemistry Leveraging Sparsity and Low Rank Factorization”, [arXiv preprint arXiv:1902.02134](https://arxiv.org/abs/1902.02134) (2019).
- [23] Cameron Hepburn, Ella Adlen, John Beddington, Emily A. Carter, Sabine Fuss, Niall Mac Dowell, Jan C. Minx, Pete Smith, and Charlotte K. Williams, “The technological and economic prospects for CO₂ utilization and removal”, *Nature* **575**, 87–97 (2019).
- [24] Yueshen Wu, Zhan Jiang, Xu Lu, Yongye Liang, and Hailiang Wang, “Domino electroreduction of CO₂ to methanol on a molecular catalyst”, *Nature* **575**, 639–642 (2019).
- [25] Fengwang Li, Arnaud Thevenon, Alonso Rosas-Hernández, Ziyun Wang, Yilin Li, Christine M. Gabardo, Adnan Ozden, Cao Thang Dinh, Jun Li, Yuhang Wang, Jonathan P. Edwards, Yi Xu, Christopher McCallum, Lizhi Tao, Zhi-Qin Liang, Mingchuan Luo, Xue Wang, Huihui Li, Colin P. O’Brien, Chih-Shan Tan, Dae-Hyun Nam, Rafael Quintero-Bermudez, Tao-Tao Zhuang, Yuguang C. Li, Zhiji Han, R. David Britt, David Sinton, Theodor Agapie, Jonas C. Peters, and Edward H. Sargent, “Molecular tuning of CO₂-to-ethylene conversion”, *Nature* **577**, 509–513 (2020).
- [26] Sayan Kar, Jotheeswari Kothandaraman, Alain Goeppert, and G. K. Surya Prakash, “Advances in catalytic homogeneous hydrogenation of carbon dioxide to methanol”, *J. CO₂ Util.* **23**, 212–218 (2018).
- [27] Sebastian Wesselbaum, Verena Moha, Markus Meuresch, Sandra Brosinski, Katharina M. Thener, Jens Kothe, Thorsten vom Stein, Ulli Englert, Markus Hölscher, Jürgen Klankermayer, and Walter Leitner, “Hydrogenation of carbon dioxide to methanol using a homogeneous ruthenium–Triphos catalyst: From mechanistic investigations to multiphase catalysis”, *Chem. Sci.* **6**, 693–704 (2015).
- [28] Aron J. Cohen, Paula Mori-Sánchez, and Weitao Yang, “Challenges for Density Functional Theory”, *Chem. Rev.* **112**, 289–320 (2012).
- [29] Narbe Mardirossian and Martin Head-Gordon, “Thirty years of density functional theory in computational chemistry: An overview and extensive assessment of 200 density functionals”, *Mol. Phys.* **115**, 2315–2372 (2017).
- [30] Thomas Weymuth, Erik P. A. Couzijn, Peter Chen, and Markus Reiher, “New Benchmark Set of Transition-Metal Coordination Reactions for the Assessment of Density Functionals”, *J. Chem. Theory Comput.* **10**, 3092–3103 (2014).
- [31] Gregor N. Simm and Markus Reiher, “Systematic Error Estimation for Chemical Reaction Energies”, *J. Chem. Theory Comput.* **12**, 2762–2773 (2016).
- [32] Tamara Husch, Leon Freitag, and Markus Reiher, “Calculation of Ligand Dissociation Energies in Large Transition-Metal Complexes”, *J. Chem. Theory Comput.* **14**, 2456–2468 (2018).
- [33] Yan Zhao and Donald G. Truhlar, “A new local density functional for main-group thermochemistry, transition metal bonding, thermochemical kinetics, and noncovalent interactions”, *J. Chem. Phys.* **125**, 194101 (2006).

- [34] John P. Perdew, Kieron Burke, and Matthias Ernzerhof, “Generalized Gradient Approximation Made Simple”, *Phys. Rev. Lett.* **77**, 3865–3868 (1996).
- [35] John P. Perdew, Matthias Ernzerhof, and Kieron Burke, “Rationale for mixing exact exchange with density functional approximations”, *J. Chem. Phys.* **105**, 9982–9985 (1996).
- [36] Christopher J. Cramer, *Essentials of Computational Chemistry: Theories and Models*, 2nd ed. (Wiley, Chichester, 2006).
- [37] Frank Jensen, *Introduction to Computational Chemistry* (Wiley, 2007).
- [38] Gregor N. Simm, Alain C. Vaucher, and Markus Reiher, “Exploration of Reaction Pathways and Chemical Transformation Networks”, *J. Phys. Chem. A* **123**, 385–399 (2019).
- [39] Qianli Ma and Hans-Joachim Werner, “Explicitly correlated local coupled-cluster methods using pair natural orbitals”, *Wiley Interdiscip. Rev. Comput. Mol. Sci.*, e1371 (2018).
- [40] Ignacio Fdez. Galván, Morgane Vacher, Ali Alavi, Celestino Angeli, Francesco Aquilante, Jochen Autschbach, Jie J. Bao, Sergey I. Bokarev, Nikolay A. Bogdanov, Rebecca K. Carlson, Liviu F. Chibotaru, Joel Creutzberg, Nike Dattani, Mickaël G. Delcey, Sijia S. Dong, Andreas Dreuw, Leon Freitag, Luis Manuel Frutos, Laura Gagliardi, Frédéric Gendron, Angelo Giussani, Leticia González, Gilbert Grell, Meiyuan Guo, Chad E. Hoyer, Marcus Johansson, Sebastian Keller, Stefan Knecht, Goran Kovačević, Erik Källman, Giovanni Li Manni, Marcus Lundberg, Yingjin Ma, Sebastian Mai, João Pedro Malhado, Per Åke Malmqvist, Philipp Marquetand, Stefanie A. Mewes, Jesper Norell, Massimo Olivucci, Markus Oppel, Quan Manh Phung, Kristine Pierloot, Felix Plasser, Markus Reiher, Andrew M. Sand, Igor Schapiro, Prachi Sharma, Christopher J. Stein, Lasse Kragh Sørensen, Donald G. Truhlar, Mihkel Ugandi, Liviu Ungur, Alessio Valentini, Steven Vancoillie, Valera Veryazov, Oskar Weser, Tomasz A. Wesolowski, Per-Olof Widmark, Sebastian Wouters, Alexander Zech, J. Patrick Zobel, and Roland Lindh, “OpenMolcas: From Source Code to Insight”, *J. Chem. Theory Comput.* **15**, 11 (2019).
- [41] Konstantinos D. Vogiatzis, Dongxia Ma, Jeppe Olsen, Laura Gagliardi, and Wibe A. de Jong, “Pushing configuration-interaction to the limit: Towards massively parallel MCSCF calculations”, *J. Chem. Phys.* **147**, 184111 (2017).
- [42] Björn O. Roos, Peter R. Taylor, and Per E. M. Siegbahn, “A complete active space SCF method (CASSCF) using a density matrix formulated super-CI approach”, *Chem. Phys.* **48**, 157–173 (1980).
- [43] Klaus Ruedenberg, Michael W. Schmidt, Mary M. Gilbert, and S. T. Elbert, “Are atoms intrinsic to molecular electronic wavefunctions? I. The FORS model”, *Chem. Phys.* **71**, 41–49 (1982).
- [44] Sebastian Keller, Katharina Boguslawski, Tomasz Janowski, Markus Reiher, and Peter Pulay, “Selection of active spaces for multiconfigurational wavefunctions”, *J. Chem. Phys.* **142**, 244104 (2015).
- [45] Christopher J. Stein and Markus Reiher, “Automated Selection of Active Orbital Spaces”, *J. Chem. Theory Comput.* **12**, 1760–1771 (2016).
- [46] Christopher J. Stein, Vera von Burg, and Markus Reiher, “The Delicate Balance of Static and Dynamic Electron Correlation”, *J. Chem. Theory Comput.* **12**, 3764–3773 (2016).
- [47] Christopher J. Stein and Markus Reiher, “autoCAS: A Program for Fully Automated Multiconfigurational Calculations”, *J. Comput. Chem.* **40**, 2216–2226 (2019).
- [48] Leticia González and Roland Lindh, *Quantum Chemistry and Dynamics of Excited States: Methods and Applications*. (John Wiley, 2020).
- [49] Emmanuel Fromager, Julien Toulouse, and Hans Jørgen Aa. Jensen, “On the universality of the long-/short-range separation in multiconfigurational density-functional theory”, *J. Chem. Phys.* **126**, 074111 (2007).
- [50] Erik Donovan Hedegård, Stefan Knecht, Jesper Skau Kielberg, Hans Jørgen Aagaard Jensen, and Markus Reiher, “Density matrix renormalization group with efficient dynamical electron correlation through range separation”, *J. Chem. Phys.* **142**, 224108 (2015).
- [51] Erik Donovan Hedegård, Julien Toulouse, and Hans Jørgen Aagaard Jensen, “Multiconfigurational short-range density-functional theory for open-shell systems”, *J. Chem. Phys.* **148**, 214103 (2018).
- [52] Hongjun Luo and Ali Alavi, “Combining the Transcorrelated Method with Full Configuration Interaction Quantum Monte Carlo: Application to the Homogeneous Electron Gas”, *J. Chem. Theory Comput.* **14**, 1403–1411 (2018).
- [53] Bo Peng and Karol Kowalski, “Highly efficient and scalable compound decomposition of two-electron integral tensor and its application in coupled cluster calculations”, *J. Chem. Theory Comput.* **13**, 4179–4192 (2017).
- [54] Francesco Aquilante, Linus Boman, Jonas Boström, Henrik Koch, Roland Lindh, Alfredo Sánchez de Merás, and Thomas Bondo Pedersen, “Cholesky Decomposition Techniques in Electronic Structure Theory”, in *Linear-Scaling Techniques in Computational Chemistry and Physics: Methods and Applications*, Challenges and Advances in Computational Chemistry and Physics, edited by Robert Zalesny, Manthos G. Papadopoulos, Paul G. Mezey, and Jerzy Leszczynski (Springer Netherlands, Dordrecht, 2011) pp. 301–343.
- [55] Alberto Peruzzo, Jarrod McClean, Peter Shadbolt, Man-Hong Yung, Xiao-Qi Zhou, Peter J. Love, Alán Aspuru-Guzik, and Jeremy L. O’Brien, “A variational eigenvalue solver on a photonic quantum processor”, *Nat Commun* **5**, 1–7 (2014).
- [56] Harper R. Grimsley, Sophia E. Economou, Edwin Barnes, and Nicholas J. Mayhall, “An adaptive variational algorithm for exact molecular simulations on a quantum computer”, *Nat Commun* **10**, 1–9 (2019).

- [57] John Preskill, “Quantum Computing in the NISQ era and beyond”, *Quantum* **2**, 79 (2018).
- [58] Michael Kühn, Sebastian Zanker, Peter Deglmann, Michael Marthaler, and Horst Weiß, “Accuracy and Resource Estimations for Quantum Chemistry on a Near-Term Quantum Computer”, *J. Chem. Theory Comput.* **15**, 4764–4780 (2019).
- [59] Dave Wecker, Matthew B. Hastings, and Matthias Troyer, “Progress towards practical quantum variational algorithms”, *Phys. Rev. A* **92**, 042303 (2015).
- [60] Nathan Wiebe and Chris Granade, “Efficient bayesian phase estimation”, *Phys. Rev. Lett.* **117**, 010503 (2016).
- [61] Michael A. Nielsen and Isaac L. Chuang, *Quantum Computation and Quantum Information*, 1st ed. (Cambridge University Press, 2004).
- [62] Wojciech Górecki, Rafał Demkowicz-Dobrzański, Howard M. Wiseman, and Dominic W. Berry, “ π -corrected heisenberg limit”, *Phys. Rev. Lett.* **124**, 030501 (2020).
- [63] Dave Wecker, Matthew B. Hastings, Nathan Wiebe, Bryan K. Clark, Chetan Nayak, and Matthias Troyer, “Solving strongly correlated electron models on a quantum computer”, *Phys. Rev. A* **92**, 062318 (2015).
- [64] Masuo Suzuki, “Fractal decomposition of exponential operators with applications to many-body theories and Monte Carlo simulations”, *Phys. Lett. A* **146**, 319–323 (1990).
- [65] Guang Hao Low, “Hamiltonian simulation with nearly optimal dependence on spectral norm”, in *Proceedings of the 51st Annual ACM Symposium on Theory of Computing - STOC '19* (ACM Press, New York, New York, USA, 2019) pp. 491–502.
- [66] Andrew M Childs and Nathan Wiebe, “Hamiltonian Simulation Using Linear Combinations of Unitary Operations”, *Quantum Inf Comput* **12**, 901–924 (2012).
- [67] Markus Reiher and Alexander Wolf, *Relativistic Quantum Chemistry: The Fundamental Theory of Molecular Science*, 2nd ed. (Wiley-VCH, Weinheim, 2015).
- [68] David Poulin, Alexei Kitaev, Damian S. Steiger, Matthew B. Hastings, and Matthias Troyer, “Quantum algorithm for spectral measurement with a lower gate count”, *Phys. Rev. Lett.* **121**, 010501 (2018).
- [69] Dominic W. Berry, Mária Kieferová, Artur Scherer, Yuval R. Sanders, Guang Hao Low, Nathan Wiebe, Craig Gidney, and Ryan Babbush, “Improved techniques for preparing eigenstates of fermionic Hamiltonians”, *npj Quantum Inf* **4**, 22 (2018).
- [70] Dmitri Maslov, “Optimal and asymptotically optimal NCT reversible circuits by the gate types”, *Quantum Information and Computation* **16**, 1096–1112 (2016).
- [71] Craig Gidney and Austin G. Fowler, “Efficient magic state factories with a catalyzed $|CCZ\rangle$ to $2|T\rangle$ transformation”, *Quantum* **3**, 135 (2019).
- [72] David Poulin, Matthew B. Hastings, Dave Wecker, Nathan Wiebe, Andrew C. Doberty, and Matthias Troyer, “The trotter step size required for accurate quantum simulation of quantum chemistry”, *Quantum Info. Comput.* **15**, 361–384 (2015).
- [73] Mario Motta, Erika Ye, Jarrod R. McClean, Zhen-dong Li, Austin J. Minnich, Ryan Babbush, and Garnet Kin-Lic Chan, “Low rank representations for quantum simulation of electronic structure”, *arXiv preprint arXiv:1808.02625* (2018).
- [74] Mario Motta, James Shee, Shiwei Zhang, and Garnet Kin-Lic Chan, “Efficient ab initio auxiliary-field quantum monte carlo calculations in gaussian bases via low-rank tensor decomposition”, *J. Chem. Theory Comput.* **15**, 3510–3521 (2019), pMID: 31091103.
- [75] Dominic W. Berry, Andrew M. Childs, Richard Cleve, Robin Kothari, and Rolando D. Somma, “Simulating Hamiltonian dynamics with a truncated Taylor series”, *Phys. Rev. Lett.* **114**, 090502 (2015).
- [76] Austin G. Fowler, Matteo Mariantoni, John M. Martinis, and Andrew N. Cleland, “Surface codes: Towards practical large-scale quantum computation”, *Phys. Rev. A* **86**, 032324 (2012).
- [77] Paul Pham and Krysta M. Svore, “A 2D nearest-neighbor quantum architecture for factoring in polylogarithmic depth”, *Quantum Info. Comput.* **13**, 937–962 (2013).
- [78] Katharina Boguslawski, Konrad H. Marti, and Markus Reiher, “Construction of CASCI-type wave functions for very large active spaces”, *J. Chem. Phys.* **134**, 224101 (2011).
- [79] Norm M. Tubman, Carlos Mejuto-Zaera, Jeffrey M. Epstein, Diptarka Hait, Daniel S. Levine, William Huggins, Zhang Jiang, Jarrod R. McClean, Ryan Babbush, Martin Head-Gordon, and K. Birgitta Whaley, “Postponing the orthogonality catastrophe: efficient state preparation for electronic structure simulations on quantum devices”, *arXiv preprint arXiv:1809.05523* (2018).
- [80] Nelson H. F. Beebe and Jan Linderberg, “Simplifications in the generation and transformation of two-electron integrals in molecular calculations”, *Int. J. Quantum Chem.* **12**, 683–705 (1977).

Supplementary Material for *Quantum Computing Enhanced Computational Catalysis*

Vera von Burg,¹ Guang Hao Low,² Thomas Häner,³ Damian S. Steiger,³
Markus Reiher,¹ Martin Roetteler,² and Matthias Troyer²

¹*Laboratorium für Physikalische Chemie, ETH Zürich,
Vladimir-Prelog-Weg 2, 8093 Zürich, Switzerland*

²*Microsoft Quantum, Redmond, Washington 98052, USA*

³*Microsoft Quantum, 8038 Zürich, Switzerland*

(Dated: February 2, 2022)

CONTENTS

I. General notes on the [Ru] catalyst	4
II. DFT calculations	4
A. Single-point M06-L energies for small molecules	4
B. Single-point PBE and PBE0 electronic energies and PBE electronic energies for fully optimized structures	5
III. HF and post-HF calculations	7
A. HF, CASSCF, and DMRG-CI electronic energies	8
B. DMRG-CI electronic energies of linear chains of Hydrogen atoms, II-III, and IX for two-electron integrals at different truncation levels	11
C. General procedure for the selection of molecular orbitals for the integral files	18
IV. Overview of the integral files	18
V. Graphical representation of active orbitals chosen for integral files	21
A. CAS(4,5)SCF active molecular orbitals chosen for integral files of stable intermediate I	21
B. CAS(8,6)SCF active molecular orbitals chosen for integral files of stable intermediate II	22
C. CAS(8,6)SCF active molecular orbitals chosen for integral files of transition state II-III	23
D. CAS(12,11)SCF active molecular orbitals chosen for integral files of stable intermediate V	24
E. CAS(2,2)SCF active molecular orbitals chosen for integral files of stable intermediate VIII	25
F. CAS(4,4)SCF active molecular orbitals chosen for integral files of transition state VIII-IX	26
G. CAS(16,16)SCF active molecular orbitals chosen for integral files of stable intermediate IX	27
H. CAS(4,4)SCF active molecular orbitals chosen for integral files of stable intermediate XVIII	28
VI. Resource analysis	29
A. Product formula and low-rank factorization of the Hamiltonian	29
B. Results	30
VII. Qubitization of double-factorized Hamiltonian	38
A. Standard quantum circuit primitives	38
1. Data-lookup oracle	40
2. State preparation unitary	41
3. Block-encoding framework	44
4. Qubitization	45
B. New quantum circuit primitives	45
1. Programmable rotation gate array	45

2. Multiplexed sparse data-lookup	47
C. Double-factorized Hamiltonian	49
1. Block-encoded, basis-transformed Majorana operator	51
2. Block-encoded product of Majorana operators	52
3. Block-encoded one-electron operator and its square	54
4. Block-encoded two-electron operator	56
5. Asymptotic costs	58
VIII. Matrix Schatten and entrywise 1-norm	59
IX. M06-L/def2-SVP optimized Cartesian coordinates for stable intermediate I	60
X. PBE/def2-TZVP optimized Cartesian coordinates of intermediates and transition states	63
A. Stable intermediate I	63
B. Stable intermediate II	65
C. Transition state II-III	67
D. Stable intermediate V	69
E. Stable intermediate VIII	72
F. Transition state VIII-IX	74
G. Stable intermediate IX	76
H. Stable intermediate XVIII	78
References	81

I. GENERAL NOTES ON THE [RU] CATALYST

We chose seven key intermediates and transition states from the supporting information of Wesselbaum et al. [1], therein labeled as complex structures II, II-III, V, VIII, VIII-IX, IX, and XVIII. These structures had been optimized with the M06-L/def2-SVP combination of exchange-correlation density functional and basis set, and single-point M06-L/def2-TZVP energies were obtained [1] which we used for the diagram in the main text. In this work, we continue to use the roman numerals as labels. Hyphenated labels (i.e., II-III and VIII-IX) correspond to transition states whereas the others are stable intermediates. The Cartesian coordinates of intermediate I were erroneous in the supporting information of the original paper and we obtained the correct ones through a private communication [2] (see [Section IX](#)). All of the complexes are monocations and were considered in the lowest-energy singlet state.

II. DFT CALCULATIONS

To be able to obtain relative reaction energies (see [Table II](#)), we optimized the small molecules CO₂, H₂, H₂O, THF, and methanol with GAUSSIAN09, revision D.01 including density fitting and the *UltraFine* keyword for the integration grid in accordance with the supporting information of Ref. [1]. For all other density functional theory (DFT) calculations reported herein we employed TURBOMOLE [3], version 7.0.2. We then carried out single-point, unrestricted PBE [4] and PBE0 [5] calculations in the def2-TZVP [6] basis for each complex and the small molecules on the M06-L/def2-SVP structures reported in the supporting information of Ref. [1] or the newly obtained ones in the case of the small molecules, respectively. To ensure that we obtained the correct global minima in the molecular orbital coefficient parameter space, we perturbed the α and β orbitals of the converged calculation with the orbital steering protocol of Ref. [7]. We repeated the respective calculation with the perturbed orbitals as starting orbitals to probe whether a solution of lower energy could be obtained.

We additionally optimized the structures with the PBE/def2-TZVP combination of density functional and basis set and carried out frequency calculations to ensure we had obtained the correct type of stationary points (no imaginary frequencies for intermediates, one for transition states).

A. Single-point M06-L energies for small molecules

For comparison, we report here the M06-L/def2-SVP electronic energies for the small molecules which we re-optimized.

Table I. M06-L/def2-SVP electronic energies for the optimized structures given in Hartree atomic units.

Compound	$E_{\text{M06-L}}^{\text{el}}$
H ₂	-1.16721
H ₂ O	-76.35053
CO ₂	-188.43534
CH ₃ OH	-115.61382
THF	-232.24308

B. Single-point PBE and PBE0 electronic energies and PBE electronic energies for fully optimized structures

The electronic energies of the unrestricted, single-point PBE/def2-TZVP and PBE0/def2-TZVP DFT calculations for the complexes and remaining compounds as well as the relative reaction energies of the complexes are collected in [Table III](#) and the ones of the re-optimized structures in [Table IV](#). The relative reaction energies reported in these Tables were obtained in accordance with the supporting information of Ref. [1] and their formulaic calculation is given in [Table II](#). We employ the double slash notation where the labels before the double slash denote the combination of exchange-correlation functional and basis set for the single-point calculation whereas the exchange-density functional and basis set employed for the structure optimization is given after the double slash.

Table II. Formulae for the calculation of relative reaction energies $\Delta E_{\text{rel}}^{\text{el}}$ for the complexes, where $E^{\text{el}}(i)$ is the electronic energy of compound i computed with a certain combination of exchange-correlation density functional and basis set.

Complex	Calculation of $\Delta E_{\text{rel}}^{\text{el}}$
I	0.0
II	$E^{\text{el}}(\text{II}) + E^{\text{el}}(\text{THF}) - E^{\text{el}}(\text{I}) - E^{\text{el}}(\text{CO}_2)$
II-III	$E^{\text{el}}(\text{II-III}) + E^{\text{el}}(\text{THF}) - E^{\text{el}}(\text{I}) - E^{\text{el}}(\text{CO}_2)$
V	$E^{\text{el}}(\text{V}) + E^{\text{el}}(\text{H}_2) - E^{\text{el}}(\text{I}) - E^{\text{el}}(\text{CO}_2)$
VIII	$E^{\text{el}}(\text{VIII}) + E^{\text{el}}(\text{THF}) - E^{\text{el}}(\text{H}_2) - E^{\text{el}}(\text{I}) - E^{\text{el}}(\text{CO}_2)$
VIII-IX	$E^{\text{el}}(\text{VIII-IX}) + E^{\text{el}}(\text{THF}) - E^{\text{el}}(\text{I}) - E^{\text{el}}(\text{CO}_2)$
IX	$E^{\text{el}}(\text{IX}) + E^{\text{el}}(\text{THF}) - E^{\text{el}}(\text{I}) - E^{\text{el}}(\text{CO}_2)$
XVIII	$E^{\text{el}}(\text{XVIII}) + E^{\text{el}}(\text{H}_2\text{O}) - 2 \cdot E^{\text{el}}(\text{H}_2) - E^{\text{el}}(\text{I}) - E^{\text{el}}(\text{CO}_2)$

Table III. PBE/def2-TZVP//M06-L/def2-SVP and PBE0/def2-TZVP//M06-L/def2-SVP electronic single-point energies E^{el} and relative reaction energies $\Delta E_{\text{rel}}^{\text{el}}$ given in Hartree atomic units.

Compound	$E_{\text{PBE}}^{\text{el}}$	$\Delta E_{\text{rel}}^{\text{el,PBE}}$	$E_{\text{PBE0}}^{\text{el}}$	$\Delta E_{\text{rel}}^{\text{el,PBE0}}$
I	-2936.85035	0.0	-2937.09522	0.0
II	-2893.07375	0.01824933	-2893.27797	0.01845670
II-III	-2893.06593	0.02630769	-2893.26673	0.02969426
V	-3124.16485	-0.00142320	-3124.39830	-0.00479493
VIII	-2894.26852	-0.01061211	-2894.47992	-0.01533001
VIII-IX	-2893.06125	0.03075055	-2893.26757	0.02886085
IX	-2893.08016	0.01184458	-2893.28802	0.00840579
XVIII	-3051.28933	-0.00472200	-3051.53350	-0.01268354
H ₂	-1.16590	—	-1.16817	—
H ₂ O	-76.37653	—	-76.37717	—
CO ₂	-188.47898	—	-188.46644	—
CH ₃ OH	-115.62907	—	-115.63697	—
THF	-232.23733	—	-232.26523	—

Table IV. PBE/def2-TZVP//PBE/def2-TZVP electronic energies $E^{\text{el,opt}}$ after structure optimization and corresponding relative reaction energies $\Delta E_{\text{rel}}^{\text{el,opt}}$ given in Hartree atomic units.

Compound	$E_{\text{PBE}}^{\text{el,opt}}$	$\Delta E_{\text{rel}}^{\text{el,PBE,opt}}$
I	-2936.85482	0.0
II	-2893.07854	0.01743994
II-III	-2893.06962	0.02635768
V	-3124.17151	-0.00331186
VIII	-2894.27315	-0.01126172
VIII-IX	-2893.06751	0.02846465
IX	-2893.08609	0.00988447
XVIII	-3051.29506	-0.00590696
H ₂	-1.16591	—
H ₂ O	-76.37676	—
CO ₂	-188.47928	—
CH ₃ OH	-115.62962	—
THF	-232.23812	—

III. HF AND POST-HF CALCULATIONS

We obtained Hartree-Fock (HF) and Complete Active Space Self-Consistent Field (CAS-SCF) [8–11] molecular orbitals (MOs) in an ANO-RCC-VTZP [12, 13] atomic orbital (AO) basis for the light elements and ANO-RCC-VQZP [14] for Ruthenium with OPENMOL-CAS [15]. We employed a Cholesky Decomposition (CD) of the two-electron repulsion integrals and generated two sets of integrals with decomposition thresholds of 10^{-4} and 10^{-8} , respectively (note that this decomposition which occurs during the quantum chemical calculations is separate from a later truncation of the two-electron integrals in the context of the quantum computing algorithms). To distinguish the two sets of integrals, those that were obtained with a threshold of 10^{-8} are labeled as “highCD” (e.g., I-highCD-cas5-fb-48e52o). We observed that the choice of this threshold has a negligible effect on the resource estimates, as seen in Tables XXII and XXIII. The choices for the molecular and atomic orbital bases in this study are summarized in Table V.

We performed exploratory calculations in a so-called minimal basis (mb) (ANO-RCC-MB [12–14] for this study). For quantitative results, it is necessary to employ a much larger AO basis, in this study, the ANO-RCC-VTZP for light elements and ANO-RCC-VQZP for Ruthenium, which we will term the full atomic orbital basis (fb). Table VI lists the number of one-electron basis functions resulting from the choice of these bases for each complex. Note that the number of MOs equals the number of AOs and the numbers in Table VI therefore apply to both types of one-electron basis sets.

The MOs are generally labeled by the type of method with which they have been obtained, i.e. HF and CASSCF. When necessary, the active space employed in the CASSCF calculation is given explicitly through the notation (N,L) (e.g., CAS(6,6)SCF), where N is the number of electrons and L the number of orbitals in the active space.

Table V. Overview of different types of one-electron basis sets employed in this study.

Basis	Basis set	Comment
Atomic orbitals	ANO-RCC-MB	Abbreviation: mb
	ANO-RCC-VTZP for light elements } ANO-RCC-VQZP for Ruthenium }	Abbreviation: fb
Molecular orbitals	HF	
	CAS(N,L)SCF	(N,L): Active space of N electrons in L orbitals

Table VI. Number of one-electron basis functions for each complex for the two choices of atomic orbital bases. ‘mb’ and ‘fb’ denote the minimal and full atomic orbital basis, respectively, as described in the text and in [Table V](#).

Complex	Number of basis functions	
	mb	fb
I	334	2286
II	316	2114
II-III	316	2114
V	347	2348
VIII	318	2142
VIII-IX	316	2114
IX	316	2114
XVIII	346	2374

A. HF, CASSCF, and DMRG-CI electronic energies

The CASSCF molecular orbitals from calculations with a Cholesky Decomposition threshold of the two-electron integrals of 10^{-4} were obtained in the following manner: HF orbitals in the ANO-RCC-MB atomic orbital basis were split-localized [16] with the Pipek-Mezey method [17]. From these localized orbitals, we selected the orbitals corresponding to the $4d$ orbitals of Ruthenium, the $2p$ and $2s$ orbitals of Oxygen and Carbon atoms (i.e. the bonding and antibonding π orbitals of carbon dioxide and derivatives), the bonding and antibonding σ orbitals of H_2 as well as the s -orbitals of Hydrogen atoms to evaluate their orbital entanglement and pair-orbital mutual information in an approximate Density Matrix Renormalization Group-Configuration Interaction (DMRG-CI) calculation with maximum bond order $m = 800$ and $n = 5$ with the QCMAQUIS [18] program. We selected the orbitals corresponding to a threshold in AUTOCAS [19, 20] as the active space for a subsequent CASSCF calculation. We repeated the approximate DMRG calculation on these new CASSCF orbitals and chose those orbitals selected by the AUTOCAS program as the final active orbital space. We then expanded these orbitals to the full atomic orbital basis with the EXPBAS module of OPENMOLCAS and re-optimized them in a final CASSCF calculation. For the calculations involving a Cholesky Decomposition threshold of 10^{-8} , we started the CASSCF calculations directly from the corresponding CASSCF orbital file of the calculations with a threshold of 10^{-4} to save computational resources.

The one- and two-electron integrals of a subset of these orbitals then served as parameters for the Coulomb Hamiltonian, for which the quantum-algorithm resource estimates were obtained. The general procedure for the selection of these active spaces is detailed in [Section III C](#) whereas the molecular orbitals resulting from this selection for each complex are reproduced in [Section V](#).

For each structure, we additionally carried out DMRG-Configuration-Interaction (CI) calculations of the orbitals corresponding to the integral file with the largest active space in order to gain qualitative information about the electronic structure. These calculations were performed with a number of sweeps $n = 10$ and a maximum bond dimension

Table VII. HF, CAS(N_c, L_c)SCF, and DMRG(N_d, L_d)CI electronic energies in Hartree for the complexes in the full atomic orbital basis obtained with different values of the Cholesky Decomposition threshold. (N_c, L_c) denotes the active space of the CASSCF calculations and (N_d, L_d) the one of the DMRG-CI calculations. For these, N_c and N_d refer to the number of electrons and L_c and L_d to the number of orbitals, respectively.

Complex	CD threshold	HF Energy	CAS(N_c, L_c)SCF Energy	(N_c, L_c)	DMRG(N_d, L_d)CI Energy	(N_d, L_d)
I	10^{-4}	-7361.315677	-7361.357885	(4,5)	-7361.461381	(48,52)
I	10^{-8}	—	-7361.360402	(4,5)	—	—
II	10^{-4}	-7317.956458	-7318.035225	(8,6)	-7318.123548	(70,62)
II	10^{-8}	—	-7318.037547	(8,6)	—	—
II-III	10^{-4}	-7317.931739	-7317.999907	(8,6)	-7318.099062	(74,65)
II-III	10^{-8}	—	-7318.002150	(8,6)	—	—
V	10^{-4}	-7548.043678	-7548.214683	(12,11)	-7548.296446	(68,60)
V	10^{-8}	—	-7548.217104	(12,11)	—	—
VIII	10^{-4}	-7319.116649	-7319.140267	(2,2)	-7319.234732	(76,65)
VIII	10^{-8}	—	-7319.142596	(2,2)	—	—
VIII-IX	10^{-4}	-7317.937509	-7317.971210	(4,4)	-7318.066197	(72,59)
VIII-IX	10^{-8}	—	-7317.973426	(4,4)	—	—
IX	10^{-4}	-7317.970467	-7318.209829	(16,16)	-7318.303045	(68,62)
IX	10^{-8}	—	-7318.212256	(16,16)	—	—
XVIII	10^{-4}	-7475.314796	-7475.367378	(4,4)	-7475.439228	(64,65)
XVIII	10^{-8}	—	-7475.369956	(4,4)	—	—

$m = 1000$ and Fiedler ordering and on the integral files with a CD truncation threshold of 10^{-4} . From the matrix product states generated in this way, we obtained the largest CI-coefficient through a reconstruction of an approximate CI wave function expansion through the sampling-reconstruction algorithm of Ref. [21]. For the latter algorithm, we employed a CI-threshold of 10^{-6} and a CI completeness measure of 10^{-6} . We confirmed that the choice of the CD threshold does not have a substantial influence on these overlap values as shown in Table VIII for complex IX (which features the smallest overlap of all structures).

Table VIII. Comparison of the overlap $|\langle \tilde{\psi}_0 | \psi_{\text{trial}} \rangle|^2$ of the dominant single-determinant state $|\psi_{\text{trial}}\rangle$ with the approximate ground state $|\tilde{\psi}_0\rangle$ obtained with DMRG-CI for complex IX. The active space is given by the number of electrons N and orbitals L . The maximum bond order dimension m and the number of sweeps n of the parent DMRG-CI calculation is given as well.

Catalyst structure	Active space (N, L)	CD threshold	m	n	Overlap $ \langle \tilde{\psi}_0 \psi_{\text{trial}} \rangle ^2$
IX	(68,62)	10^{-4}	500	8	0.8108
IX	(68,62)	10^{-8}	500	8	0.8107
IX	(68,62)	10^{-4}	1000	10	0.8069

The energies of the HF, CASSCF, and DMRG-CI calculations are reported in [Table VII](#). Note that no HF energies are tabulated for the calculations involving a tight Cholesky Decomposition threshold since these were started directly from the corresponding CASSCF orbital file of the calculations with the default threshold of 10^{-4} .

We studied the effect of the accuracy of the wave function on the overlap calculated after applying the reconstruction algorithm by comparing with DMRG results obtained for smaller bond dimensions and energetical orderings of the orbitals on the lattices (we refrain from reporting the explicit total energies of these calculations in order not to confuse the reader with less converged energy data). As expected, Fiedler ordering of the orbitals turned out to improve the energy by about 0.6 mHartree to 0.45 Hartree when comparing calculations with the same bond order but different orbital ordering. For our catalyst structures, changing m from a value of 500 to 1000 (with Fiedler ordering) lowers the energy by 1-2 mHartree. With respect to the question whether a bond order of 1000 is actually sufficient, we note that increasing the value of m from 1000 to 2048 leads to a change in energy of -1.7 mHartree for catalyst structure IX, whereas the overlap changes by 0.004. We therefore conclude that the convergence of the DMRG calculations beyond values of the bond dimension m chosen for this work has a negligible effect on the qualitative structure of the wave function and hence on the overlap.

B. DMRG-CI electronic energies of linear chains of Hydrogen atoms, II-III, and IX for two-electron integrals at different truncation levels

To obtain reasonable thresholds for the truncation parameters ϵ_{in} and ϵ_{co} , we carried out highly accurate DMRG calculations with QCMAQUIS on integral files where the two-electron integrals had been truncated at varying thresholds as well as the full integrals and report the resulting absolute error in the energy. We performed these calculations on linear chains of Hydrogen atoms of length 2, 4, 6, and 8 with an internuclear separation of 1.4 times the equilibrium H_2 bond distance (1.037 Å) as well as on the complexes II-III with an active space of (8,6) and IX with an active space of (16,16), respectively. For the catalyst structures, this means we employed the integral files II-III-highCD-cas6-fb-8e6o and IX-highCD-cas16-fb-16e16o of [Tables XV](#) and [XVI](#). The HF orbitals for the integrals of the linear chains of Hydrogen atoms were obtained with OPENMOLCAS in an ANO-RCC-VDZ basis. To determine the optimal parameters for these calculations, we carried out several ones at varying values of the maximum bond dimension m and number of sweeps n , the results of which are summarized in [Tables IX](#) and [X](#). The settings of the final production calculations, derived from these Tables, are given in [Table XI](#).

Table IX. DMRG(8,6)-CI energies and their convergence with respect to the bond dimension m and the number of sweeps n for catalyst structure II-III with integrals obtained with a Cholesky Decomposition threshold of 10^{-8} . The column “Energy change” collects, for each row, the difference in energy of the given calculation with respect to the energy of the calculation listed in the previous row. The final settings are a maximum bond dimension of 500 and 5 sweeps (second to last column).

Integral file	m	n	DMRG(8,6)-CI energy / Hartree	Energy change / mHartree
II-III-highCD-cas6-8e6o	10	2	-7318.000681	n.a.
II-III-highCD-cas6-8e6o	250	5	-7318.002150	-1.5
II-III-highCD-cas6-8e6o	500	5	-7318.002150	0.0
II-III-highCD-cas6-8e6o	500	10	-7318.002150	0.0

The resulting DMRG-CI electronic ground-state energies are given in [Tables XII](#) to [XIV](#).

Table X. DMRG(16,16)-CI energies and their convergence with respect to the bond dimension m and the number of sweeps n for catalyst structure IX with integrals obtained with a Cholesky Decomposition threshold of 10^{-8} . The column ‘‘Energy change’’ collects, for each row, the difference in energy of the given calculation with respect to the energy of the calculation listed in the previous row. The final settings are a maximum bond dimension of 2048 and 16 sweeps (second to last column).

Integral file	m	n	DMRG(16,16)-CI energy / Hartree	Energy change / mHartree
IX-highCD-cas16-fb-16e16o	512	8	-7318.21108886	n.a.
IX-highCD-cas16-fb-16e16o	1024	8	-7318.21198760	-0.90
IX-highCD-cas16-fb-16e16o	2048	8	-7318.21221455	-0.23
IX-highCD-cas16-fb-16e16o	2048	16	-7318.21221456	-10^{-6}
IX-highCD-cas16-fb-16e16o	4096	16	-7318.21225438	-0.04

Table XI. Summary of the parameters of the DMRG calculations performed to evaluate the error in the ground-state electronic energy due to a truncation of the two-electron integrals of the catalyst structures II-III and IX and the linear chains of Hydrogen atoms H_2 , H_4 , H_6 , and H_8 . The active space for the DMRG calculations for II-III and IX corresponds to the small and intermediate active space of the respective catalyst structure (see [Tables XV](#) and [XVI](#), the ‘highCD’ integrals) whereas for the linear chains of Hydrogen atoms, the full orbital space was employed. The maximum bond dimension and number of sweeps of the DMRG calculations are given by m and n , respectively.

System	Active electrons	Active orbitals	m	n
H_2	2	4	1000	10
H_4	4	8	1000	10
H_6	6	12	1000	10
H_8	8	16	1000	10
II-III	8	6	500	5
IX	16	16	2048	16

Table XII: DMRG-CI electronic energies in Hartree atomic units for the linear chains of Hydrogen atoms H_2 , H_4 , H_6 , and H_8 evaluated from low-rank approximations to the double-factorized Hamiltonian at two different truncation schemes. $\epsilon_{\text{in/co}}$ denotes the value of the truncation parameter ϵ of either the incoherent truncation (ϵ_{in}) of the two-electron integrals or the coherent one (ϵ_{co}). The resulting ground-state DMRG-CI energy of the integral file at a given truncation level is denoted by $E_{\text{el}}^{\text{DMRG-CI}}(\epsilon_{\text{in}})$ for the incoherent truncation scheme and $E_{\text{el}}^{\text{DMRG-CI}}(\epsilon_{\text{co}})$ for the coherent truncation scheme. The energy associated with the non-truncated integrals is given as the energy at the truncation value of 0.0 Hartree.

System	$\epsilon_{\text{in/co}}$ / Hartree	$E_{\text{el}}^{\text{DMRG-CI}}(\epsilon_{\text{in}})$ / Hartree	$E_{\text{el}}^{\text{DMRG-CI}}(\epsilon_{\text{co}})$ / Hartree	System	$\epsilon_{\text{in/co}}$ / Hartree	$E_{\text{el}}^{\text{DMRG-CI}}(\epsilon_{\text{in}})$ / Hartree	$E_{\text{el}}^{\text{DMRG-CI}}(\epsilon_{\text{co}})$ / Hartree
H_2	0.000000	-1.12158913	-1.12158913	H_4	0.000000	-2.22021372	-2.22021372
H_2	0.000001	-1.12158913	-1.12158913	H_4	0.000001	-2.22021393	-2.22021374

H ₂	0.000002	-1.12158913	-1.12158913	H ₄	0.000002	-2.22021378	-2.22021374
H ₂	0.000003	-1.12158913	-1.12158913	H ₄	0.000003	-2.22021414	-2.22021386
H ₂	0.000004	-1.12158913	-1.12158913	H ₄	0.000004	-2.22021422	-2.22021397
H ₂	0.000005	-1.12158913	-1.12158913	H ₄	0.000005	-2.22021428	-2.22021397
H ₂	0.000006	-1.12158913	-1.12158913	H ₄	0.000006	-2.22021468	-2.22021396
H ₂	0.000008	-1.12158913	-1.12158913	H ₄	0.000008	-2.22021653	-2.22021397
H ₂	0.000010	-1.12158913	-1.12158913	H ₄	0.000010	-2.22021770	-2.22021393
H ₂	0.000013	-1.12158913	-1.12158913	H ₄	0.000013	-2.22021642	-2.22021394
H ₂	0.000016	-1.12158913	-1.12158913	H ₄	0.000016	-2.22022156	-2.22021378
H ₂	0.000020	-1.12158913	-1.12158913	H ₄	0.000020	-2.22022139	-2.22021378
H ₂	0.000025	-1.12158913	-1.12158913	H ₄	0.000025	-2.22022737	-2.22021417
H ₂	0.000032	-1.12158913	-1.12158913	H ₄	0.000032	-2.22022689	-2.22021422
H ₂	0.000040	-1.12158913	-1.12158913	H ₄	0.000040	-2.22022945	-2.22021428
H ₂	0.000050	-1.12158913	-1.12158913	H ₄	0.000050	-2.22023611	-2.22021468
H ₂	0.000063	-1.12158913	-1.12158913	H ₄	0.000063	-2.22023841	-2.22021633
H ₂	0.000079	-1.12158913	-1.12158913	H ₄	0.000079	-2.22023851	-2.22021711
H ₂	0.000100	-1.12158913	-1.12158913	H ₄	0.000100	-2.22023926	-2.22021770
H ₂	0.000126	-1.12158913	-1.12158913	H ₄	0.000126	-2.22025864	-2.22021642
H ₂	0.000158	-1.12160508	-1.12158913	H ₄	0.000158	-2.22026109	-2.22021956
H ₂	0.000200	-1.12160508	-1.12158913	H ₄	0.000200	-2.22025525	-2.22022226
H ₂	0.000251	-1.12164293	-1.12158913	H ₄	0.000251	-2.22025040	-2.22022578
H ₂	0.000316	-1.12164896	-1.12160508	H ₄	0.000316	-2.22025288	-2.22022734
H ₂	0.000398	-1.12165993	-1.12160508	H ₄	0.000398	-2.22025826	-2.22022919
H ₂	0.000501	-1.12165993	-1.12160508	H ₄	0.000501	-2.22026298	-2.22022954
H ₂	0.000631	-1.12165993	-1.12164293	H ₄	0.000631	-2.22028388	-2.22023802
H ₂	0.000794	-1.12166545	-1.12164293	H ₄	0.000794	-2.22023929	-2.22023851
H ₂	0.001000	-1.12166545	-1.12164896	H ₄	0.001000	-2.22041577	-2.22023742
H ₂	0.001259	-1.12167101	-1.12164896	H ₄	0.001259	-2.22045034	-2.22025864
H ₂	0.001585	-1.12195357	-1.12165993	H ₄	0.001585	-2.22075130	-2.22026109
H ₂	0.001995	-1.12223966	-1.12165993	H ₄	0.001995	-2.22085576	-2.22025509
H ₂	0.002512	-1.12223266	-1.12165993	H ₄	0.002512	-2.22097745	-2.22025040
H ₂	0.003162	-1.12223266	-1.12166545	H ₄	0.003162	-2.22179419	-2.22025566
H ₂	0.003981	-1.12226773	-1.12166545	H ₄	0.003981	-2.22188997	-2.22025826
H ₂	0.005012	-1.12293938	-1.12167101	H ₄	0.005012	-2.22213743	-2.22029173
H ₂	0.006310	-1.12456443	-1.12167101	H ₄	0.006310	-2.22269565	-2.22028388
H ₂	0.007943	-1.12457007	-1.12195357	H ₄	0.007943	-2.22264060	-2.22030357
H ₂	0.010000	-1.12521364	-1.12194658	H ₄	0.010000	-2.22413315	-2.22024464
H ₂	0.012589	-1.12478454	-1.12223266	H ₄	0.012589	-2.22570303	-2.22041314
H ₂	0.015849	-1.12599035	-1.12226773	H ₄	0.015849	-2.22713724	-2.22055674
H ₂	0.019953	-1.12599176	-1.12293938	H ₄	0.019953	-2.22977827	-2.22075130
H ₂	0.025119	-1.12789093	-1.12293938	H ₄	0.025119	-2.23257326	-2.22085576
H ₂	0.031623	-1.13295508	-1.12456443	H ₄	0.031623	-2.23862926	-2.22097745
H ₂	0.039811	-1.13508558	-1.12457007	H ₄	0.039811	-2.25219293	-2.22172800
H ₂	0.050119	-1.15524671	-1.12521364	H ₄	0.050119	-2.26286296	-2.22184603
H ₂	0.063096	-1.15524671	-1.12478454	H ₄	0.063096	-2.26411098	-2.22280707

H ₂	0.079433	-1.16115222	-1.12478867	H ₄	0.079433	-2.27453848	-2.22285026
H ₂	0.100000	-1.16973021	-1.12599176	H ₄	0.100000	-2.28592300	-2.22277314
H ₆	0.000000	-3.32158066	-3.32158066	H ₈	0.000000	-4.34617684	-4.34617684
H ₆	0.000001	-3.32158106	-3.32158069	H ₈	0.000001	-4.34617730	-4.34617686
H ₆	0.000002	-3.32158141	-3.32158070	H ₈	0.000002	-4.34617766	-4.34617687
H ₆	0.000003	-3.32158160	-3.32158073	H ₈	0.000003	-4.34617815	-4.34617688
H ₆	0.000004	-3.32158154	-3.32158076	H ₈	0.000004	-4.34617880	-4.34617690
H ₆	0.000005	-3.32158200	-3.32158075	H ₈	0.000005	-4.34617900	-4.34617692
H ₆	0.000006	-3.32158238	-3.32158079	H ₈	0.000006	-4.34617932	-4.34617694
H ₆	0.000008	-3.32158325	-3.32158084	H ₈	0.000008	-4.34617947	-4.34617696
H ₆	0.000010	-3.32158386	-3.32158086	H ₈	0.000010	-4.34618052	-4.34617700
H ₆	0.000013	-3.32158445	-3.32158093	H ₈	0.000013	-4.34618092	-4.34617706
H ₆	0.000016	-3.32158222	-3.32158095	H ₈	0.000016	-4.34618121	-4.34617709
H ₆	0.000020	-3.32158388	-3.32158102	H ₈	0.000020	-4.34618138	-4.34617716
H ₆	0.000025	-3.32158395	-3.32158112	H ₈	0.000025	-4.34618025	-4.34617723
H ₆	0.000032	-3.32158764	-3.32158109	H ₈	0.000032	-4.34618418	-4.34617720
H ₆	0.000040	-3.32159475	-3.32158111	H ₈	0.000040	-4.34619035	-4.34617730
H ₆	0.000050	-3.32160131	-3.32158169	H ₈	0.000050	-4.34619473	-4.34617740
H ₆	0.000063	-3.32161010	-3.32158159	H ₈	0.000063	-4.34619620	-4.34617764
H ₆	0.000079	-3.32161480	-3.32158184	H ₈	0.000079	-4.34620736	-4.34617808
H ₆	0.000100	-3.32161479	-3.32158215	H ₈	0.000100	-4.34621712	-4.34617875
H ₆	0.000126	-3.32162599	-3.32158266	H ₈	0.000126	-4.34622564	-4.34617877
H ₆	0.000158	-3.32165812	-3.32158330	H ₈	0.000158	-4.34623466	-4.34617920
H ₆	0.000200	-3.32167318	-3.32158434	H ₈	0.000200	-4.34624784	-4.34617919
H ₆	0.000251	-3.32167606	-3.32158422	H ₈	0.000251	-4.34625387	-4.34617953
H ₆	0.000316	-3.32176286	-3.32158239	H ₈	0.000316	-4.34628688	-4.34618063
H ₆	0.000398	-3.32171852	-3.32158342	H ₈	0.000398	-4.34621573	-4.34618099
H ₆	0.000501	-3.32171439	-3.32158481	H ₈	0.000501	-4.34627616	-4.34618128
H ₆	0.000631	-3.32171118	-3.32158902	H ₈	0.000631	-4.34629912	-4.34618081
H ₆	0.000794	-3.32173600	-3.32159451	H ₈	0.000794	-4.34629439	-4.34618028
H ₆	0.001000	-3.32189021	-3.32160091	H ₈	0.001000	-4.34628547	-4.34618546
H ₆	0.001259	-3.32193984	-3.32160671	H ₈	0.001259	-4.34640554	-4.34619096
H ₆	0.001585	-3.32202636	-3.32161480	H ₈	0.001585	-4.34649770	-4.34619721
H ₆	0.001995	-3.32251898	-3.32161759	H ₈	0.001995	-4.34663895	-4.34620128
H ₆	0.002512	-3.32283885	-3.32162047	H ₈	0.002512	-4.34653313	-4.34621092
H ₆	0.003162	-3.32301884	-3.32165725	H ₈	0.003162	-4.34747627	-4.34621651
H ₆	0.003981	-3.32324022	-3.32167319	H ₈	0.003981	-4.34793027	-4.34622811
H ₆	0.005012	-3.32388399	-3.32167315	H ₈	0.005012	-4.34849946	-4.34623794
H ₆	0.006310	-3.32508229	-3.32171495	H ₈	0.006310	-4.34944662	-4.34625163
H ₆	0.007943	-3.32543283	-3.32172159	H ₈	0.007943	-4.34993224	-4.34625462
H ₆	0.010000	-3.32541755	-3.32171487	H ₈	0.010000	-4.34921153	-4.34629028
H ₆	0.012589	-3.32710745	-3.32173575	H ₈	0.012589	-4.35177484	-4.34621821
H ₆	0.015849	-3.33011387	-3.32174741	H ₈	0.015849	-4.35336244	-4.34625426
H ₆	0.019953	-3.33237130	-3.32180721	H ₈	0.019953	-4.35525855	-4.34629940
H ₆	0.025119	-3.33587433	-3.32193798	H ₈	0.025119	-4.35984793	-4.34629900

H ₆	0.031623	-3.33689545	-3.32205172	H ₈	0.031623	-4.36466842	-4.34629188
H ₆	0.039811	-3.34292326	-3.32242166	H ₈	0.039811	-4.36972018	-4.34638023
H ₆	0.050119	-3.34354251	-3.32278773	H ₈	0.050119	-4.37083690	-4.34652382
H ₆	0.063096	-3.37708344	-3.32295246	H ₈	0.063096	-4.37667930	-4.34650941
H ₆	0.079433	-3.39476016	-3.32307469	H ₈	0.079433	-4.39344403	-4.34648766
H ₆	0.100000	-3.40138205	-3.32346661	H ₈	0.100000	-4.43190074	-4.34675691

Table XIII. DMRG -CI electronic energies in Hartree atomic units for the catalyst structure II-III with a CAS(8,6), evaluated from low-rank approximations to the double-factorized Hamiltonian at two different truncation schemes. The base integral file with the non-truncated integrals is II-III-highCD-cas6-fb-8e6o. $\epsilon_{\text{in/co}}$ denotes the value of the truncation parameter ϵ of either the incoherent truncation (ϵ_{in}) of the two-electron integrals or the coherent one (ϵ_{co}). The resulting ground-state DMRG(8,6)-CI energy of the integral file at a given truncation level is denoted by $E_{\text{el}}^{\text{DMRG-CI}}(\epsilon_{\text{in}})$ for the incoherent truncation scheme and $E_{\text{el}}^{\text{DMRG-CI}}(\epsilon_{\text{co}})$ for the coherent one. The energy associated with the non-truncated integrals is given in the first row at a truncation value of 0.0 Hartree.

$\epsilon_{\text{in/co}}$ / Hartree	$E_{\text{el}}^{\text{DMRG-CI}}(\epsilon_{\text{in}})$ / Hartree	$E_{\text{el}}^{\text{DMRG-CI}}(\epsilon_{\text{co}})$ / Hartree
0.000000	-7318.00215013	-7318.00215013
0.000100	-7318.00215864	-7318.00215187
0.000126	-7318.00215503	-7318.00215187
0.000158	-7318.00213043	-7318.00215274
0.000200	-7318.00216079	-7318.00215274
0.000251	-7318.00215679	-7318.00215864
0.000316	-7318.00213123	-7318.00215864
0.000398	-7318.00216705	-7318.00216409
0.000501	-7318.00221220	-7318.00216409
0.000631	-7318.00220470	-7318.00213948
0.000794	-7318.00219296	-7318.00216986
0.001000	-7318.00229250	-7318.00216625
0.001259	-7318.00250109	-7318.00214070
0.001585	-7318.00280990	-7318.00217604
0.001995	-7318.00249959	-7318.00216705
0.002512	-7318.00254140	-7318.00218788
0.003162	-7318.00262988	-7318.00221220
0.003981	-7318.00333674	-7318.00220470
0.005012	-7318.00680238	-7318.00219296
0.006310	-7318.00737955	-7318.00220866
0.007943	-7318.00814157	-7318.00241234
0.010000	-7318.01010856	-7318.00271304
0.012589	-7318.00987156	-7318.00263355
0.015849	-7318.01217928	-7318.00249959
0.019953	-7318.01212307	-7318.00247483
0.025119	-7318.01908891	-7318.00262988
0.031623	-7318.02160123	-7318.00301686
0.039811	-7318.03507773	-7318.00526335
0.050119	-7318.04053844	-7318.00683148
0.063096	-7318.04732502	-7318.00769067
0.079433	-7318.08057598	-7318.00814157
0.100000	-7318.10412106	-7318.00829295

Table XIV. DMRG-CI electronic energies in Hartree atomic units for the catalyst structure IX with a CAS(16,16), evaluated from low-rank approximations to the double-factorized Hamiltonian at two different truncation schemes. The base integral file with the non-truncated integrals is IX-highCD-cas16-fb-16e16o. $\epsilon_{\text{in/co}}$ denotes the value of the truncation parameter ϵ of either the incoherent truncation (ϵ_{in}) of the two-electron integrals or the coherent one (ϵ_{co}). The resulting ground-state DMRG(16,16)-CI energy of the integral file at a given truncation level is denoted by $E_{\text{el}}^{\text{DMRG-CI}}(\epsilon_{\text{in}})$ for the incoherent truncation scheme and $E_{\text{el}}^{\text{DMRG-CI}}(\epsilon_{\text{co}})$ for the coherent one. The energy associated with the non-truncated integrals is given in the first row at a truncation value of 0.0 Hartree.

$\epsilon_{\text{in/co}}$ / Hartree	$E_{\text{el}}^{\text{DMRG-CI}}(\epsilon_{\text{in}})$ / Hartree	$E_{\text{el}}^{\text{DMRG-CI}}(\epsilon_{\text{co}})$ / Hartree
0.000000	-7318.21221456	-7318.21221456
0.000100	-7318.21230964	-7318.21221600
0.000126	-7318.21234289	-7318.21221644
0.000158	-7318.21237029	-7318.21221704
0.000200	-7318.21240692	-7318.21221761
0.000251	-7318.21246425	-7318.21221840
0.000316	-7318.21251053	-7318.21221965
0.000398	-7318.21259187	-7318.21222093
0.000501	-7318.21268462	-7318.21222356
0.000631	-7318.21281515	-7318.21222591
0.000794	-7318.21297009	-7318.21222853
0.001000	-7318.21312759	-7318.21223208
0.001259	-7318.21330936	-7318.21223602
0.001585	-7318.21365065	-7318.21224246
0.001995	-7318.21397040	-7318.21224753
0.002512	-7318.21431504	-7318.21225796
0.003162	-7318.21484663	-7318.21227019
0.003981	-7318.21581205	-7318.21228159
0.005012	-7318.21688967	-7318.21230107
0.006310	-7318.21781895	-7318.21233012
0.007943	-7318.21914577	-7318.21235753
0.010000	-7318.22001812	-7318.21239445
0.012589	-7318.22199964	-7318.21243973
0.015849	-7318.22428406	-7318.21248711
0.019953	-7318.22385766	-7318.21254718
0.025119	-7318.22690256	-7318.21263369
0.031623	-7318.22795625	-7318.21273693
0.039811	-7318.24170762	-7318.21286327
0.050119	-7318.27394958	-7318.21307670
0.063096	-7318.30682217	-7318.21319792
0.079433	-7318.35577244	-7318.21351128
0.100000	-7318.43110749	-7318.21376772

C. General procedure for the selection of molecular orbitals for the integral files

During the selection of the small active spaces for the CASSCF calculations, it became evident that the intermediates and transition states in this study are mainly dynamically correlated, as indicated by e.g. low values of our multi-configurational measure $Z_{s(1)}$ [22]. While the orbitals are sufficiently correlated to allow for the determination of a small active space for the CASSCF calculations, the selection becomes ambiguous for larger active space sizes because of the dominant dynamic correlation that renders the active space concept arbitrary. For the selection of the active spaces for the integral files, we therefore chose a scheme that is as reproducible as possible while still maintaining chemical relevance. For each complex, we selected at least three different active spaces from the valence space of the CAS(N,L)SCF orbitals, termed the *small*, *intermediate*, and *large* active spaces. The small active space consists of the L orbitals of the underlying CAS(N,L)SCF calculation. The intermediate one includes the small active space plus the orbitals which are primarily localized on CO_2 , HCO_2^- , HCOOH , CH_2OOH^- , CH_3O^- , H_2 , H, Ruthenium or in the bonding region between the metal and the ligands. The large one comprises the intermediate active space plus the 18 π and 18 π^* orbitals of the 6 phenyl groups that are part of the triphos ligand.

To investigate the performance of the quantum algorithms in the limit of very large active spaces, we additionally generated integral files with 100, 150, and 250 active orbitals for the complex XVIII. As a selection guided by manual inspection becomes unfeasible for these active space sizes, we chose to include the $n/2$ orbitals below (and including) the HOMO and the $n/2$ orbitals above it (with $n=100, 150, 250$).

For complex II, we also generated integral files from HF orbitals to understand the effect of the orbital type on the resource estimates. We selected the active space analogously to the CASSCF active spaces but without the small active space (as it is not defined for the HF orbitals).

IV. OVERVIEW OF THE INTEGRAL FILES

The files containing the one- and two-electron integrals for a selection of molecular orbitals as defined in Section III C are summarized in Table XV, which also lists the atomic and molecular orbital bases used as well as the active spaces for the integrals. The notation for the files is *catalyst-integralAccuracy-MObasis-AObasis- $n_e n_o$* , where *catalyst* is one of the catalyst structure identifiers I, II, II-III, V, VIII, VIII-IX, IX, or XVIII, *integralAccuracy* denotes the tightness of the CD threshold, with *highCD* standing for a threshold of 10^{-8} and no string for a threshold of 10^{-4} ; *MObasis* denotes the molecular orbitals basis, *AObasis* the atomic orbital basis, and n_e and n_o are the number of electrons and orbitals, respectively.

Table XV. List of the integral files resulting from the active space selection outlined in [Section III C](#) for complexes I to VIII with the notation explained in the text. The MO active space is the one of the underlying CASSCF calculation through which the orbitals have been obtained, whereas the integral active space denotes the size of the active space chosen for the integral file under consideration. Calculations were performed with a Cholesky Decomposition of the two-electron integrals with two thresholds of 10^{-4} and 10^{-8} . Files that were obtained with the high-accuracy threshold 10^{-8} are labeled “highCD”, whereas the absence of that label indicates the default threshold of 10^{-4} .

Name of file	AO basis	MO basis	MO active space	Integral active space
I-cas5-fb-4e5o	fb	CASSCF	(4,5)	(4,5)
I-cas5-fb-14e16o	fb	CASSCF	(4,5)	(14,16)
I-cas5-fb-48e52o	fb	CASSCF	(4,5)	(48,52)
I-highCD-cas5-fb-4e5o	fb	CASSCF	(4,5)	(4,5)
I-highCD-cas5-fb-14e16o	fb	CASSCF	(4,5)	(14,16)
I-highCD-cas5-fb-48e52o	fb	CASSCF	(4,5)	(48,52)
II-cas6-fb-8e6o	fb	CASSCF	(8,6)	(8,6)
II-cas6-fb-34e26o	fb	CASSCF	(8,6)	(34,26)
II-cas6-fb-70e62o	fb	CASSCF	(8,6)	(70,62)
II-highCD-cas6-fb-8e6o	fb	CASSCF	(8,6)	(8,6)
II-highCD-cas6-fb-34e26o	fb	CASSCF	(8,6)	(34,26)
II-highCD-cas6-fb-70e62o	fb	CASSCF	(8,6)	(70,62)
II-hf-fb-38e33o	fb	HF	n.a.	(38,33)
II-hf-fb-74e71o	fb	HF	n.a.	(74,71)
II-III-cas6-fb-8e6o	fb	CASSCF	(8,6)	(8,6)
II-III-cas6-fb-38e29o	fb	CASSCF	(8,6)	(38,29)
II-III-cas6-fb-74e65o	fb	CASSCF	(8,6)	(74,65)
II-III-highCD-cas6-fb-8e6o	fb	CASSCF	(8,6)	(8,6)
II-III-highCD-cas6-fb-38e29o	fb	CASSCF	(8,6)	(38,29)
II-III-highCD-cas6-fb-74e65o	fb	CASSCF	(8,6)	(74,65)
V-cas11-fb-12e11o	fb	CASSCF	(12,11)	(12,11)
V-cas11-fb-32e24o	fb	CASSCF	(12,11)	(32,24)
V-cas11-fb-68e60o	fb	CASSCF	(12,11)	(68,60)
V-highCD-cas11-fb-12e11o	fb	CASSCF	(12,11)	(12,11)
V-highCD-cas11-fb-32e24o	fb	CASSCF	(12,11)	(32,24)
V-highCD-cas11-fb-68e60o	fb	CASSCF	(12,11)	(68,60)
VIII-cas2-fb-2e2o	fb	CASSCF	(2,2)	(2,2)
VIII-cas2-fb-40e29o	fb	CASSCF	(2,2)	(40,29)
VIII-cas2-fb-76e65o	fb	CASSCF	(2,2)	(76,65)
VIII-highCD-cas2-fb-2e2o	fb	CASSCF	(2,2)	(2,2)
VIII-highCD-cas2-fb-40e29o	fb	CASSCF	(2,2)	(40,29)
VIII-highCD-cas2-fb-76e65o	fb	CASSCF	(2,2)	(76,65)

Table XVI. List of the integral files resulting from the active space selection outlined in [Section III C](#) for complexes VIII-IX to XVIII with the notation explained in the text. The MO active space is the one of the underlying CASSCF calculation through which the orbitals have been obtained, whereas the integral active space denotes the size of the active space chosen for the integral file under consideration. Calculations were performed with a Cholesky decomposition of the two-electron integrals with two thresholds of 10^{-4} and 10^{-8} . Files that were obtained with the high-accuracy threshold 10^{-8} are labeled “highCD”, whereas the absence of that label indicates the default threshold of 10^{-4} .

VIII-IX-cas4-fb-4e4o	fb	CASSCF	(4,4)	(4,4)
VIII-IX-cas4-fb-36e23o	fb	CASSCF	(4,4)	(36,23)
VIII-IX-cas4-fb-72e59o	fb	CASSCF	(4,4)	(72,59)
VIII-IX-highCD-cas4-fb-4e4o	fb	CASSCF	(4,4)	(4,4)
VIII-IX-highCD-cas4-fb-36e23o	fb	CASSCF	(4,4)	(36,23)
VIII-IX-highCD-cas4-fb-72e59o	fb	CASSCF	(4,4)	(72,59)
IX-cas16-fb-16e16o	fb	CASSCF	(16,16)	(16,16)
IX-cas16-fb-32e26o	fb	CASSCF	(16,16)	(32,26)
IX-cas16-fb-68e62o	fb	CASSCF	(16,16)	(68,62)
IX-highCD-cas4-cas16-fb-16e16o	fb	CASSCF	(16,16)	(16,16)
IX-highCD-cas4-cas16-fb-32e26o	fb	CASSCF	(16,16)	(32,26)
IX-highCD-cas4-cas16-fb-68e62o	fb	CASSCF	(16,16)	(68,62)
XVIII-cas4-fb-4e4o	fb	CASSCF	(4,4)	(4,4)
XVIII-cas4-fb-28e20o	fb	CASSCF	(4,4)	(28,20)
XVIII-cas4-fb-64e56o	fb	CASSCF	(4,4)	(64,56)
XVIII-cas4-fb-100e100o	fb	CASSCF	(4,4)	(100,100)
XVIII-cas4-fb-150e150o	fb	CASSCF	(4,4)	(150,150)
XVIII-cas4-fb-250e250o	fb	CASSCF	(4,4)	(250,250)
XVIII-highCD-cas4-fb-4e4o	fb	CASSCF	(4,4)	(4,4)
XVIII-highCD-cas4-fb-28e20o	fb	CASSCF	(4,4)	(28,20)
XVIII-highCD-cas4-fb-64e56o	fb	CASSCF	(4,4)	(64,56)
XVIII-highCD-cas4-fb-100e100o	fb	CASSCF	(4,4)	(100,100)
XVIII-highCD-cas4-fb-150e150o	fb	CASSCF	(4,4)	(150,150)
XVIII-highCD-cas4-fb-250e250o	fb	CASSCF	(4,4)	(250,250)

V. GRAPHICAL REPRESENTATION OF ACTIVE ORBITALS CHOSEN FOR INTEGRAL FILES

We provide in the following figures of the active orbitals chosen for each catalyst structure.

A. CAS(4,5)SCF active molecular orbitals chosen for integral files of stable intermediate I

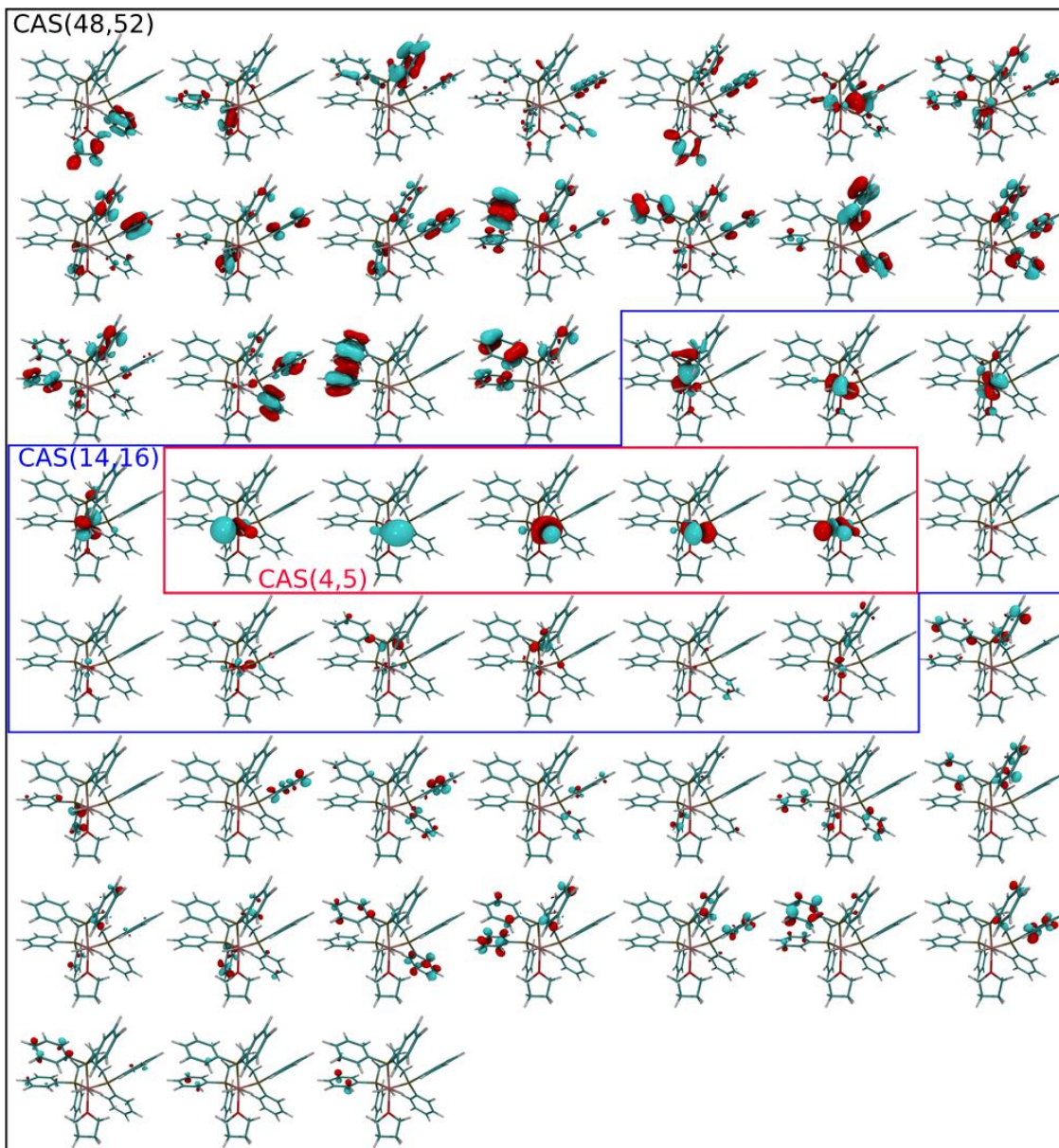


Figure 1. Active spaces yielding integral files for complex structure I produced from CAS(4,5)SCF molecular orbitals in the full atomic orbital basis.

B. CAS(8,6)SCF active molecular orbitals chosen for integral files of stable intermediate II

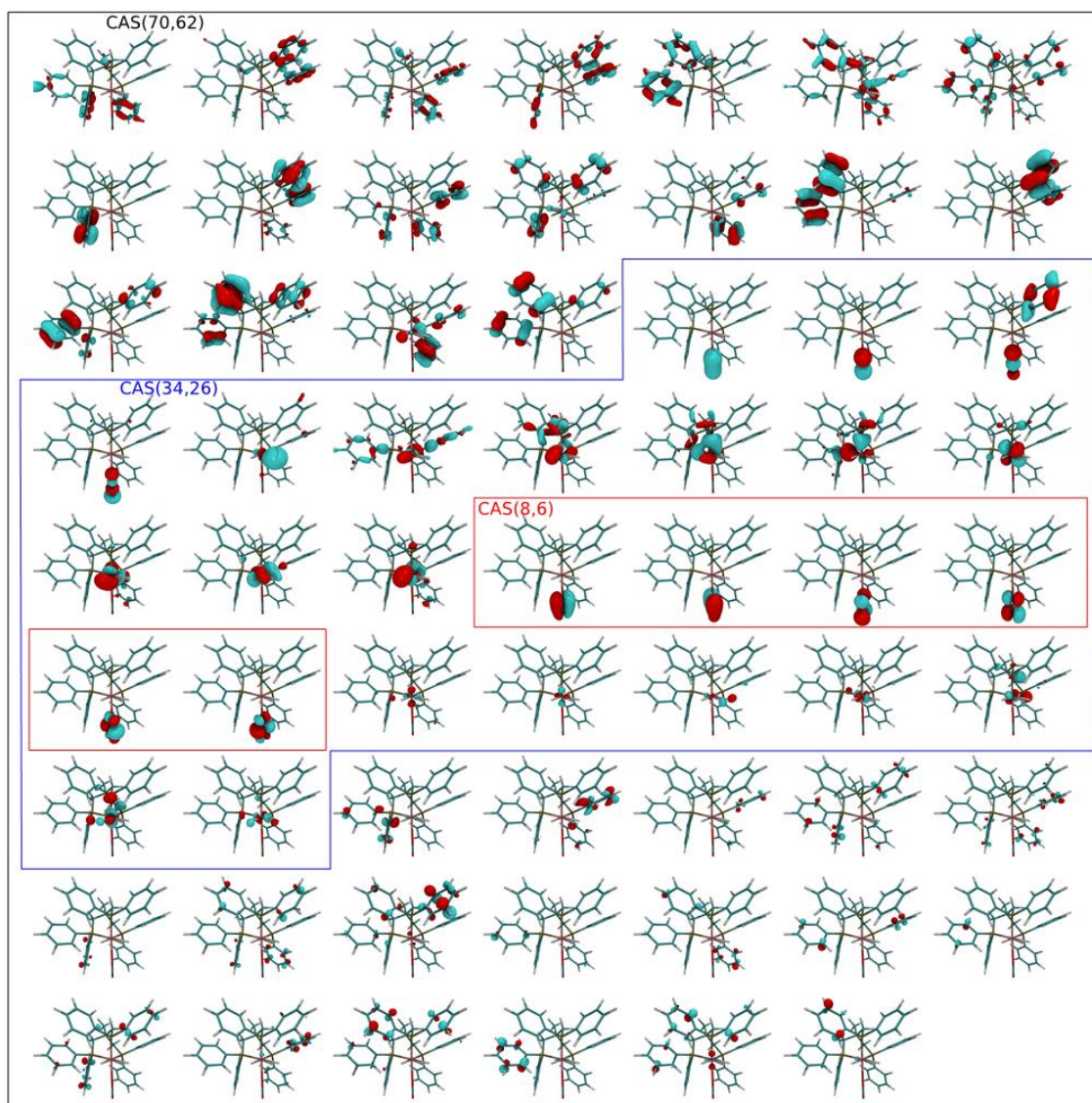


Figure 2. Active spaces yielding integral files for complex structure II produced from CAS(8,6)SCF molecular orbitals in the full atomic orbital basis.

C. CAS(8,6)SCF active molecular orbitals chosen for integral files of transition state II-III

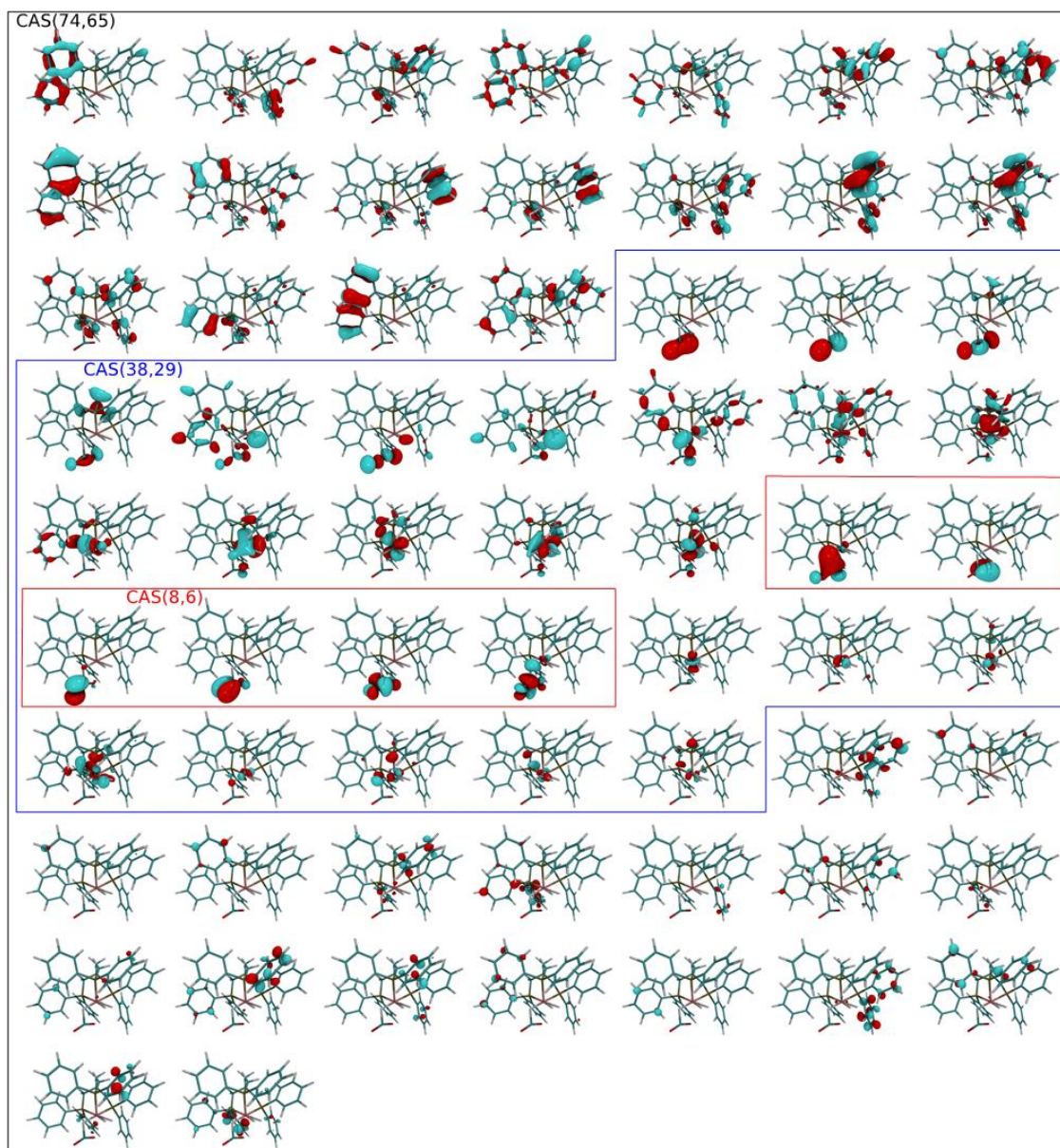


Figure 3. Active spaces yielding integral files for complex structure II-III produced from CAS(8,6)SCF molecular orbitals in the full atomic orbital basis.

D. CAS(12,11)SCF active molecular orbitals chosen for integral files of stable intermediate V

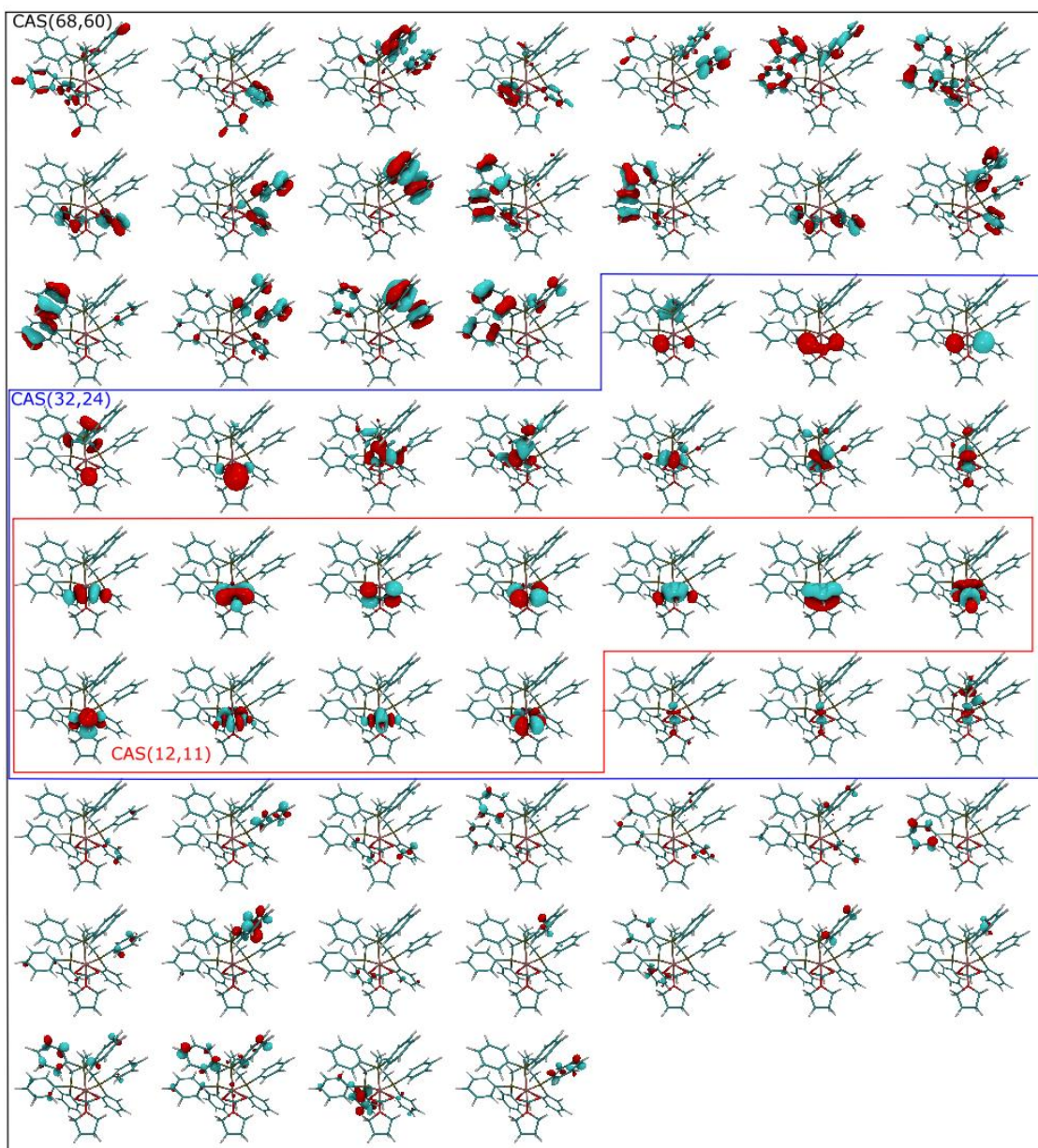


Figure 4. Active spaces yielding integral files for complex structure V produced from CAS(12,11)SCF molecular orbitals in the full atomic orbital basis.

E. CAS(2,2)SCF active molecular orbitals chosen for integral files of stable intermediate VIII

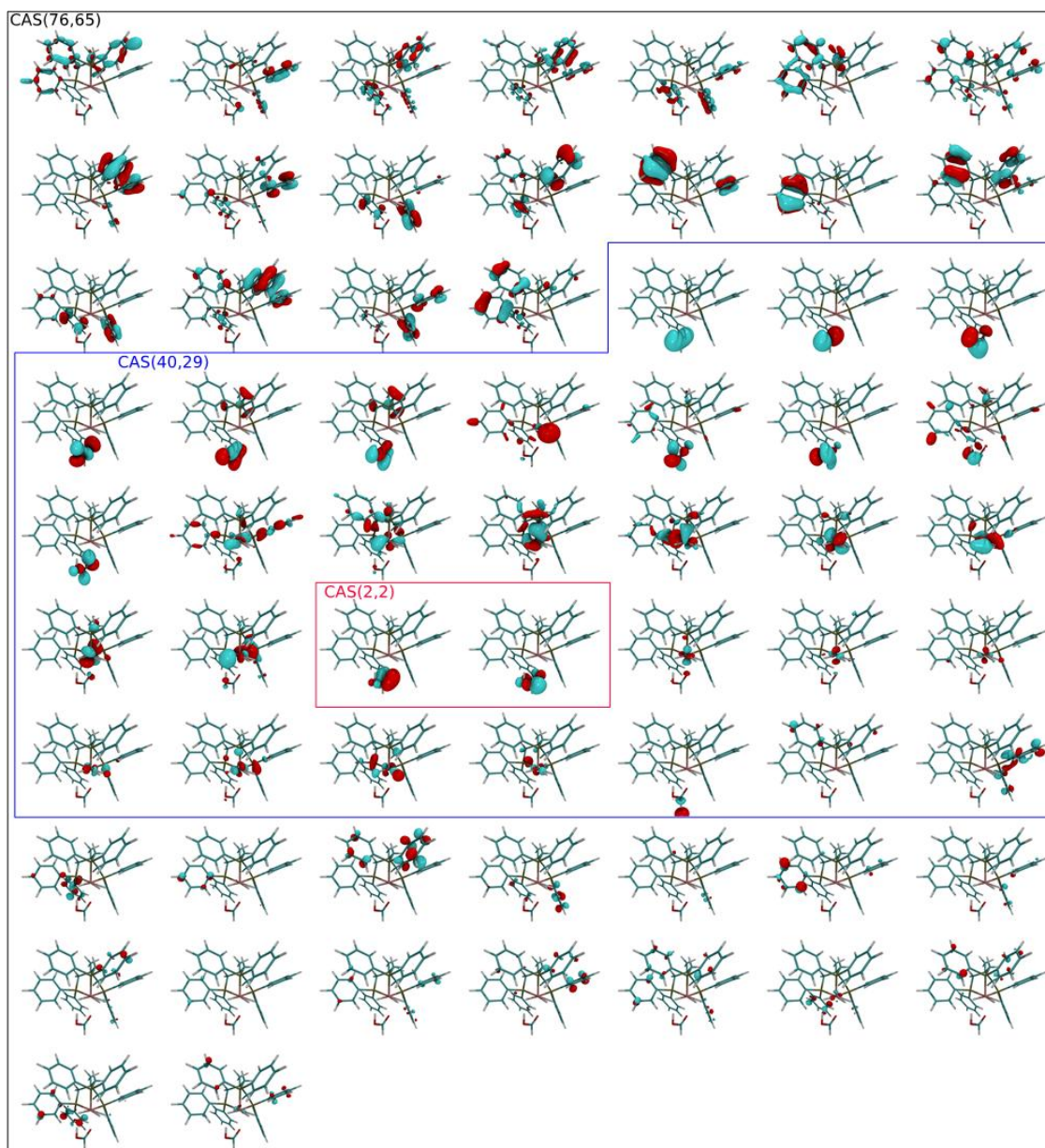


Figure 5. Active spaces yielding integral files for complex structure VIII produced from CAS(2,2)SCF molecular orbitals in the full atomic orbital basis.

F. CAS(4,4)SCF active molecular orbitals chosen for integral files of transition state VIII-IX

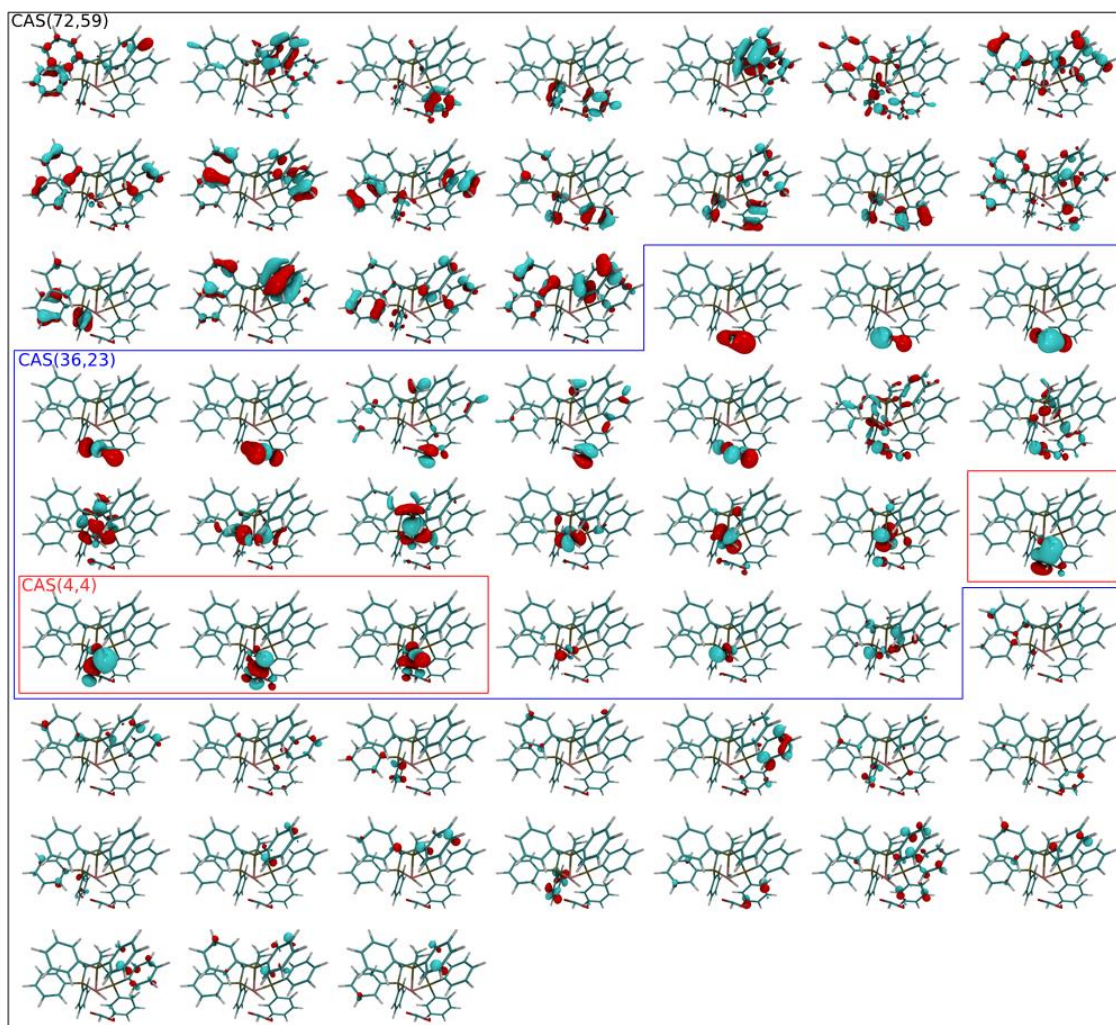


Figure 6. Active spaces yielding integral files for complex structure VIII-IX produced from CAS(4,4)SCF molecular orbitals in the full atomic orbital basis.

G. CAS(16,16)SCF active molecular orbitals chosen for integral files of stable intermediate IX

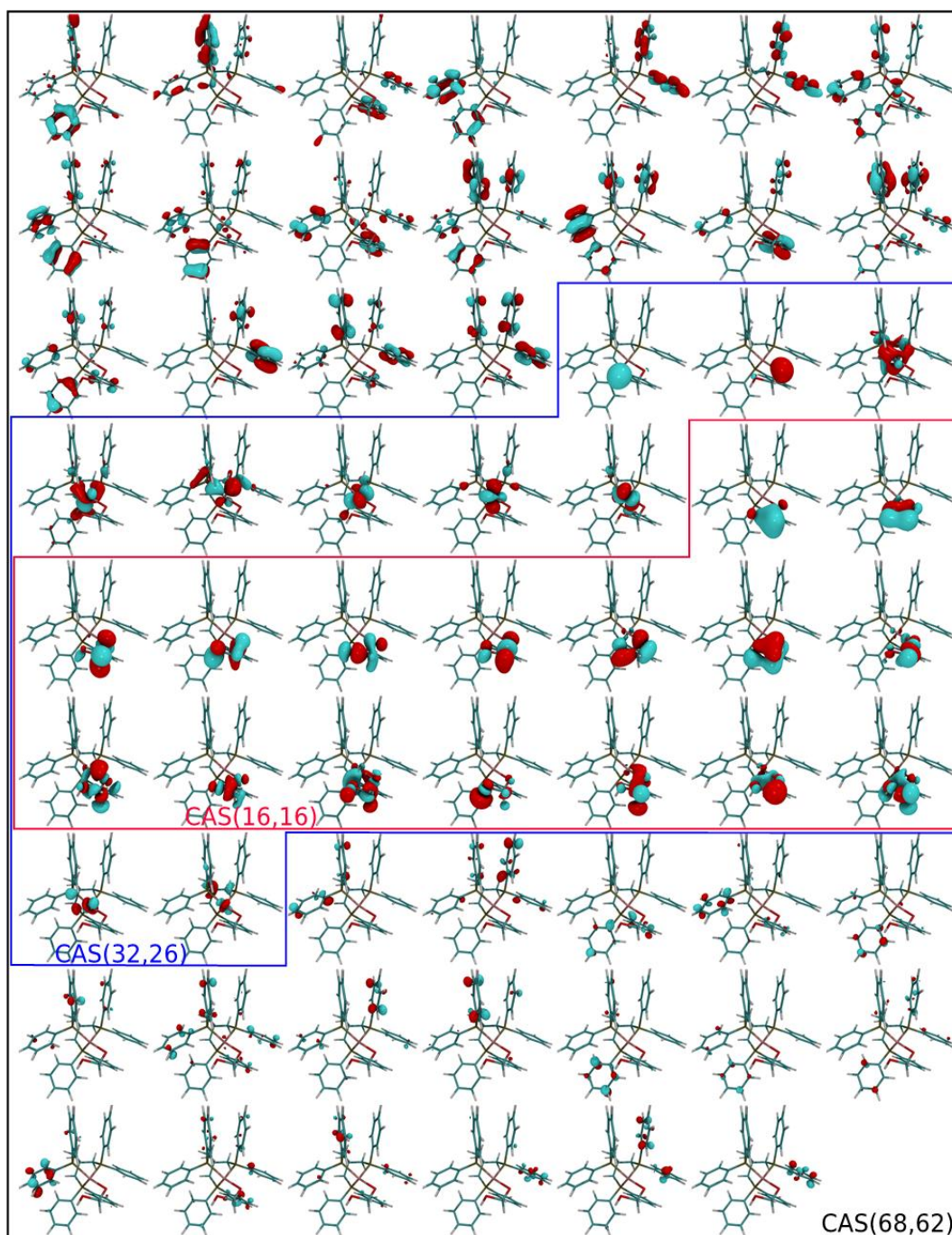


Figure 7. Active spaces yielding integral files for complex structure IX produced from CAS(16,16)SCF molecular orbitals in the full atomic orbital basis.

H. CAS(4,4)SCF active molecular orbitals chosen for integral files of stable intermediate XVIII

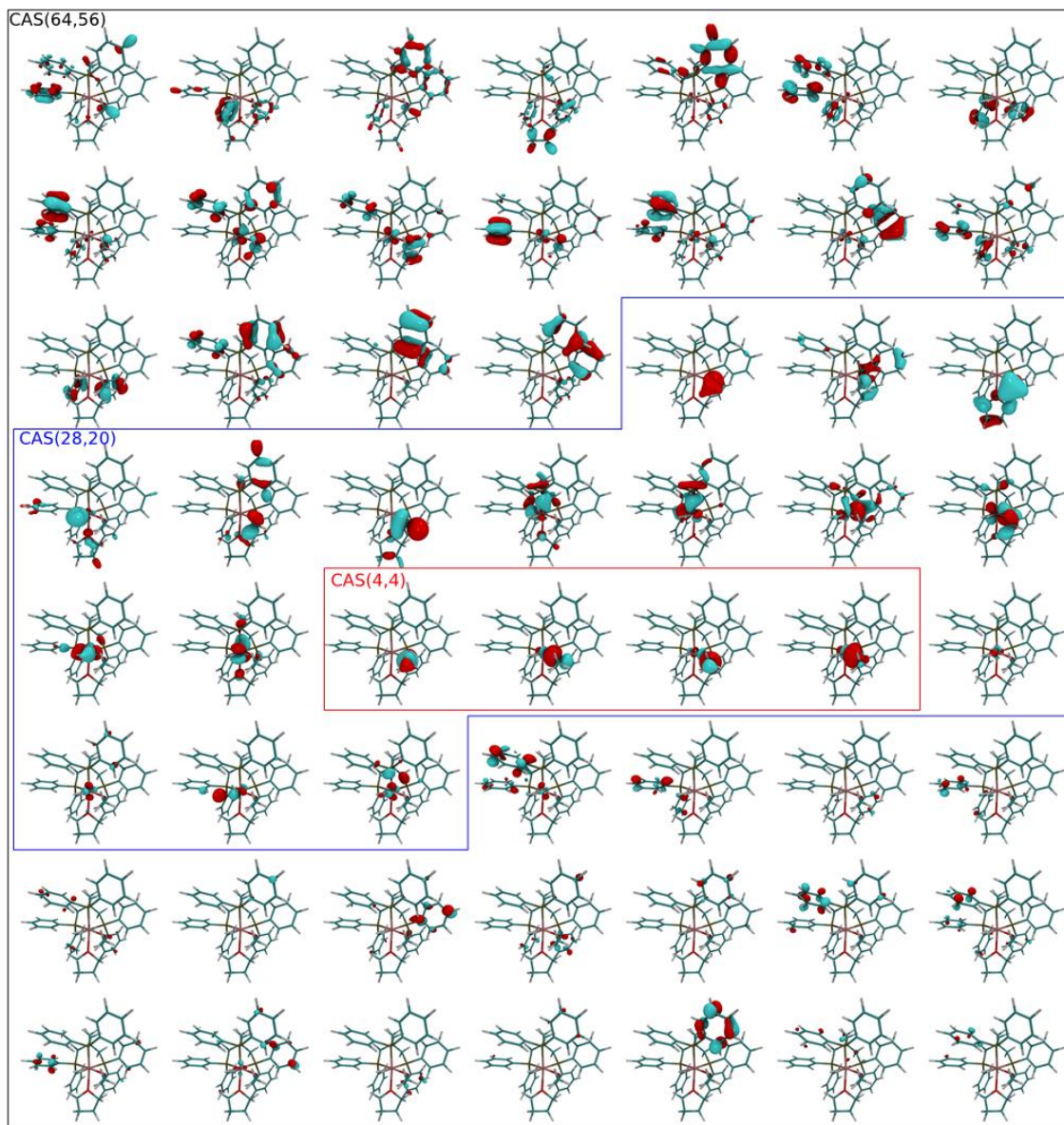


Figure 8. Active spaces yielding integral files for complex structure XVIII produced from CAS(4,4)SCF molecular orbitals in the full atomic orbital basis.

VI. RESOURCE ANALYSIS

There exists a plethora of quantum algorithms that allow one to obtain energies of a given Hamiltonian. Our previous work [23] focused on a product-formula based implementation of the time evolution operator, where the Hamiltonian was given in a standard second-quantized representation. In this work, we evaluated a variety of different approaches and focused on the ones that yield the lowest resource costs.

An initial screening of methods left us with the following methods to consider:

- Trotter based implementation of the low-rank factorized Hamiltonian [24]
- Qubitization of the standard (unfactorized) second-quantized representation [25]
- Qubitization of the single-factorized Hamiltonian [26]
- Qubitization of the double-factorized Hamiltonian (this work)

We found that a qubitization based implementation of a doubly-factorized Hamiltonian resulted in the lowest costs. This method is discussed in the main text with a comparison to the single-factorized Hamiltonian, and also thoroughly detailed in [Section VII C](#) of this supporting document. We also ruled out qubitization in the standard and single-factorized second-quantized representation based on highly-optimized algorithms targeting these representations [26]. In the remainder of this section, we summarize our evaluation of remaining Trotter based implementation, and compare resource estimates in [Table XVII](#) with the best qubitization implementations. Finally, we tabulate resource estimates of all carbon dioxide fixation complexes mentioned in the main text.

A. Product formula and low-rank factorization of the Hamiltonian

This method was introduced in [24]. The idea is to approximate the Hamiltonian using a low-rank factorization, i.e., using $R < N^2$ components, and to then simulate time-evolution using a product formula. Each step of the product formula based implementation consists of a sequence of rotations that diagonalize the current component of the low-rank factorization, followed by a sequence of controlled phase gates that correspond to the eigenvalues of the component. This is repeated for all R components of the low-rank factorization. As the simulation basis size N is increased, it has been shown that $R \sim \mathcal{O}(N)$ [27]. Additionally, the eigenvalues of each component in the factorization may be truncated, allowing one to further reduce the resource requirements. For a more detailed description of this method, we refer the reader to [24].

We provide gate counts for estimating the electronic energies of some of our chosen systems using this method in [Table XVII](#). The resource estimation uses the same truncation method as discussed in Section 5.1 of the main text. We note that this product formula based implementation naturally offers more parallelism than, e.g., a qubitization based implementation at comparable qubit numbers. We leave the detailed investigation of such space/time tradeoffs for future work.

The time step for the second order Trotter method was chosen using the following upper bound [28]

$$\|e^{-iHt} - e^{-iH_{\text{eff}}t}\| \leq \frac{t^3}{12} \sum_p \left(\sum_{c>b} \sum_{a>b} \| [H_a, [H_b, H_c]] \| + \frac{1}{2} \sum_{c>b} \| [H_b, [H_b, H_c]] \| \right), \quad (1)$$

which applies to any Hamiltonian $H = \sum_{j=0}^{M-1} H_j$ where time-evolution by each term can be applied without any error. In the context of electronic structure, time-evolution by the one-electron term and each rank component of the two-electron terms can be applied exactly by diagonalizing them with fermionic basis transformations that are implemented by Givens rotations [29].

Since such bounds have been shown to be loose by many orders of magnitude, we carried out an empirical study of the required Trotter step size for linear chains of Hydrogen atoms. We depict the bound and empirically determined step sizes in Fig. 9. The results for linear chains of Hydrogen atoms indicate that the upper bound yields Trotter numbers that may be up to $10\sqrt{n}$ larger than what empirical data suggests. Rescaling the T -count estimates for our catalyst systems by this factor results in an optimistic estimate that can also be found in Table XVII.

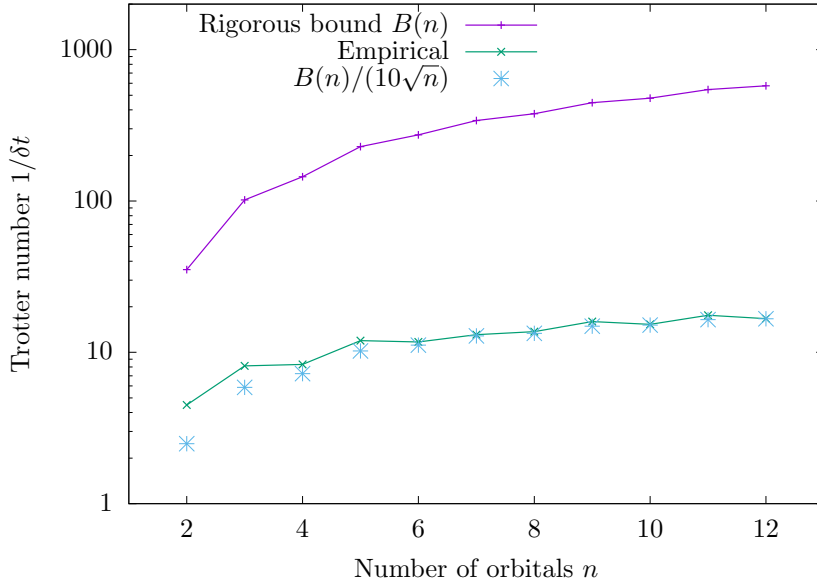


Figure 9. Comparing Trotter numbers $1/\delta t$, where δt is the Trotter step size, derived from simulations (labeled “empirical”) to rigorous upper bounds. The gap between the empirical data and the bound is approximately $10\sqrt{n}$, as indicated by the rescaled points.

B. Results

In this section, we compare the T -gate and qubit counts of Trotter- and qubitization-based each method in Table XVII – note that any Toffoli gate can be synthesized from 4

T gates. Qubitization using a doubly-factorized representation of the Hamiltonian offers the lowest T -counts at reasonable qubit numbers. The main text therefore focuses on this approach, and thus we tabulate, for completeness, the cost of phase estimation to 1mHartree and problem parameters of all the carbon dioxide fixation complex structures mentioned in the main text using this approach. We also briefly compare with qubitization using the unfactorized or single-factorized representation using the algorithms of Berry et al. [26]. In all these examples, we reduce the number of non-zero terms by using the incoherent truncation scheme discussed in the main text at an error threshold of $\epsilon_{in} = 1\text{mHartree}$.

Table XVII. Comparison of resource estimates for estimating electronic energies on a quantum computer. Results for Trotter (DF) follow from Section VI A, results for Qubitization (DF) follow from Section VII C, and results for unfactorized and single-factorized qubitization follow from the algorithms described by Berry et al. [26]

Step	Trotter (DF)				Qubitization (DF)			
	R	M	Qubits	T -count	optimistic / Hartree	α	Qubits	Toffoli-count
I-cas5-fb-48e52o	613	23566	104	8.29×10^{14}	1.15×10^{13}	177.3	3400	1.3×10^{10}
II-cas6-fb-70e62o	734	33629	124	3.50×10^{15}	4.45×10^{13}	374.4	4200	3.6×10^{10}
II-III-cas6-fb-74e65o	783	38122	130	4.17×10^{15}	5.18×10^{13}	416.0	4400	4.5×10^{10}
V-cas11-fb-68e60o	670	29319	120	2.76×10^{15}	3.57×10^{13}	372.1	4100	3.3×10^{10}
VIII-cas2-fb-76e65o	794	39088	130	4.52×10^{15}	5.61×10^{13}	425.7	4400	4.6×10^{10}
VIII-IX-cas4-fb-72e59o	666	29286	118	2.58×10^{15}	3.36×10^{13}	384.4	4000	3.4×10^{10}
IX-cas16-fb-68e62o	638	28945	124	2.97×10^{15}	3.77×10^{13}	396.6	4200	3.5×10^{10}
XVIII-cas4-fb-64e56o	705	29594	112	2.09×10^{15}	2.80×10^{13}	293.5	3700	2.5×10^{10}

Step	Qubitization (Unfactorized)			Qubitization (Single-factorized)				
	n.n.z	α	Toffoli	n.n.z	α	Toffoli	Toffoli	
I-cas5-fb-48e52o	911134	5775	9832	2.8×10^{11}	628549	19725	5480	7.0×10^{11}
II-cas6-fb-70e62o	1757237	8683	9980	7.9×10^{11}	1052858	31790	5628	1.9×10^{12}
II-III-cas6-fb-74e65o	2181633	10714	11010	9.3×10^{11}	1251855	42037	5762	2.1×10^{12}
V-cas11-fb-68e60o	1526106	7332	9976	3.6×10^{11}	887611	25725	5624	8.4×10^{11}
VIII-cas2-fb-76e65o	2169817	10617	11010	9.3×10^{11}	1292050	42160	5762	2.1×10^{12}
VIII-IX-cas4-fb-72e59o	1485406	8950	9974	7.2×10^{11}	880955	33100	5622	1.7×10^{12}
IX-cas16-fb-68e62o	1751213	9651	9980	7.9×10^{11}	897570	34973	5628	1.7×10^{12}
XVIII-cas4-fb-64e56o	1213076	6708	9968	3.2×10^{11}	847812	25611	5616	8.2×10^{11}

Table XVIII. Double-factorization resource estimates for all steps of carbon dioxide fixation for active space sizes from 52–65 orbitals at a truncation threshold between $\epsilon_{\text{in}} = 0.1\text{mHartree}$ and 0.1Hartree .

Step	ϵ_{in} / Hartree	Orbitals N	R	M	α_{DF} / Hartree	Qubits	#Toffoli gates
I-cas5-fb-48e52o	1.00×10^{-4}	52	855	37242	177.4	3448	1.72×10^{10}
I-cas5-fb-48e52o	1.58×10^{-4}	52	808	34633	177.4	3448	1.63×10^{10}
I-cas5-fb-48e52o	2.51×10^{-4}	52	761	31937	177.4	3447	1.55×10^{10}
I-cas5-fb-48e52o	3.98×10^{-4}	52	713	29187	177.4	3447	1.46×10^{10}
I-cas5-fb-48e52o	6.31×10^{-4}	52	665	26399	177.4	3447	1.38×10^{10}
I-cas5-fb-48e52o	1.00×10^{-3}	52	613	23566	177.3	3447	1.29×10^{10}
I-cas5-fb-48e52o	1.58×10^{-3}	52	561	20739	177.3	3447	1.20×10^{10}
I-cas5-fb-48e52o	2.51×10^{-3}	52	509	17950	177.2	3447	1.11×10^{10}
I-cas5-fb-48e52o	3.98×10^{-3}	52	457	15198	177.2	3446	1.02×10^{10}
I-cas5-fb-48e52o	6.31×10^{-3}	52	403	12516	177.0	3446	9.38×10^9
I-cas5-fb-48e52o	1.00×10^{-2}	52	343	9993	176.8	3446	8.57×10^9
I-cas5-fb-48e52o	1.58×10^{-2}	52	280	7695	176.3	3445	7.83×10^9
I-cas5-fb-48e52o	2.51×10^{-2}	52	224	5739	175.7	3445	7.18×10^9
I-cas5-fb-48e52o	3.98×10^{-2}	52	167	4161	174.7	3445	6.65×10^9
I-cas5-fb-48e52o	6.31×10^{-2}	52	125	2959	173.3	3444	6.22×10^9
I-cas5-fb-48e52o	1.00×10^{-1}	52	93	2117	171.5	3444	5.89×10^9
II-cas6-fb-70e62o	1.00×10^{-4}	62	998	51731	374.5	4232	4.84×10^{10}
II-cas6-fb-70e62o	1.58×10^{-4}	62	947	48215	374.5	4232	4.60×10^{10}
II-cas6-fb-70e62o	2.51×10^{-4}	62	893	44655	374.4	4232	4.37×10^{10}
II-cas6-fb-70e62o	3.98×10^{-4}	62	840	41036	374.4	4232	4.13×10^{10}
II-cas6-fb-70e62o	6.31×10^{-4}	62	790	37348	374.4	4232	3.89×10^{10}
II-cas6-fb-70e62o	1.00×10^{-3}	62	734	33629	374.4	4232	3.64×10^{10}
II-cas6-fb-70e62o	1.58×10^{-3}	62	678	29874	374.4	4231	3.39×10^{10}
II-cas6-fb-70e62o	2.51×10^{-3}	62	622	26143	374.3	4231	3.14×10^{10}
II-cas6-fb-70e62o	3.98×10^{-3}	62	555	22497	374.2	4231	2.90×10^{10}
II-cas6-fb-70e62o	6.31×10^{-3}	62	491	19012	374.0	4231	2.67×10^{10}
II-cas6-fb-70e62o	1.00×10^{-2}	62	432	15702	373.7	4230	2.45×10^{10}
II-cas6-fb-70e62o	1.58×10^{-2}	62	370	12580	373.3	4230	2.24×10^{10}
II-cas6-fb-70e62o	2.51×10^{-2}	62	309	9700	372.6	4230	2.04×10^{10}
II-cas6-fb-70e62o	3.98×10^{-2}	62	248	7150	371.4	4229	1.87×10^{10}
II-cas6-fb-70e62o	6.31×10^{-2}	62	183	5096	369.3	4229	1.72×10^{10}
II-cas6-fb-70e62o	1.00×10^{-1}	62	136	3609	366.8	4228	1.61×10^{10}

Table XIX. (Continued) Double-factorization resource estimates for all steps of carbon dioxide fixation for active space sizes from 52–65 orbitals at a truncation threshold between $\epsilon_{\text{in}} = 0.1\text{mHartree}$ and 0.1Hartree .

Step	ϵ_{in} / Hartree	Orbitals N	R	M	α_{DF} / Hartree	Qubits	#Toffoli gates
II-III-cas6-fb-74e65o	1.00×10^{-4}	65	1064	58020	416.1	4436	5.91×10^{10}
II-III-cas6-fb-74e65o	1.58×10^{-4}	65	1011	54104	416.1	4436	5.62×10^{10}
II-III-cas6-fb-74e65o	2.51×10^{-4}	65	954	50154	416.1	4436	5.33×10^{10}
II-III-cas6-fb-74e65o	3.98×10^{-4}	65	895	46172	416.0	4436	5.04×10^{10}
II-III-cas6-fb-74e65o	6.31×10^{-4}	65	839	42153	416.0	4436	4.75×10^{10}
II-III-cas6-fb-74e65o	1.00×10^{-3}	65	783	38122	416.0	4436	4.45×10^{10}
II-III-cas6-fb-74e65o	1.58×10^{-3}	65	725	34075	416.0	4436	4.15×10^{10}
II-III-cas6-fb-74e65o	2.51×10^{-3}	65	665	30026	415.9	4435	3.85×10^{10}
II-III-cas6-fb-74e65o	3.98×10^{-3}	65	604	26032	415.8	4435	3.56×10^{10}
II-III-cas6-fb-74e65o	6.31×10^{-3}	65	536	22119	415.6	4435	3.27×10^{10}
II-III-cas6-fb-74e65o	1.00×10^{-2}	65	462	18383	415.2	4435	2.99×10^{10}
II-III-cas6-fb-74e65o	1.58×10^{-2}	65	400	14890	414.8	4434	2.73×10^{10}
II-III-cas6-fb-74e65o	2.51×10^{-2}	65	339	11652	414.1	4434	2.49×10^{10}
II-III-cas6-fb-74e65o	3.98×10^{-2}	65	273	8757	412.7	4434	2.27×10^{10}
II-III-cas6-fb-74e65o	6.31×10^{-2}	65	213	6312	410.7	4433	2.08×10^{10}
II-III-cas6-fb-74e65o	1.00×10^{-1}	65	160	4463	407.9	4433	1.93×10^{10}
V-cas11-fb-68e60o	1.00×10^{-4}	60	938	46425	372.2	4096	4.41×10^{10}
V-cas11-fb-68e60o	1.58×10^{-4}	60	883	43035	372.2	4096	4.19×10^{10}
V-cas11-fb-68e60o	2.51×10^{-4}	60	828	39623	372.2	4096	3.97×10^{10}
V-cas11-fb-68e60o	3.98×10^{-4}	60	778	36188	372.2	4096	3.74×10^{10}
V-cas11-fb-68e60o	6.31×10^{-4}	60	724	32739	372.1	4095	3.52×10^{10}
V-cas11-fb-68e60o	1.00×10^{-3}	60	670	29319	372.1	4095	3.29×10^{10}
V-cas11-fb-68e60o	1.58×10^{-3}	60	612	25946	372.1	4095	3.07×10^{10}
V-cas11-fb-68e60o	2.51×10^{-3}	60	558	22638	372.0	4095	2.85×10^{10}
V-cas11-fb-68e60o	3.98×10^{-3}	60	501	19412	371.9	4095	2.64×10^{10}
V-cas11-fb-68e60o	6.31×10^{-3}	60	444	16335	371.8	4094	2.43×10^{10}
V-cas11-fb-68e60o	1.00×10^{-2}	60	383	13448	371.5	4094	2.24×10^{10}
V-cas11-fb-68e60o	1.58×10^{-2}	60	329	10819	371.1	4094	2.07×10^{10}
V-cas11-fb-68e60o	2.51×10^{-2}	60	273	8462	370.5	4094	1.91×10^{10}
V-cas11-fb-68e60o	3.98×10^{-2}	60	222	6436	369.5	4093	1.77×10^{10}
V-cas11-fb-68e60o	6.31×10^{-2}	60	174	4781	368.0	4093	1.65×10^{10}
V-cas11-fb-68e60o	1.00×10^{-1}	60	138	3519	366.1	4092	1.56×10^{10}

Table XX. (Continued) Double-factorization resource estimates for all steps of carbon dioxide fixation for active space sizes from 52–65 orbitals at a truncation threshold between $\epsilon_{\text{in}} = 0.1\text{mHartree}$ and 0.1Hartree .

Step	ϵ_{in} / Hartree	Orbitals N	R	M	α_{DF} / Hartree	Qubits	#Toffoli gates
VIII-cas2-fb-76e65o	1.00×10^{-4}	65	1081	59349	425.8	4436	6.15×10^{10}
VIII-cas2-fb-76e65o	1.58×10^{-4}	65	1028	55420	425.8	4436	5.85×10^{10}
VIII-cas2-fb-76e65o	2.51×10^{-4}	65	969	51442	425.8	4436	5.55×10^{10}
VIII-cas2-fb-76e65o	3.98×10^{-4}	65	914	47379	425.8	4436	5.25×10^{10}
VIII-cas2-fb-76e65o	6.31×10^{-4}	65	856	43246	425.7	4436	4.94×10^{10}
VIII-cas2-fb-76e65o	1.00×10^{-3}	65	794	39088	425.7	4436	4.63×10^{10}
VIII-cas2-fb-76e65o	1.58×10^{-3}	65	735	34927	425.7	4436	4.31×10^{10}
VIII-cas2-fb-76e65o	2.51×10^{-3}	65	675	30767	425.6	4435	4.00×10^{10}
VIII-cas2-fb-76e65o	3.98×10^{-3}	65	615	26636	425.5	4435	3.69×10^{10}
VIII-cas2-fb-76e65o	6.31×10^{-3}	65	548	22559	425.3	4435	3.38×10^{10}
VIII-cas2-fb-76e65o	1.00×10^{-2}	65	483	18623	425.0	4435	3.08×10^{10}
VIII-cas2-fb-76e65o	1.58×10^{-2}	65	414	14912	424.5	4434	2.80×10^{10}
VIII-cas2-fb-76e65o	2.51×10^{-2}	65	344	11494	423.7	4434	2.54×10^{10}
VIII-cas2-fb-76e65o	3.98×10^{-2}	65	277	8424	422.4	4434	2.30×10^{10}
VIII-cas2-fb-76e65o	6.31×10^{-2}	65	206	5912	420.1	4433	2.10×10^{10}
VIII-cas2-fb-76e65o	1.00×10^{-1}	65	146	4112	416.8	4433	1.95×10^{10}
VIII-IX-cas4-fb-72e59o	1.00×10^{-4}	59	915	45289	384.4	4028	4.46×10^{10}
VIII-IX-cas4-fb-72e59o	1.58×10^{-4}	59	866	42119	384.4	4028	4.24×10^{10}
VIII-IX-cas4-fb-72e59o	2.51×10^{-4}	59	819	38956	384.4	4028	4.03×10^{10}
VIII-IX-cas4-fb-72e59o	3.98×10^{-4}	59	768	35764	384.4	4028	3.81×10^{10}
VIII-IX-cas4-fb-72e59o	6.31×10^{-4}	59	712	32538	384.4	4027	3.59×10^{10}
VIII-IX-cas4-fb-72e59o	1.00×10^{-3}	59	666	29286	384.4	4027	3.37×10^{10}
VIII-IX-cas4-fb-72e59o	1.58×10^{-3}	59	609	26030	384.3	4027	3.15×10^{10}
VIII-IX-cas4-fb-72e59o	2.51×10^{-3}	59	553	22780	384.3	4027	2.93×10^{10}
VIII-IX-cas4-fb-72e59o	3.98×10^{-3}	59	496	19598	384.1	4027	2.71×10^{10}
VIII-IX-cas4-fb-72e59o	6.31×10^{-3}	59	443	16506	384.0	4027	2.50×10^{10}
VIII-IX-cas4-fb-72e59o	1.00×10^{-2}	59	386	13588	383.7	4026	2.30×10^{10}
VIII-IX-cas4-fb-72e59o	1.58×10^{-2}	59	330	10863	383.3	4026	2.11×10^{10}
VIII-IX-cas4-fb-72e59o	2.51×10^{-2}	59	275	8405	382.7	4026	1.94×10^{10}
VIII-IX-cas4-fb-72e59o	3.98×10^{-2}	59	222	6264	381.6	4025	1.79×10^{10}
VIII-IX-cas4-fb-72e59o	6.31×10^{-2}	59	178	4558	380.2	4025	1.67×10^{10}
VIII-IX-cas4-fb-72e59o	1.00×10^{-1}	59	128	3327	377.6	4024	1.57×10^{10}

Table XXI. (Continued) Double-factorization resource estimates for all steps of carbon dioxide fixation for active space sizes from 52–65 orbitals at a truncation threshold between $\epsilon_{\text{in}} = 0.1\text{mHartree}$ and 0.1Hartree .

Step	ϵ_{in} / Hartree	Orbitals N	R	M	α_{DF} / Hartree	Qubits	#Toffoli gates
IX-cas16-fb-68e62o	1.00×10^{-4}	62	886	45264	396.7	4232	4.67×10^{10}
IX-cas16-fb-68e62o	1.58×10^{-4}	62	834	42011	396.7	4232	4.44×10^{10}
IX-cas16-fb-68e62o	2.51×10^{-4}	62	787	38764	396.7	4232	4.22×10^{10}
IX-cas16-fb-68e62o	3.98×10^{-4}	62	738	35493	396.7	4232	3.99×10^{10}
IX-cas16-fb-68e62o	6.31×10^{-4}	62	686	32226	396.6	4231	3.76×10^{10}
IX-cas16-fb-68e62o	1.00×10^{-3}	62	638	28945	396.6	4231	3.53×10^{10}
IX-cas16-fb-68e62o	1.58×10^{-3}	62	583	25694	396.6	4231	3.30×10^{10}
IX-cas16-fb-68e62o	2.51×10^{-3}	62	532	22504	396.5	4231	3.08×10^{10}
IX-cas16-fb-68e62o	3.98×10^{-3}	62	479	19401	396.4	4231	2.86×10^{10}
IX-cas16-fb-68e62o	6.31×10^{-3}	62	428	16430	396.3	4231	2.65×10^{10}
IX-cas16-fb-68e62o	1.00×10^{-2}	62	379	13616	396.1	4230	2.45×10^{10}
IX-cas16-fb-68e62o	1.58×10^{-2}	62	318	11056	395.6	4230	2.27×10^{10}
IX-cas16-fb-68e62o	2.51×10^{-2}	62	270	8809	395.0	4230	2.10×10^{10}
IX-cas16-fb-68e62o	3.98×10^{-2}	62	227	6887	394.2	4229	1.97×10^{10}
IX-cas16-fb-68e62o	6.31×10^{-2}	62	178	5282	392.8	4229	1.84×10^{10}
IX-cas16-fb-68e62o	1.00×10^{-1}	62	140	4020	390.8	4228	1.75×10^{10}
XVIII-cas4-fb-64e56o	1.00×10^{-4}	56	969	45760	293.6	3712	3.35×10^{10}
XVIII-cas4-fb-64e56o	1.58×10^{-4}	56	921	42665	293.5	3712	3.19×10^{10}
XVIII-cas4-fb-64e56o	2.51×10^{-4}	56	871	39511	293.5	3712	3.02×10^{10}
XVIII-cas4-fb-64e56o	3.98×10^{-4}	56	819	36271	293.5	3712	2.86×10^{10}
XVIII-cas4-fb-64e56o	6.31×10^{-4}	56	762	32962	293.5	3712	2.69×10^{10}
XVIII-cas4-fb-64e56o	1.00×10^{-3}	56	705	29594	293.5	3711	2.51×10^{10}
XVIII-cas4-fb-64e56o	1.58×10^{-3}	56	653	26201	293.5	3711	2.33×10^{10}
XVIII-cas4-fb-64e56o	2.51×10^{-3}	56	592	22796	293.4	3711	2.16×10^{10}
XVIII-cas4-fb-64e56o	3.98×10^{-3}	56	530	19439	293.3	3711	1.98×10^{10}
XVIII-cas4-fb-64e56o	6.31×10^{-3}	56	470	16199	293.1	3710	1.81×10^{10}
XVIII-cas4-fb-64e56o	1.00×10^{-2}	56	400	13174	292.8	3710	1.65×10^{10}
XVIII-cas4-fb-64e56o	1.58×10^{-2}	56	336	10436	292.4	3710	1.51×10^{10}
XVIII-cas4-fb-64e56o	2.51×10^{-2}	56	275	8001	291.7	3709	1.38×10^{10}
XVIII-cas4-fb-64e56o	3.98×10^{-2}	56	216	5884	290.6	3709	1.26×10^{10}
XVIII-cas4-fb-64e56o	6.31×10^{-2}	56	161	4168	288.8	3709	1.17×10^{10}
XVIII-cas4-fb-64e56o	1.00×10^{-1}	56	123	2979	286.8	3708	1.10×10^{10}

Table XXII. Double-factorization resource estimates for all steps of carbon dioxide fixation for active space sizes from 2–250 orbitals at a truncation threshold of $\epsilon_{\text{in}} = 1\text{mHartree}$. Examples with ≤ 20 orbitals marked by (*) are considered classically tractable by FCI methods.

Step	Orbitals N	R	M	α_{DF} /Hartree	λ	Qubits	#Toffoli gates
I-cas5-fb-4e5o	5*	12	54	6.5	0	126	1.3×10^7
I-cas5-fb-14e16o	16*	104	1293	25.6	1	907	2.7×10^8
I-cas5-fb-48e52o	52	613	23566	177.3	3	6879	1.1×10^{10}
I-highCD-cas5-fb-4e5o	5*	12	54	6.5	0	126	1.3×10^7
I-highCD-cas5-fb-14e16o	16*	104	1296	25.6	1	907	2.7×10^8
I-highCD-cas5-fb-48e52o	52	616	23785	177.4	3	6879	1.1×10^{10}
II-cas6-fb-8e6o	6*	15	87	13.7	0	163	3.6×10^7
II-cas6-fb-34e26o	26	203	3822	117.4	1	1624	2.5×10^9
II-cas6-fb-70e62o	62	734	33629	374.4	3	8448	3.1×10^{10}
II-hf-fb-38e33o	33	361	8795	138.6	2	3182	4.6×10^9
II-hf-fb-74e71o	71	935	50506	422.8	4	12086	4.4×10^{10}
II-highCD-cas6-fb-8e6o	6*	15	87	13.7	0	163	3.6×10^7
II-highCD-cas6-fb-34e26o	26	203	3822	117.3	1	1624	2.5×10^9
II-highCD-cas6-fb-70e64o	64	740	33861	374.5	3	8720	3.2×10^{10}
II-III-cas6-fb-8e6o	6*	19	99	12.4	0	163	3.3×10^7
II-III-cas6-fb-38e29o	29	253	5497	144.4	2	2710	3.7×10^9
II-III-cas6-fb-74e65o	65	783	38122	416.0	3	8856	3.7×10^{10}
II-III-highCD-cas6-fb-8e6o	6*	19	99	12.4	0	163	3.3×10^7
II-III-highCD-cas6-fb-38e29o	29	253	5500	144.4	2	2710	3.8×10^9
II-III-highCD-cas6-fb-74e65o	65	789	38364	416.0	3	8856	3.7×10^{10}
V-cas11-fb-12e11o	11*	49	453	31.8	0	317	1.9×10^8
V-cas11-fb-32e25o	24	146	2738	95.5	1	1500	1.7×10^9
V-cas11-fb-68e60o	60	670	29319	372.1	3	8175	2.9×10^{10}
V-highCD-cas11-fb-12e11o	11*	49	453	31.8	0	317	2.0×10^8
V-highCD-cas11-fb-32e24o	24	146	2739	122.1	1	1500	2.2×10^9
V-highCD-cas11-fb-68e60o	60	671	29503	372.7	3	8175	2.9×10^{10}
VIII-cas2-fb-2e2o	2*	3	6	1.3	0	45	8.2×10^5
VIII-cas2-fb-40e29o	29	270	5870	146.2	2	2710	3.9×10^9
VIII-cas2-fb-76e65o	65	794	39088	425.7	3	8856	3.8×10^{10}
VIII-highCD-cas2-fb-2e2o	2*	3	6	1.3	0	45	8.2×10^5
VIII-highCD-cas2-fb-40e29o	29	270	5878	146.2	2	2710	3.9×10^9
VIII-highCD-cas2-fb-76e65o	65	805	39393	425.9	3	8856	3.8×10^{10}
VIII-IX-cas4-fb-4e4o	4*	9	32	3.9	0	97	5.8×10^6
VIII-IX-cas4-fb-36e23o	23	177	3063	121.7	1	1438	2.2×10^9
VIII-IX-cas4-fb-72e59o	59	666	29286	384.4	3	8039	2.9×10^{10}
VIII-IX-highCD-cas4-fb-4e4o	4*	9	32	3.9	0	97	5.8×10^6
VIII-IX-highCD-cas4-fb-36e23o	23	177	3063	121.7	1	1438	2.2×10^9
VIII-IX-highCD-cas4-fb-72e59o	59	668	29417	384.5	3	8039	3.0×10^{10}

Table XXIII. Double-factorization resource estimates for all steps of carbon dioxide fixation for active space sizes from 2–250 orbitals at a truncation threshold of $\epsilon_{\text{in}} = 1\text{mHartree}$. Examples with ≤ 20 orbitals marked by (*) are considered classically tractable by FCI methods.

Step	Orbitals N	R	M	α_{DF} /Hartree	λ	Qubits	#Toffoli gates
IX-cas16-fb-16e16o	16*	80	1050	58.3	1	939	6.0×10^8
IX-cas16-fb-32e26o	26	155	3215	136.4	1	1624	2.8×10^9
IX-cas16-fb-68e62o	62	638	28945	396.6	3	8447	3.1×10^{10}
IX-highCD-cas16-fb-16e16o	16*	80	1050	58.3	1	939	6.0×10^8
IX-highCD-cas16-fb-32e26o	26	155	3215	136.4	2	2430	2.9×10^9
IX-highCD-cas16-fb-68e62o	62	641	29096	396.6	3	8447	3.1×10^{10}
XVIII-cas4-fb-4e4o	4*	9	36	5.2	0	102	8.0×10^6
XVIII-cas4-fb-28e20o	20*	155	2336	71.0	1	1212	1.1×10^9
XVIII-cas4-fb-64e56o	56	705	29594	293.5	3	7407	2.1×10^{10}
XVIII-cas4-fb-100e100o	100	982	75449	781.0	4	18017	1.2×10^{11}
XVIII-cas4-fb-150e150o	150	1462	174699	1919.7	5	34218	5.5×10^{11}
XVIII-cas4-fb-250e250e	250	2276	443046	6793.2	6	70019	3.9×10^{12}
XVIII-highCD-cas4-fb-4e4o	4*	9	36	5.2	0	102	8.0×10^6
XVIII-highCD-cas4-fb-28e20o	20*	155	2337	71.0	1	1212	1.1×10^9
XVIII-highCD-cas4-fb-64e56o	56	712	29763	293.5	3	7407	2.1×10^{10}
XVIII-highCD-cas4-fb-100e100o	100	995	76323	782.1	4	18017	1.2×10^{11}
XVIII-highCD-cas4-fb-150e150o	150	1490	177979	1923.8	5	34218	5.5×10^{11}
XVIII-highCD-cas4-fb-250e250o	250	2362	456067	6806.8	6	70019	4.0×10^{12}

VII. QUBITIZATION OF DOUBLE-FACTORIZED HAMILTONIAN

In this section, we present our approach for qubitizing the double-factorized Hamiltonian. We make heavy use of quantum circuit diagrams, and many of our proofs follow from combining these diagrams. Thus in [Section VII A](#), we define our notation for many standard quantum circuit primitives and their costs. Of particular importance are quantum circuits for data-lookup in [Section VII A 1](#), state preparation in [Section VII A 2](#), block-encoding in [Section VII A 3](#), and qubitization in [Section VII A 4](#). In [Section VII B](#), we also present new optimized constructions of two quantum circuit primitives. These are the programmable rotation gate array in [Section VII B 1](#), which applies a single-qubit rotation with a rotation angle controlled by an integer index, and sparse multiplexed data-lookup in [Section VII B 2](#). These primitives are then combined in our qubitization of the double-factorized Hamiltonian in [Section VII C](#).

A. Standard quantum circuit primitives

In this section, we define quantum circuit primitives and their costs. Throughout, we use the shorthand $n_x \doteq \lceil \log_2 x \rceil$ which is the number of bits needed to store an integer of size x . All the quantum circuits we use are constructed from the following primitive elements.

$$\text{Unitary and its adjoint: } |\psi\rangle_s \text{---} \boxed{U} \text{---} U|\psi\rangle_s, \quad |\psi\rangle_s \text{---} \boxed{U^\dagger} \text{---} U^\dagger|\psi\rangle_s. \quad (2)$$

$$\text{Controlled unitary: } \begin{array}{c} \bullet \\ | \\ \text{---} \\ \boxed{U} \end{array} = |0\rangle\langle 0| \otimes \mathcal{I} + |1\rangle\langle 1| \otimes U. \quad (3)$$

$$\text{Multiplexed unitaries: } \begin{array}{c} \text{---} \langle j \\ \text{---} \\ \boxed{U} \end{array} = \sum_j |j\rangle\langle j| \otimes U_j, \quad \begin{array}{c} \text{---} \langle j \\ \text{---} \langle k \\ \text{---} \\ \boxed{U} \end{array} = \sum_{j,k} |j\rangle\langle j| \otimes |k\rangle\langle k| \otimes U_{j,k}. \quad (4)$$

$$\text{Controlled multiplexed unitary: } \begin{array}{c} \bullet \\ | \\ \text{---} \\ \text{---} \langle j \\ \text{---} \\ \boxed{U} \end{array} = |0\rangle\langle 0| \otimes \mathcal{I} + |1\rangle\langle 1| \otimes \sum_j |j\rangle\langle j| \otimes U_j. \quad (5)$$

$$\text{Data-lookup that XORs } \vec{x}_k \text{ with } \vec{z}: \begin{array}{c} |k\rangle_a \text{---} \langle k \\ \text{---} \\ \text{---} \langle \vec{x}_k \\ \text{---} \\ \boxed{} \end{array} |z\rangle_s = |z \oplus \vec{x}_k\rangle_s = |z_0 \oplus x_{k,0}\rangle \cdots. \quad (6)$$

$$\text{Unitary that prepares } |\vec{a}\rangle: |0\rangle \text{---} \boxed{|\vec{a}\rangle} \text{---} |\vec{a}\rangle = \sum_j \sqrt{\frac{|a_j|}{\|\vec{a}\|_1}} |j\rangle. \quad (7)$$

Unitary that prepares $|\overline{\vec{a}}\rangle$: $|0\rangle \xrightarrow{|\overline{\vec{a}}\rangle} |\overline{\vec{a}}\rangle = \sum_j \text{sign}[a_j] \sqrt{\frac{|a_j|}{\|\vec{a}\|_1}} |j\rangle.$ (8)

Unitary that prepares $|\vec{a}, f\rangle$: $\left. \begin{array}{l} |0\rangle_1 \xrightarrow{f} \\ |0\rangle_2 \xrightarrow{|\vec{a}, f\rangle} \end{array} \right\} |\vec{a}, f\rangle = \sum_j \sqrt{\frac{|a_j|}{\|\vec{a}\|_1}} |f(j)\rangle_1 |j\rangle_2.$ (9)

Block-encoding unitary: $\left. \begin{array}{l} |0\rangle_1 \\ |\psi\rangle_2 \end{array} \right\} \xrightarrow{\mathcal{B}\left[\frac{H}{\alpha}\right]} |0\rangle_1 \frac{H}{\alpha} |\psi\rangle_2 + \dots.$ (10)

The block-encoding of a unitary is trivial: $|\psi\rangle_s \xrightarrow{U} = \mathcal{B}[U] U|\psi\rangle_s.$ (11)

Multiplexed block-encoding unitary: $\left. \begin{array}{l} |0\rangle_1 \\ |\psi\rangle_2 \end{array} \right\} \xrightarrow{\mathcal{B}\left[\frac{H_j}{\alpha_j}\right]} \sum_j |j\rangle \langle j| \otimes \left(|0\rangle_1 \frac{H_j}{\alpha_j} |\psi\rangle_2 + \dots \right).$ (12)

Adding block-encodings: $\left. \begin{array}{l} |0\rangle_{a,1} \\ |0\rangle_{a,2} \\ |\psi\rangle_s \end{array} \right\} \xrightarrow{\mathcal{B}\left[\frac{\sum_j H_j}{\|\vec{\alpha}\|_1}\right]} = \left. \begin{array}{l} |0\rangle_{a,1} \xrightarrow{|\vec{a}\rangle} \\ |0\rangle_{a,2} \xrightarrow{\mathcal{B}\left[\frac{H_j}{\alpha_j}\right]} \\ |\psi\rangle_s \end{array} \right\} |0\rangle_a \frac{\sum_j H_j}{\|\vec{\alpha}\|_1} |\psi\rangle_s + \dots.$ (13)

Multiplying block-encodings: (14)

$\left. \begin{array}{l} |0\rangle_{a,1} \\ |0\rangle_{a,2} \\ |0\rangle_{a,3} \\ |\psi\rangle_s \end{array} \right\} \xrightarrow{\mathcal{B}\left[\frac{H_1 H_2}{\alpha_1 \alpha_2}\right]} = \left. \begin{array}{l} |0\rangle_{a,1} \xrightarrow{|11\rangle} \\ |0\rangle_{a,2} \xrightarrow{\mathcal{B}\left[\frac{H_1}{\alpha_1}\right]} \\ |0\rangle_{a,3} \xrightarrow{\mathcal{B}\left[\frac{H_2}{\alpha_2}\right]} \\ |\psi\rangle_s \end{array} \right\} |0\rangle_a \frac{H_1 H_2}{\alpha_1 \alpha_2} |\psi\rangle_s + \dots.$ (15)

The costs of these quantum circuits are expressed in terms of primitive quantum gates and qubits. We define primitive quantum gates as those acting on at most two qubits, and we distinguish between Clifford gates $\{\text{HAD}, S, \text{CNOT}\}$, and the non-Clifford T gate. Note that we denote the Hadamard gate as HAD instead of the more traditional symbol H to avoid confusion with the Hamiltonian. Some of these circuits may be implemented by ancilla qubits in addition to the ‘register’ qubits. Typically, we do not show the ancilla qubits in the diagrams and implicitly assume that these invisible qubits are all borrowed, meaning that they are returned to the same initial state at the end of the circuit. We call these ancilla qubits ‘clean’ if their initial state is the computational basis state $|0\rangle$. In contrast, We call these ancilla qubits ‘dirty’ if their initial is arbitrary and unknown.

In some cases, a quantum circuit U is approximated by U' to some error $\|U - U'\| \leq \epsilon$ in spectral norm. The errors of multiple approximate quantum circuits add linearly, following the triangle inequality

$$\|U_0 U_1 \dots U_{N-1} - U'_0 U'_1 \dots U'_{N-1}\| \leq \sum_{j \in [N]} \|U_j - U'_j\|. \quad (16)$$

1. Data-lookup oracle

Given a list of d bit-strings $\vec{a} \in \{0, 1\}^{d \times b}$, each of length b , the data-lookup oracle in Eq. (6) returns the bit-string a_x , that is $D|x\rangle|z\rangle = |x\rangle|z \oplus a_x\rangle$. In addition to the $b + \lceil \log_2(d) \rceil$ qubits needed to store its inputs and outputs, this oracle has the following cost.

Lemma 1 (Data-lookup oracle [30]). *The data-lookup oracle in Eq. (6) and its controlled version can be implemented using*

- Toffoli gates: $(d - 1)$.
- Clifford gates: $\Theta(db)$.
- Clean ancillary qubits: $\lceil \log_2(d) \rceil$.

According to Low et al. [31], the Toffoli gate cost of data-lookup can be further reduced by adding λb additional qubits, where $\lambda \geq 0$ is an integer. These qubits can be clean, meaning they start in and are returned to the computational basis state $|0\rangle$. Circuit optimizations by Berry et al. [26] further reduce the cost by constant factors.

Lemma 2 (Data-lookup oracle with clean qubit assistance [26, 31]). *For any integer $\lambda \geq 0$, the data-lookup oracle in Eq. (6) and its controlled version can be implemented using*

- Toffoli gates: $d/(1 + \lambda) + \lambda b + \mathcal{O}(\log d)$.
- Clifford gates: $\Theta(db)$.
- Clean ancillary qubits: $\lambda b + \lceil \log_2(d/\lambda) \rceil + \mathcal{O}(1)$.

Note that the additional $\mathcal{O}(1)$ clean qubits and $\mathcal{O}(\log(d))$ Toffoli gates only needed when $1 + \lambda$ is not a power of two. In this case, they are used in an intermediate step to reversibly compute the remainder and quotient of $j/(1 + \lambda)$, where the numerator $j \in [N]$ is stored in a n_d qubit register. In the following, we will omit this additive cost as it is subdominant in all our applications. We find it useful to define the Toffoli gate count function

$$D_{d,b,\lambda} = \min_{\lambda' \in [0, \lambda]} (d/(1 + \lambda') + \lambda' b) \gtrsim \min \left[d, 2\sqrt{bd} \right], \quad (17)$$

which returns the smallest possible Toffoli gate count for any number of λ available clean qubits. The bit-strings output by these lookup oracles may be uncomputed by applying their adjoint. This doubles their gate complexity at most. However, the gate complexity of uncomputation can be further improved [26] used measurement-based uncomputation. By using $\lambda + \mathcal{O}(\log(d/\lambda))$ qubits, measurement-based uncomputation of data-lookup reduces the additive λb Toffoli gate term to λ , which becomes significant when $\lambda b \sim \sqrt{bd}$. More importantly, any garbage qubits produced by Lemma 2 can be measured and the results stored in classical memory for later uncomputation. This frees up clean ancilla qubits and means that the λ parameter for uncomputation can be optimized separately from that of computation in reducing Toffoli costs. Thus we also find it useful to define the cost of uncomputation as

$$\text{DU}_{d,b,\lambda} = \min_{\lambda' \in [0, \lambda]} (d/(1 + \lambda') + \lambda') \gtrsim \min \left[d, 2\sqrt{d} \right]. \quad (18)$$

In most of the cases we consider, uncomputation of data-lookup is an order of magnitude cheaper than computation.

These assisting qubits can also be dirty, meaning that start in and are returned to the same initial state. This is useful whenever the quantum algorithm has any idling qubits. To simplify notation in the following, we will assume that λ is a power of two.

Lemma 3 (Data-lookup oracle with dirty qubit assistance [26, 31]). *For any integer $\lambda \geq b$ such that $1 + \lambda$ is a power of two, the data-lookup oracle in Eq. (6) and its controlled version can be implemented using*

- *Toffoli gates:* $2d/(1 + \lambda) + 4\lambda b$.
- *Clifford gates:* $\Theta(db)$.
- *Clean ancillary qubits:* $\lceil \log_2(d/\lambda) \rceil$.
- *Dirty ancillary qubits:* λb .

Note that when $\lambda \leq 1$, there is no advantage over the original construction in Lemma 1. We find it useful to define the Toffoli gate count function

$$\begin{aligned} D_{d,b,\lambda \text{ dirty}} &= \min_{\lambda' \in [1, \lambda]} (d, 2d/(1 + \lambda') + 4\lambda'b) \gtrsim \min [d, 4\sqrt{2bd}], \\ DU_{d,b,\lambda \text{ dirty}} &= \min_{\lambda' \in [1, \lambda]} (d, 2d/(1 + \lambda') + 4\lambda') \gtrsim \min [d, 4\sqrt{2d}], \end{aligned} \quad (19)$$

which returns the smallest possible Toffoli gate count for any number of λ available dirty qubits. Note a slight difference in notation compared to Eq. (18) – there, the last subscript λ is the number of times the output register is duplicated, whereas the last subscript λb parameterizes the total number of dirty qubits available. Similar to the case using clean qubits, the Toffoli cost of uncomputation is less than that of computation [26].

2. State preparation unitary

Quantum state preparation is a unitary circuit that prepares a desired quantum state.

A number of different quantum circuit implementations of Eqs. (7) and (8) are known, each with different trade-offs in qubit count, and the various quantum gates. For instance, the approach by Shende et al. [32] uses $\lceil \log_2 d \rceil$ qubits and d arbitrary single-qubit rotations, and $\mathcal{O}(d)$ other two-qubit Clifford gates.

For our purposes, it suffices to prepare quantum states where each $|j\rangle$ is, in general, entangled with some arbitrary quantum state $|\text{Garbage}_j\rangle$.

$$|\vec{a}\rangle = \sum_{j=0}^{d-1} \sqrt{\frac{|a_j|}{\|\vec{a}\|_1}} |j\rangle |\text{Garbage}_j\rangle \quad (20)$$

As this includes Eq. (7) as a special case, quantum circuits for state preparation with garbage can use fewer T gates, though at the expense of more qubits. This garbage state may be safely ignored in the remainder of this manuscript, so we do not differentiate between the

state preparation unitaries of Eq. (7) and Eq. (20). Moreover, the circuits for $|\vec{a}\rangle$ and $|\overline{\vec{a}}\rangle$ are very similar and have the same T gate cost. We will repeatedly invoke the following implementation which approximates each coefficient to a targeted precision.

Lemma 4 (Approximate quantum state preparation with garbage [30]). *Given a list of d positive coefficients $\vec{a} \in \mathbb{R}^d$ and the desired bits of precision μ , the quantum state*

$$|\psi\rangle = \sum_{j=0}^{d-1} \sqrt{p_j} |j\rangle |\text{Garbage}_j\rangle, \quad (21)$$

where $\left| p_j - \frac{a_j}{\|\vec{a}\|_1} \right| \leq \frac{2^{-\mu}}{d}$ (which implies that $\left\| \vec{p} - \frac{\vec{a}}{\|\vec{a}\|_1} \right\|_1 \leq 2^{-\mu}$) can be prepared by a unitary U that is implemented using one application of any data-lookup oracle from Section VII A 1 for d bit-strings of length $\lceil \log_2(d) \rceil + \mu$. The total cost for implementing U is given by:

- Toffoli gates: $\mu + D_{d, \lceil \log_2(d) \rceil + \mu, \lambda} + \Theta(\log(d))$.
- Arbitrary single-qubit rotations: 1.
- Clifford gates: $\Theta(d\mu)$.
- Garbage qubits: $2\mu + n_d$.
- Clean qubits: $n_d + \mathcal{O}(1)$.
- Dirty qubits: λ .

Our implementation of Lemma 4 introduces a small modification that is useful for synthesizing the multiplexed version of state preparation. In the original procedure [30], let $L = \lceil \log_2(d) \rceil$ be the number of bits needed to store any integer between 0 and $d - 1$, and let μ be the bits of precision to which p_j/d is specified. Then one prepares a uniform superposition over $d \times 2^\mu$ elements $\frac{1}{\sqrt{d}} \sum_{j=0}^{d-1} |j\rangle |+\rangle^{\otimes \mu}$ and applies data-lookup that writes out two bitstrings $k = f(j) \in [d]$ and $\tilde{p}_j \in [2^\mu]$. Note that the map from j to $f(j)$ can be surjective so $f^{-1}(k) = \{j : f(j) = k\}$. This produces the state

$$\frac{1}{\sqrt{d}} \sum_{j=0}^{d-1} |j\rangle |f(j)\rangle |+\rangle^{\otimes \mu} |\tilde{p}_j\rangle. \quad (22)$$

Let COMP be a unitary that compares two integers x, y and writes the result in a qubit.

$$\text{COMP}|x\rangle|y\rangle|0\rangle = |x\rangle|y\rangle|x \geq y\rangle. \quad (23)$$

When applied to compare $|+\rangle^{\otimes \mu}$ and $|\tilde{p}_j\rangle$, this results in

$$\frac{1}{\sqrt{d}} \sum_{j=0}^{d-1} |j\rangle |f(j)\rangle \left(\sqrt{\frac{\tilde{p}_j}{2^\mu}} |\phi_j\rangle |0\rangle + \sqrt{\frac{2^\mu - \tilde{p}_j}{2^\mu}} |\chi_j\rangle |1\rangle \right), \quad (24)$$

For instance, we have the following approximation due to error in the coefficient of the quantum state.

Lemma 6 (Approximate block-encoding using approximate state preparation). *Using the approximate state preparation circuit of Lemma 4 with precision parameter μ in the block-encoding circuit of Definition 1 produces an ϵ -approximate block-encoding $\mathcal{B}_\epsilon [H/\|\vec{a}\|_1]$, where $\epsilon = 2^{-\mu}$.*

Proof. Let \vec{p} be such that $\|\vec{p} - \vec{a}/\|\vec{a}\|_1\|_1 \leq 2^{-\mu}$. Let $H' = \sum_j p_j U_j$, and $H = \sum_j a_j U_j$. Then

$$\left\| \frac{H}{\|\vec{a}\|_1} - H' \right\| = \left\| \sum_j \left(\frac{a_j}{\|\vec{a}\|_1} - p_j \right) U_j \right\| \leq 2^{-\mu}. \quad (31)$$

□

4. Qubitization

We also use the following result on qubitization, which is a generalization of quantum walks.

Theorem 1 (Qubitization). *Let $\mathcal{B} [H]$ be a block-encoding of a Hamiltonian H with spectral norm $\|H\| \leq 1$, and an ancillary register with M qubits. Then there is a quantum circuit $\mathcal{B} [T_j[H]]$ that block-encodes $T_j[H]$, where $T_j[x] = \cos(j \cos^{-1}(x))$ is a Chebyshev polynomial of the first kind.*

$$\mathcal{B} [H] = \begin{pmatrix} H & \cdots \\ \vdots & \ddots \end{pmatrix} \Rightarrow \mathcal{B} [T_j[H]] = \begin{pmatrix} T_j[H] & \cdots \\ \vdots & \ddots \end{pmatrix}. \quad (32)$$

In particular, following the work of Low and Chuang [33], this circuit

$$\begin{array}{c} |0\rangle_a \\ |\psi\rangle_s \end{array} \begin{array}{|c} \boxed{\mathcal{B} [T_j[H]]} \\ \hline \end{array} = \underbrace{\begin{array}{|c} \boxed{\mathcal{B} [H]} \quad \boxed{\text{REF}} \quad \boxed{\mathcal{B} [H]^\dagger} \quad \boxed{\text{REF}} \quad \cdots \quad \boxed{\mathcal{B} [H]} \\ \hline \end{array}}_{\text{Alternate } \mathcal{B} [H] \text{ and } \mathcal{B} [H]^\dagger \text{ } j \text{ times.}} \left. \vphantom{\begin{array}{|c} \boxed{\mathcal{B} [H]} \quad \boxed{\text{REF}} \quad \boxed{\mathcal{B} [H]^\dagger} \quad \boxed{\text{REF}} \quad \cdots \quad \boxed{\mathcal{B} [H]} \\ \hline \end{array}} \right\} |0\rangle_a T_j [H] |\psi\rangle_s + \cdots, \quad (33)$$

costs j total queries to $\mathcal{B} [H]$ and its inverse, and $j - 1$ reflections $\text{REF} = 2|0\rangle\langle 0|_a - \mathcal{I}_a$ on the ancilla register.

Each reflection can be understood as a multi-controlled Z gate, and so has a Toffoli cost equal to the number of qubits it acts on.

B. New quantum circuit primitives

1. Programmable rotation gate array

In this section, we present an implementation of the multiplexed single-qubit Z -rotation gate. Given a list of N angles $\vec{\theta}$ where each $\theta_k = \sum_{b=0}^{\beta-1} \theta_{k,b}/2^{1+b} \in [0, 1 - 2^{-\beta}]$ is specified to

β bits of precision, we synthesize the unitary

$$\begin{array}{c} \langle k | \\ \hline e^{i2\pi\theta_k Z} \\ \hline |k\rangle \end{array} = \sum_{k \in [N]} |k\rangle\langle k| \otimes e^{i2\pi\theta_k Z} = \begin{array}{c} \langle k | \\ \hline e^{i2\pi\theta_{k,0} Z/2^1} \\ \hline \end{array} \begin{array}{c} \langle k | \\ \hline e^{i2\pi\theta_{k,1} Z/2^2} \\ \hline \end{array} \cdots \begin{array}{c} \langle k | \\ \hline e^{i2\pi\theta_{k,\beta-1} Z/2^\beta} \\ \hline \end{array}. \quad (34)$$

For brevity, let $R_b = e^{i2\pi Z/2^{1+b}}$, and $R_{-1}^\theta = e^{i2\pi\theta Z}$.

In our approach, we define a data register with κ qubits that will store κ bits of θ_k . Let $\vec{\theta}_{k, [\mu: \mu+\kappa-1]} = (\theta_{k,\mu}, \theta_{k,\mu+1}, \dots, \theta_{k,\mu+\kappa-1})$. Now define the data-lookup oracle that outputs κ contiguous bits of θ_k , conditioned on index k .

$$\begin{array}{c} |k\rangle_a \\ \hline \langle k | \\ \hline |\vec{z}\rangle_s \xrightarrow{\kappa} \vec{\theta}_{k, [\mu: \mu+\kappa-1]} \\ \hline |z \oplus \theta_{k,\mu} \theta_{k,\mu+1} \cdots \theta_{k,\mu+\kappa-1}\rangle_s \end{array}. \quad (35)$$

Then Eq. (34) is implemented by the following circuit.

$$\begin{array}{c} \langle k | \\ \hline |0\rangle \\ \vdots \\ |0\rangle \\ \hline e^{i2\pi\theta_k Z} \end{array} = \begin{array}{c} \langle k | \\ \hline \vec{\theta}_{k, [0: \kappa-1]}^\dagger \\ \hline R_0 \end{array} \cdots \begin{array}{c} \langle k | \\ \hline \vec{\theta}_{k, [(\kappa-1): 2\kappa-1]}^\dagger \\ \hline R_{\kappa-1} \end{array} \begin{array}{c} \langle k | \\ \hline \vec{\theta}_{k, [\kappa: 2\kappa-1]}^\dagger \\ \hline R_\kappa \end{array} \cdots \begin{array}{c} \langle k | \\ \hline \vec{\theta}_{k, [2\kappa-1: 3\kappa-1]}^\dagger \\ \hline R_{2\kappa-1} \end{array} \cdots |0\rangle^{\otimes \kappa}. \quad (36)$$

With only κ qubits, clearly $\lceil b/\kappa \rceil$ slices of the circuit within the dotted regions are required. Note that the middle pair of data-lookup oracles in the j^{th} slice can be merged also into one that writes the bits $\vec{\theta}_{k, [j\kappa: (j+1)\kappa-1]} \oplus \vec{\theta}_{k, [(j+1)\kappa: (j+2)\kappa-1]}$. Accounting for this merging, this circuit applies $\lceil b/\kappa \rceil + 1$ data-lookup oracles each storing at most κ entries.

Another useful situation is where arbitrary unitaries are applied on the system register are interspersed between M multiplexed rotations.

$$\begin{array}{c} \langle k | \\ \hline R_{-1}^{(\theta_0)_k} \\ \hline U_0 \\ \hline R_{-1}^{(\theta_1)_k} \\ \hline U_1 \\ \hline R_{-1}^{(\theta_2)_k} \\ \hline U_2 \\ \hline \cdots \\ \hline U_{M-2} \\ \hline R_{-1}^{(\theta_{M-1})_k} \end{array}. \quad (37)$$

We may use the same construction as in Eq. (36) to implement this. The number of data-lookup oracles required is then $M\lceil b/\kappa \rceil + 1$. We may reduce this to just $\lceil Mb/\kappa \rceil + 1$. When b is not an integer multiplier of κ , the data-lookup in the last slice might store fewer than κ entries. Thus we fill these empty entries with bit-strings from the next data-lookup. This filling procedure is illustrated by the following example, where the bits of precision $b = 2 \leq \kappa = 3$.

$$\begin{array}{c} \langle k | \\ \hline |0\rangle \\ |0\rangle \\ |0\rangle \\ \hline R_0 \quad R_1 \\ \hline U \\ \hline R_0 \quad R_1 \end{array} = \begin{array}{c} \langle k | \\ \hline (\theta_0, \phi_1, \phi_0)^\dagger \\ \hline R_0 \quad R_1 \\ \hline U \\ \hline R_0 \\ \hline (\theta_0, \phi_1, \phi_0)^\dagger \\ \hline (\phi_1)^\dagger \\ \hline (\phi_1)^\dagger \end{array}. \quad (38)$$

In the case where many data qubits are available $\kappa \gg b$, we may similarly merge multiple bit-strings into the same lookup oracle. Thus, the Toffoli cost of Eq. (37) is equal to $\lceil Mb/\kappa + 1 \rceil$ data lookup oracles with K bit-strings of length κ in addition to that of all the U_j . Moreover, the number of qubits required for the data and index k is equals to $\kappa + \lceil \log_2(M) \rceil$. It is valuable to express these costs with respect to a tunable number of qubits κ . According to Section VII A 1, the Toffoli gate cost of data-lookup with K elements that outputs κ bits an be reduced by using λ ancillary qubits. When these qubits are clean, the Toffoli cost is $K/\lceil 1 + \frac{\lambda}{\kappa} \rceil + \lambda$. Thus the Toffoli count of all the data-lookup oracles is

$$\left\lceil \frac{Mb}{\kappa} + 1 \right\rceil \left(K / \left\lceil 1 + \frac{\lambda}{\kappa} \right\rceil + \lambda \right), \quad (39)$$

which is minimized by choosing $\lambda \sim \sqrt{K\kappa}$.

We now bound the bits of precision required to approximate Eq. (37) to an overall error of ϵ in the spectral norm. Suppose we are given angles $\vec{\theta}_{\text{exact}}$ that are real numbers. Then the error of approximating each angle $\theta_{\text{exact},k}$ with a β -bit number θ_k is at most $2^{-\beta-1}$. Thus the error of each rotation compared to its binary approximation is $\|R_{-1}^{\theta_{\text{exact},k}} - R_{-1}^{\theta_k}\| \leq \|R^{2^{-\beta-1}} - \mathcal{I}\| = \|\cos(2^{-\beta}\pi) - i\sin(2^{-\beta}\pi)Z - \mathcal{I}\| = \sqrt{(\cos(2^{-\beta}\pi) - 1)^2 + \sin^2(2^{-\beta}\pi)} = \sqrt{2}|\sin(2^{-\beta}\pi)| \leq \pi 2^{-\beta+1/2}$. The cumulative error $\epsilon \leq M\pi 2^{-\beta+1/2}$ of all rotations then follows by the triangle inequality on unitary operators $\|(\prod_j U_j) - (\prod_j \tilde{U}_j)\| \leq \sum_j \|U_j - \tilde{U}_j\|$. Thus the bits of precision required is

$$\beta = \left\lceil \frac{1}{2} + \log_2 \left(\frac{M\pi}{\epsilon} \right) \right\rceil. \quad (40)$$

There can be an additional error introduced from approximating each single-qubit rotation gate with Clifford + T gates. However, using the phase gradient technique [34] eliminates this error with a worst-case cost of one Toffoli gate per R_b rotation.

2. Multiplexed sparse data-lookup

In this section, we describe an implementation of a multiplexed data-lookup oracle. This can be non-trivial as standard data-lookup constructions [30, 31] are controlled by a single index register. Whereas in this case, there can be two or more index registers such as below.

$$\begin{array}{l} |j\rangle_a \text{---} \langle j \rangle \text{---} |j\rangle_a \\ |k\rangle_b \text{---} \langle k \rangle \text{---} |k\rangle_b \\ |\vec{z}\rangle_s \text{---} \langle \vec{x}_{j,k} \rangle \text{---} |z \oplus \vec{x}_{j,k}\rangle_s = |z_0 \oplus x_{j,k,0}\rangle |z_0 \oplus x_{j,k,1}\rangle \cdots \end{array} \quad (41)$$

In the above, $j \in [J]$ and $k \in [K]$. Thus there are at most KJ bit-strings $\vec{x}_{j,k}$. One solution is to map the indices (j, k) to a unique integer $q = jK + k$. Thus Eq. (41) can be implemented by a data-lookup oracle controlled by a single index $q \in [JK]$, combined with an arithmetic circuit that computes q from j and k as follows.

$$\begin{array}{l} |j\rangle_a \text{---} \boxed{q = jK + k} \text{---} \langle q \rangle \text{---} |j\rangle_a \\ |k\rangle_b \text{---} \boxed{q = jK + k} \text{---} \langle q \rangle \text{---} |k\rangle_b \\ |\vec{z}\rangle_s \text{---} \boxed{\vec{x}_q} \text{---} |z \oplus \vec{x}_{j,k}\rangle_s \end{array} \quad (42)$$

□

In most applications, particularly later when we use this to block-encode the molecular Hamiltonian, the total number of bit-strings Q is significantly larger than J . Thus the cost of computation in [Lemma 7](#) is dominated by $D_{Q,b,\lambda} + \mathcal{O}(n_Q + D_{J,n_Q,n})$.

C. Double-factorized Hamiltonian

The electronic Hamiltonian in first-quantization is

$$H_{\text{first}} = \left(- \sum_{n \in \text{electrons}} \frac{\nabla_n^2}{2} - \sum_{m \in \text{nuclei}} \frac{Z_m}{|x_n - r_m|} \right) + \left(\sum_{n_1, n_2 \in \text{electrons}} \frac{1}{|x_{n_1} - x_{n_2}|} \right), \quad (44)$$

where ∇_n^2 is the Laplace operator on the n^{th} electron, Z_m is the nuclear charge, and r_m is the nucleus coordinate. By choosing a basis of orbitals $\psi_i(x)$, this implies the second-quantized representation

$$\begin{aligned} H &= \sum_{ij,\sigma} h_{ij} a_{(i,\sigma)}^\dagger a_{(j,\sigma)} + \frac{1}{2} \sum_{ijkl,\sigma\rho} h_{ijkl} a_{(i,\sigma)}^\dagger a_{(k,\rho)}^\dagger a_{(l,\rho)} a_{(j,\sigma)}, \quad (45) \\ h_{ij} &= \int \psi_i^*(x_1) \left(-\frac{\nabla^2}{2} - \sum_m \frac{Z_m}{|x_1 - r_m|} \right) \psi_j(x_1) d^3x_1, \\ h_{ijkl} &= \int \psi_i^*(x_1) \psi_j(x_1) \left(\frac{1}{|x_1 - x_2|} \right) \psi_k^*(x_2) \psi_l(x_2) d^3x_1 d^3x_2. \end{aligned}$$

This is equal to the single-factorized H_{CD} and double-factorized H_{DF} Hamiltonians

$$\begin{aligned} H_{\text{CD}} &\doteq \sum_{ij,\sigma} \tilde{h}_{ij} a_{(i,\sigma)}^\dagger a_{(j,\sigma)} + \frac{1}{2} \sum_{r \in [R]} \left(\sum_{ij,\sigma} L_{ij}^{(r)} a_{(i,\sigma)}^\dagger a_{(j,\sigma)} \right)^2, \quad \tilde{h}_{ij} \doteq h_{ij} - \frac{1}{2} \sum_l h_{illj}, \quad (46) \\ H_{\text{DF}} &= \sum_{ij,\sigma} \tilde{h}_{ij} a_{(i,\sigma)}^\dagger a_{(j,\sigma)} + \frac{1}{2} \sum_{r \in [R]} \left(\sum_{ij,\sigma} \sum_{m \in [M^{(r)}]} \lambda_m^{(r)} \vec{R}_{m,i}^{(r)} \cdot \vec{R}_{m,j}^{(r)\top} a_{(i,\sigma)}^\dagger a_{(j,\sigma)} \right)^2, \end{aligned}$$

where the $\lambda_m^{(r)}$ are eigenvalues of $L^{(r)}$.

The dominant cost in qubitizing a Hamiltonian is the synthesis of a unitary quantum circuit $\mathcal{B}[H/\alpha]$ with the property

$$\mathcal{B}[H/\alpha] = \begin{pmatrix} H/\alpha & \cdots \\ \vdots & \ddots \end{pmatrix}. \quad (47)$$

This implies that $\mathcal{B}[H/\alpha] |0\rangle_a |\psi\rangle_s = |0\rangle_a \frac{H}{\alpha} |\psi\rangle_s + |0\psi^\perp\rangle_{as}$, where the unnormalized residual state $|0\psi^\perp\rangle_{as}$ has no support on the ancilla state $|0\rangle_a$. As H is embedded in a contiguous block of the unitary, we say that $\mathcal{B}[H/\alpha]$ ‘block-encodes’ the Hamiltonian H .

The block-encoding framework supports the addition and multiplication of encoded matrices. For instance, one may add block-encoded Hamiltonians $H = \sum_j H_j$ with a new normalizing constant such as $\alpha = \sum_j \alpha_j$, using the following quantum circuit

$$\mathcal{B}[H/\alpha] = \left(\sum_j \langle j|_a \otimes \mathcal{I}_s \sqrt{\frac{\alpha_j}{\alpha}} \right) \left(\sum_j |j\rangle\langle j|_a \otimes \mathcal{B}[H_j/\alpha_j] \right) \left(\sum_j \sqrt{\frac{\alpha_j}{\alpha}} |j\rangle_a \otimes \mathcal{I}_s \right). \quad (48)$$

As mentioned in eq. (14), block-encoded Hamiltonians may also be multiplied to obtain $\mathcal{B}[H_2 H_1 / \alpha_2 \alpha_1]$. In general, these addition and multiplication operations increase the ancilla register size in a straightforward manner. Using these ingredients, one may block-encode matrices specified by a variety of common input models, such as sparse matrix oracle, linear-combination-unitaries, or other quantum data structures.

In qubitizing H_{DF} , we find it more natural to work in the Majorana representation of the fermion operators

$$\gamma_{p,0} = a_p + a_p^\dagger, \quad \gamma_{p,1} = -i(a_p - a_p^\dagger), \quad \{\gamma_{p,x}, \gamma_{q,y}\} = 2\delta_{pq}\delta_{xy}\mathcal{I}. \quad (49)$$

Thus $a_p = (\gamma_{p,0} + i\gamma_{p,1})/2$ and $a_q = (\gamma_{p,0} - i\gamma_{p,1})/2$, where $p \doteq (i, \sigma)$ is a combined orbital and spin index. Some useful identities are

$$a_{(i,\sigma)}^\dagger a_{(j,\sigma)} + a_{(j,\sigma)}^\dagger a_{(i,\sigma)} = \begin{cases} \mathcal{I} + i(\gamma_{i,\sigma,0}\gamma_{i,\sigma,1}), & i = j, \\ \frac{i}{2}(\gamma_{i,\sigma,0}\gamma_{j,\sigma,1} + \gamma_{j,\sigma,0}\gamma_{i,\sigma,1}), & i \neq j, \end{cases} \quad (50)$$

which implies the Majorana representation for one-electron Hamiltonian

$$\sum_{ij,\sigma} L_{ij} a_{(i,\sigma)}^\dagger a_{(j,\sigma)} = \sum_i L_{ii} \mathcal{I} + \text{One}_L, \quad \text{One}_L \doteq \frac{i}{2} \sum_{ij} \sum_{\sigma} L_{ij} \gamma_{i,\sigma,0} \gamma_{j,\sigma,1} \quad (51)$$

that separates into a trivial identity component, and a non-trivial one-electron component One_L . As L is a symmetric matrix, it has the eigendecomposition $L = \sum_k \lambda_k \vec{R}_k \cdot \vec{R}_k^\top$. Thus we may diagonalize the one-electron Hamiltonian to obtain

$$\text{One}_L = \frac{i}{2} \sum_k \lambda_k \sum_{\sigma} \gamma_{\vec{R}_k, \sigma, 0} \gamma_{\vec{R}_k, \sigma, 1}, \quad \gamma_{\vec{u}, \sigma, x} \doteq \sum_j u_j \gamma_{j, \sigma, x}. \quad (52)$$

One should verify that $\gamma_{\vec{u}, \sigma, x}^2 = \mathcal{I}$, which follows from Eq. (49) and the unit-length normalization Eq. (52) of \vec{u} .

Thus the spectral norm $\|\text{One}_L\| = \|L\|_{\text{SC}}$ is seen to be the one-norm of the eigenvalues of L . Substituting the Majorana representation into the doubly-factorized Hamiltonian results in

$$H_{\text{DF}} = \left(\sum_i h_{ii} - \frac{1}{2} \sum_{il} h_{illi} + \frac{1}{2} \sum_{il} h_{llii} \right) \mathcal{I} + \text{One}_{L^{(-1)}} + \frac{1}{2} \sum_r \text{One}_{L^{(r)}}^2, \quad (53)$$

$$L_{ij}^{(-1)} \doteq h_{ij} - \frac{1}{2} \sum_l h_{illj} + \sum_l h_{llij}.$$

Our strategy for block-encoding Eq. (53) is to build it up from block-encodings of its component pieces. Let us further collect terms as follows.

$$\begin{aligned}
H_{\text{DF}} &= \left(\sum_i h_{ii} - \frac{1}{2} \sum_{il} h_{illi} + \frac{1}{2} \sum_{il} h_{llii} + \frac{1}{4} \sum_r \|L^{(r)}\|_{\text{SC}}^2 \right) \mathcal{I} + \text{One}_{L^{(-1)}} + \text{Two}_H, \\
\text{Two}_H &\doteq \frac{1}{4} \sum_r \|L^{(r)}\|_{\text{SC}}^2 T_2 \left[\frac{\text{One}_{L^{(r)}}}{\|L^{(r)}\|_{\text{SC}}} \right],
\end{aligned} \tag{54}$$

where $T_2(x) = 2x^2 - 1$ is a Chebyshev polynomial of the first kind. The identity term only contributes a constant shift in energy and may be ignored. Observe that we have reduced the double-factorized Hamiltonian to sums of products of basis-rotated Majorana operators $\gamma_{\vec{u},\sigma,x}$.

We thus block-encode the two-body term as follows.

1. Block-encode $\mathcal{B}[\gamma_{\vec{u},\sigma,x}]$ of the basis transformed Majorana operator [Section VII C 1](#).
2. Block-encode $\mathcal{B}[\gamma_{\vec{u},\sigma,0}\gamma_{\vec{u},\sigma,1}]$ by multiplying $\mathcal{B}[\gamma_{\vec{u},\sigma,x}]$ [Section VII C 2](#).
3. Block-encode $\mathcal{B}\left[\frac{\text{One}_L}{\|L\|_{\text{SC}}}\right]$ by taking a linear combination of $\lambda_k \mathcal{B}\left[\gamma_{\vec{R}_k,\sigma,0}\gamma_{\vec{R}_k,\sigma,1}\right]$ over the eigenvalues and eigenvectors of L and the spins [Section VII C 3](#).
4. Block-encode $\mathcal{B}\left[T_2\left[\frac{\text{One}_L}{\|L\|_{\text{SC}}}\right]\right]$ by applying $\mathcal{B}\left[\frac{\text{One}_L}{\|L\|_{\text{SC}}}\right]$ twice using qubitization [\[33\]](#).
5. Block-encode $\mathcal{B}\left[\frac{\text{Two}_H}{\frac{1}{4}\sum_r \|L^{(r)}\|_{\text{SC}}^2}\right]$ by taking a linear combination of $\|L^{(r)}\|_{\text{SC}}^2 \mathcal{B}\left[T_2\left[\frac{\text{One}_{L^{(r)}}}{\|L^{(r)}\|_{\text{SC}}}\right]\right]$ over the rank components of the two-electron tensor [Section VII C 4](#).
6. Block-encode $\mathcal{B}\left[\frac{H_{\text{DF}}}{\|L^{(-1)}\|_{\text{SC}} + \frac{1}{4}\sum_r \|L^{(r)}\|_{\text{SC}}^2}\right]$ by adding one- and two-body terms [Section VII C 5](#).

Generally, the cost of block-encoding the large number of two-electron terms dominate that of the smaller number of one-electron terms. A common theme throughout will be the use of symmetries. Many coefficients turn out to be identical. For instance, $L_{ij}^{(r)} = L_{ji}^{(r)}$, and is independent of spin. Moreover, the same coefficients $\vec{R}_k^{(r)}$ occur in both of $\gamma_{\vec{u},\sigma,0}\gamma_{\vec{u},\sigma,1}$. Wherever possible, we use this redundancy to optimize the number of bits of classical data we need to encode into our quantum circuits. These optimizations are combined with recent advances using ancillary qubits [\[31\]](#) to substantially reduce Toffoli gate count

We now provide optimized quantum circuits that implement the above steps. We make heavy use of quantum circuit notation, outlined in [Section VII A](#).

1. Block-encoded, basis-transformed Majorana operator

We synthesize the basis-transformed Majorana operator $\gamma_{\vec{u},\sigma,x}$ by conjugating $\gamma_{0,\sigma,x}$ with a sequence of unitary rotations. The required sequence of unitary rotations follows from the following observation.

Lemma 8 (Sum of Majorana operators by Majorana rotations). *Let the unitary $U_{\vec{u}}$ be the sequence*

$$U_{\vec{u},\sigma,x} \doteq V_{\vec{u},\sigma,x}^{(0)} V_{\vec{u},\sigma,x}^{(1)} \cdots V_{\vec{u},\sigma,x}^{(N-2)}, \quad V_{\vec{u},\sigma,x}^{(p)} \doteq e^{\theta_p \gamma_{p,\sigma,x} \gamma_{p+1,\sigma,x}}. \quad (55)$$

Then for all $\sigma \in \{0, 1\}$ and $x \in \{0, 1\}$, there exists rotation angles $\theta_p \doteq \theta_{\vec{u},p}$ that are function of \vec{u} such that $U_{\vec{u},\sigma,x}^\dagger \cdot \gamma_{0,\sigma,x} \cdot U_{\vec{u},\sigma,x} = \gamma_{\vec{u},\sigma,x}$.

Proof. In the interests of clarity, we drop the σ, x subscript in the following. By taking a Taylor series expansion, observe that $V_{\vec{u}}^{(p)} = \cos(\theta_p) \mathcal{I} + \sin(\theta_p) \gamma_p \gamma_{p+1}$. Thus

$$V_{\vec{u}}^{(p)\dagger} \gamma_q V_{\vec{u}}^{(p)} = \begin{cases} \gamma_q, & q \neq p, p+1, \\ \cos(2\theta_p) \gamma_p + \sin(2\theta_p) \gamma_{p+1}, & q = p, \\ \cos(2\theta_p) \gamma_{p+1} - \sin(2\theta_p) \gamma_p, & q = p+1. \end{cases} \quad (56)$$

Thus $U_{\vec{u}}^\dagger \cdot \gamma_0 \cdot U_{\vec{u}} = \sum_{p \in [N]} u_p \gamma_p$, by choosing

$$u_0 = \cos(2\theta_0), \quad u_1 = \sin(2\theta_0) \cos(2\theta_1), \quad \cdots, \quad u_p = \cos(2\theta_p) \prod_{j < p} \sin(2\theta_j). \quad (57)$$

We obtain the angles θ_p by recursively solving this linear chain of equations. \square

As $\gamma_{\vec{u},\sigma,x}$ is unitary, it is also trivially its own block-encoding $\mathcal{B}[\gamma_{\vec{u},\sigma,x}] = \gamma_{\vec{u},\sigma,x}$.

2. Block-encoded product of Majorana operators

We synthesize the product $\gamma_{\vec{u},\sigma,0} \gamma_{\vec{u},\sigma,1}$ using the implementation described in [Lemma 8](#). Observe that the commutator $[\gamma_{p,\sigma,x} \gamma_{p+1,\sigma,x}, \gamma_{q,\rho,y} \gamma_{q+1,\rho,y}]$ is zero for all $\sigma \neq \rho$ or $x \neq y$. Thus all rotations in $U_{\vec{u},\sigma,0}$ and $U_{\vec{u},\sigma,1}$ commute with each other. This allows us to collect rotations in the product

$$\gamma_{\vec{u},\sigma,0} \gamma_{\vec{u},\sigma,1} = \left((V_{\vec{u},\sigma,0}^{(0)} V_{\vec{u},\sigma,1}^{(0)}) \cdots (V_{\vec{u},\sigma,0}^{(N-2)} V_{\vec{u},\sigma,1}^{(N-2)}) \right)^\dagger \gamma_{0,\sigma,0} \gamma_{0,\sigma,1} \underbrace{(V_{\vec{u},\sigma,0}^{(0)} V_{\vec{u},\sigma,1}^{(0)}) \cdots (V_{\vec{u},\sigma,0}^{(N-2)} V_{\vec{u},\sigma,1}^{(N-2)})}_{U_{\vec{u},\sigma,0} U_{\vec{u},\sigma,1}}. \quad (58)$$

In a Pauli representation of the Majorana operators, each rotation

$$V_{\vec{u},p,x} = C_{p,x}^\dagger \cdot e^{i\theta_{\vec{u},p} Z} \cdot C_{p,x} \quad (59)$$

is implemented by a single-qubit Z rotation conjugated by some Clifford gate $C_{p,x}$ such that $C_{p,x}^\dagger \cdot iZ \cdot C_{p,x} = \gamma_{p,\sigma,x} \gamma_{p+1,\sigma,x}$. We use the Jordan-Wigner representation (momentarily ignoring the spin index) that maps

$$\gamma_{p,0} \gamma_{p+1,0} \rightarrow -iY_p X_{p+1}, \quad \gamma_{p,1} \gamma_{p+1,1} \rightarrow iX_p Y_{p+1}, \quad \gamma_{0,0} \gamma_{0,1} \rightarrow iZ_0. \quad (60)$$

In the example where $N = 4$, the rotated Majorana operator is hence implemented by the circuit

$$\gamma_{\bar{u},0}\gamma_{\bar{u},1} = U_{\bar{u},0}U_{\bar{u},1} iZ (U_{\bar{u},0}U_{\bar{u},1})^\dagger, \quad (61)$$

where the basis transformation is

$$(U_{\bar{u},0}U_{\bar{u},1})^\dagger = e^{-i\theta_0 X_0 Y_1} e^{i\theta_0 Y_0 X_1} e^{-i\theta_1 X_1 Y_2} e^{i\theta_1 Y_1 X_2} \dots, \quad (62)$$

which, upon substituting the Jordan-Wigner representation and defining the Z Pauli rotation $R_\theta \doteq e^{i\theta Z}$, is equal to

$$(U_{\bar{u},0}U_{\bar{u},1})^\dagger = C_{0,0} R_{\theta_0}^\dagger C_{0,0}^\dagger C_{0,1} R_{\theta_0}^\dagger C_{0,1}^\dagger C_{1,0} R_{\theta_1}^\dagger C_{1,0}^\dagger C_{1,1} R_{\theta_1}^\dagger C_{1,1}^\dagger \dots \quad (63)$$

With the spin indices restored, the Jordan-Wigner representation maps

$$\gamma_{p,1,0}\gamma_{p+1,1,0} \rightarrow -iY_{p+N}X_{p+1+N}, \quad \gamma_{p,1,1}\gamma_{p+1,1,1} \rightarrow iX_{p+N}Y_{p+1+N}, \quad \gamma_{0,1,0}\gamma_{0,1,1} \rightarrow iZ_N, \quad (64)$$

for $\sigma = 1$. The case $\sigma = 0$ is identical to Eq. (60). Thus the quantum circuit for

$$\gamma_{\bar{u},1,0}\gamma_{\bar{u},1,1} = \prod_{j=0}^{N-1} (\text{SWAP}_{j \leftrightarrow j+N}) \cdot \gamma_{\bar{u},0}\gamma_{\bar{u},1} \prod_{j=0}^{N-1} (\text{SWAP}_{j \leftrightarrow j+N}), \quad (65)$$

is implemented by swapping all pairs of qubits $j \leftrightarrow j + N$. Thus the spin-multiplexed unitary $|0\rangle\langle 0| \otimes \gamma_{\bar{u},0,0}\gamma_{\bar{u},0,1} + |1\rangle\langle 1| \otimes \gamma_{\bar{u},1,0}\gamma_{\bar{u},1,1}$ is implemented by adding a control to the SWAP gates, as illustrated below (for $N = 4$).

$$\gamma_{\bar{u},\sigma,0}\gamma_{\bar{u},\sigma,1} = U_{\bar{u},0}U_{\bar{u},1} iZ (U_{\bar{u},0}U_{\bar{u},1})^\dagger. \quad (66)$$

As $\gamma_{\bar{u},\sigma,0}\gamma_{\bar{u},\sigma,1}$ is unitary, it is also trivially its own block-encoding $\mathcal{B}[\gamma_{\bar{u},\sigma,0}\gamma_{\bar{u},\sigma,1}] = \gamma_{\bar{u},\sigma,0}\gamma_{\bar{u},\sigma,1}$.

3. Block-encoded one-electron operator and its square

The one-electron operator is

$$\text{One}_L \doteq \frac{1}{2} \sum_{k \in [K]} \lambda_k \sum_{\sigma} \gamma_{\vec{R}_k, \sigma, 0} \gamma_{\vec{R}_k, \sigma, 1}, \quad L = \sum_{k \in [K]} \lambda_k \vec{R}_k \vec{R}_k^\dagger. \quad (67)$$

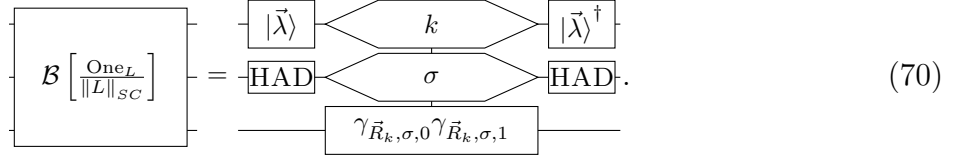
The block-encoding of One_L is accomplished by adding block-encodings of $\mathcal{B}[\gamma_{\vec{u}, \sigma, 0} \gamma_{\vec{u}, \sigma, 1}]$, each weighted by the eigenvalue λ_k , following the construction in Eq. (13). This requires synthesizing the quantum state

$$|\vec{\lambda}\rangle = \sum_k \sqrt{|\lambda_k| / \|L\|_{\text{SC}}} |k\rangle |\text{sign}[\lambda_k]\rangle \quad (68)$$

and the multiplexed unitary

$$Z \otimes \sum_k \sum_{\sigma} |k\rangle \langle k| \otimes |\sigma\rangle \langle \sigma| \otimes \mathcal{B}[\gamma_{\vec{u}, \sigma, 0} \gamma_{\vec{u}, \sigma, 1}]. \quad (69)$$

Note that we encode the sign of λ_k in a single qubit using the Pauli Z operation, as described in Eq. (29), which uses the fact $\langle \text{sign}[\lambda_k] | Z | \text{sign}[\lambda_k] \rangle = \text{sign}[\lambda_k]$. In the following circuit diagrams, this sign qubit is assumed to be implicitly present and will not be shown. Given these two components, the block-encoding is implemented by the quantum circuit



$$\mathcal{B} \left[\frac{\text{One}_L}{\|L\|_{\text{SC}}} \right] = \begin{array}{c} \begin{array}{c} |\vec{\lambda}\rangle \\ \text{HAD} \end{array} \begin{array}{c} \text{---} \\ \text{---} \end{array} \\ \begin{array}{c} \text{---} \\ \text{---} \end{array} \end{array} \quad (70)$$

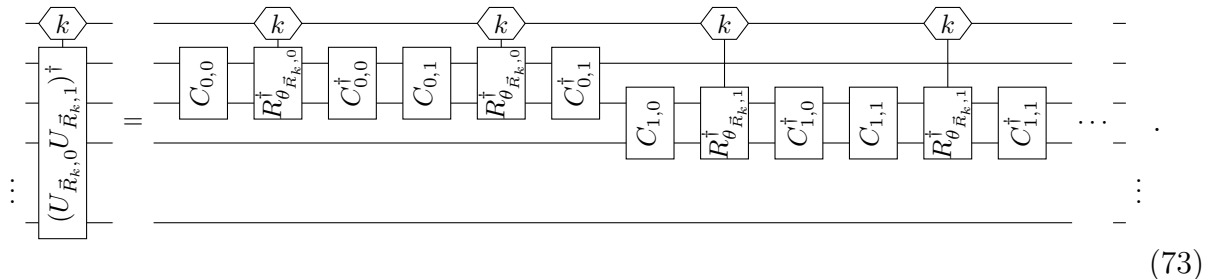
We now discuss the implementation of Eq. (69) which is controlled by the spin index σ and the eigenvalue index k . Control by the spin index remains unchanged from Eq. (66). Control by the eigenvalue index is implemented by multiplexing the basis transformation

$$\sum_k |k\rangle \langle k| \otimes U_{\vec{R}_k, 0} U_{\vec{R}_k, 1}. \quad (71)$$

From Eq. (63), $U_{\vec{R}_k, 0} U_{\vec{R}_k, 1}$ is a sequence of Z -rotations by a k -dependent angle $\theta_{\vec{R}_k, p}$, each conjugated by a Clifford gate that is independent of k . Thus Eq. (71) may be implemented by multiplexing the phase-rotations

$$\sum_k |k\rangle \langle k| \otimes e^{i\theta_{\vec{R}_k, p} Z}, \quad (72)$$

as follows



$$\begin{array}{c} \begin{array}{c} \text{---} \\ \text{---} \end{array} \\ \begin{array}{c} \text{---} \\ \text{---} \end{array} \end{array} \quad (73)$$

We implement multiplexed phase-rotations using a data-lookup oracle $D_p|k\rangle|z\rangle = |k\rangle|z \oplus \tilde{\theta}_{\tilde{R}_{k,p}}\rangle$ on K β -bit entries. This oracle computes a β -bit binary representation of the rotation angle $\frac{\theta_{\tilde{R}_{k,p}}}{2\pi} \approx \tilde{\theta}_{\tilde{R}_{k,p}} = \sum_{b=0}^{\beta-1} \tilde{\theta}_{\tilde{R}_{k,p},b}/2^{1+b} \in [0, 1 - 2^{-\beta}]$, and may be implemented according to [Section VII A 1](#). With this oracle, we perform the following sequence

$$\begin{aligned}
D_p|k\rangle|0\rangle|\psi\rangle &= |k\rangle|\tilde{\theta}_{\tilde{R}_{k,p}}\rangle|\psi\rangle = |k\rangle \left(\bigotimes_{b=0}^{\beta-1} |\tilde{\theta}_{\tilde{R}_{k,p},b}\rangle \right) |\psi\rangle \\
\text{Controlled rotations} &\rightarrow |k\rangle \left(\bigotimes_{b=0}^{\beta-1} |\tilde{\theta}_{\tilde{R}_{k,p},b}\rangle \right) \prod_{b=0}^{\beta-1} e^{i2\pi\tilde{\theta}_{\tilde{R}_{k,p},b}Z} |\psi\rangle = |k\rangle|\tilde{\theta}_{\tilde{R}_{k,p}}\rangle e^{i2\pi\tilde{\theta}_{\tilde{R}_{k,p}}Z} |\psi\rangle \\
\text{Uncompute} &\rightarrow |k\rangle|0\rangle e^{i2\pi\tilde{\theta}_{\tilde{R}_{k,p}}Z} |\psi\rangle.
\end{aligned} \tag{74}$$

This costs two queries to data-lookup D_p and β arbitrary single-qubit rotations. As the circuit for [Eq. \(69\)](#) contains $4N$ multiplexed rotations, these rotations costs at most $8N$ queries to data-lookup on K β -bit entries, and $4N\beta$ arbitrary single-qubit rotations.

However, some optimizations are possible. First, the rotation angle bits computed once by D_p may be used to implement both rotations $R_{\tilde{\theta}_{\tilde{R}_{k,p}}}$ in [Eq. \(73\)](#). This reduces queries by a factor of two to $4N$. Second, the uncomputation of $|\tilde{\theta}_{\tilde{R}_{k,p}}\rangle$ may be merged with the computation of $\tilde{\theta}_{\tilde{R}_{k,p+1}}$. Instead of applying D_p and D_{p+1} , we merge them into a single data-lookup oracle $D_{p,p+1}|k\rangle|z\rangle = |p\rangle|z \oplus \tilde{\theta}_{\tilde{R}_{k,p}} \oplus \tilde{\theta}_{\tilde{R}_{k,p+1}}\rangle$. This reduces queries by another factor of two to $2N$. Third, the data-lookup oracles may output $\kappa > \beta$ bits. Thus multiple angles may be written out at once, e.g. $|z_0 \oplus \tilde{\theta}_{\tilde{R}_{k,p}}\rangle|z_1 \oplus \tilde{\theta}_{\tilde{R}_{k,p+1}}\rangle \cdots |z_{\kappa/\beta-1} \oplus \tilde{\theta}_{\tilde{R}_{k,p+\kappa/\beta-1}}\rangle$. These angles allow the application of more controlled-rotations for each application of data-lookup. This is detailed in [Section VII B 1](#), and reduces the number of queries to $2\lceil \frac{N\beta}{\kappa} \rceil$, but now to data-lookup on K κ -bit entries. Fourth, many of arbitrary single-qubit rotations are by identical angles (powers of 2). These may be implemented exactly using $4N\beta$ Toffoli gates by the phase gradient technique [34]. This also requires a one-time cost of preparing and storing β single-qubit resource states whose cost is negligible and thus ignored. Fifth, using the choice $\kappa = N\beta$, only one computation and uncomputation step is required. This can be advantageous as uncomputation as described in [Section VII A 1](#) has a Toffoli cost that can be smaller than computation when many ancillary qubits are used.

We now bound the bits of precision β required to approximate [Eq. \(69\)](#) to an overall error of ϵ in spectral norm. As each rotation angle $\theta_{\tilde{R}_{k,p}}$ is approximated to an error of at most $\pi 2^{-\beta}$, the error of each unitary rotation compared to its binary approximation is

$$\|R_{\theta_{\tilde{R}_{k,p}}} - R_{2\pi\tilde{\theta}_{\tilde{R}_{k,p}}}\| \leq \|R_{\pi 2^{-\beta}} - \mathcal{I}\| = \|\cos(2^{-\beta}\pi) - i\sin(2^{-\beta}\pi)Z - \mathcal{I}\| \tag{75}$$

The cumulative error $\epsilon \leq (4N)\pi 2^{-\beta+1/2}$ of all rotations then follows by the triangle inequality on unitary operators $\|(\prod_j U_j) - (\prod_j \tilde{U}_j)\| \leq \sum_j \|U_j - \tilde{U}_j\|$. Thus the bits of precision required is

$$\beta = \left\lceil \frac{1}{2} + \log_2 \left(\frac{4N\pi}{\epsilon} \right) \right\rceil. \tag{76}$$

Including the error μ of state-preparation results in an $\epsilon' = \epsilon + \mu$ -approximate block-encoding $\mathcal{B}_{\epsilon+\mu} \left[\frac{\text{One}_L}{\|L\|_{\text{SC}}} \right]$ instead of the exact $\mathcal{B} \left[\frac{\text{One}_L}{\|L\|_{\text{SC}}} \right]$. A simple choice of error budgeting is $\epsilon = \epsilon'/2$

Table XXIV. Resources used to block-encode a one-electron operator $\mathcal{B}_\epsilon \left[\frac{\text{One}_L}{\|L\|_{\text{SC}}} \right]$ on N orbitals where L has K eigenvectors. The parameters $\beta = \lceil 5.152 + \log_2 \left(\frac{N}{\epsilon} \right) \rceil$ and $\mu = 2 + \lceil \log_2(1/\epsilon) \rceil$.

Operation	#	Toffoli cost each	Ancillary qubits
Data-lookup Lemma 2	1	$D_{K,N\beta,\lambda} + \text{DU}_{K,N\beta,\lambda}$	$2\lceil \log_2 K \rceil + N\beta(1 + \lambda)$
Arbitrary rotations [34]	$4N\beta$	1	0
Controlled-SWAPs	$2N$	1	0
State-preparation Lemma 4	2	$\mu + D_{K,n_{K+\mu+1},N\beta(1+\lambda)+2N+1}$ dirty	$\lceil \log_2 K \rceil + 2\mu + 1$

and $\mu = \epsilon'/2$, though this may be optimized with more weight on ϵ as its data-lookup oracles are more costly.

The overall cost of block-encoding the one-electron operator is summarized in [Table XXIV](#), and is dominated by data-lookup in multiplexing the basis transformation rotations. As state-preparation is cheap in comparison, we choose an implementation that is assisted by $\kappa + \lambda + 2N$ dirty qubits. Given $\mathcal{B}_\epsilon \left[\frac{\text{One}_L}{\|L\|_{\text{SC}}} \right]$, qubitization in [Theorem 1](#) describes how it may be applied twice, hence doubling the cost, to block-encode $\mathcal{B}_{2\epsilon} \left[T_2 \left[\frac{\text{One}_L}{\|L\|_{\text{SC}}} \right] \right]$. This also applies a reflection about the all-zero state $|0 \cdots 0\rangle$ on $\mathcal{O}(\log_K + \mu)$ qubits, whose cost is negligible and thus ignored.

4. Block-encoded two-electron operator

In this section, we describe a block-encoding of the double-factorized Hamiltonian in [Eq. \(54\)](#). We focus on the two-body term, which is the most costly component.

$$\text{Two}_H \doteq \frac{1}{4} \sum_{r \in [R]} \|L^{(r)}\|_{\text{SC}}^2 T_2 \left[\frac{\text{One}_{L^{(r)}}}{\|L^{(r)}\|_{\text{SC}}} \right], \quad \overrightarrow{\Lambda}_{\text{SH}} \doteq (\|L^{(1)}\|_{\text{SC}}^2, \|L^{(2)}\|_{\text{SC}}^2, \dots, \|L^{(R)}\|_{\text{SC}}^2)^\top, \quad (77)$$

$$L^{(r)} = \sum_{k \in [M^{(r)}]} \lambda_k^{(r)} \vec{R}_k^{(r)} \vec{R}_k^{(r)\top}.$$

and its uncomputation has a cost

$$\text{DU}_{M,R,N\beta,\lambda''} = \min_{\lambda' \in [0, \lambda'']} \left(\frac{M}{1 + \lambda'} + \lambda' \right) + \mathcal{O}(\sqrt{Rn_M}). \quad (85)$$

As the number of clean ancilla qubits used by the computation step is $\sim \lambda' N\beta$, the uncomputation step may choose $\lambda'' = \lambda' N\beta$. With this choice, the Toffoli cost of $\text{DU}_{M,R,N\beta,\lambda''}$ is always a factor of at least $\sqrt{N\beta}$ smaller than $\text{D}_{M,R,N\beta,\lambda}$, so long as $M = \Omega(N\beta)$, and is sub-dominant. For instance, in the case of $\lambda = 0$, we obtain almost-linear scaling with respect to M as follows.

$$\text{D}_{M,R,N\beta,0} = M + \mathcal{O}(\sqrt{Rn_M}) = \mathcal{O}(N \log N). \quad (86)$$

Choosing $\lambda = \Theta(\sqrt{M/(N\beta)})$ minimizes this as $\text{D}_{M,R,N\beta,\Theta(\sqrt{M/(N\beta)})} = \mathcal{O}(\sqrt{MN\beta}) + \mathcal{O}(\sqrt{Rn_M})$.

State-preparation has a cost that is sub-dominant to data-lookup. It suffices to use $\mu = \lceil 2.5 + \log_2(1/\epsilon) \rceil$ bits of precision.

$$\begin{aligned} \text{STATE}_{M,2n_R+\mu+1} &= \mu + \text{D}_{M,b,\lambda+\kappa+2N} \text{ dirty} \\ &= \min_{\lambda' \in [0, \lambda+N(2+\beta)]} \left(2 \frac{M}{1 + \lfloor \frac{\lambda'}{b} \rfloor} + 4b \left\lfloor \frac{\lambda'}{b} \right\rfloor \right) + \mu, \end{aligned} \quad (87)$$

where $b = 2n_{\max_{r \in [R]} M^{(r)}} + 2n_R + \mu + 1 = \mathcal{O}(\log N + \mu)$. As the number of dirty qubits $N(2 + \beta) \gg b$,

$$\text{STATE}_{M,2n_R+\mu+1} \lesssim \min \left[M, 4\sqrt{2Mb} \right] + \mu = \mathcal{O}(\sqrt{M \log(1/\epsilon)}). \quad (88)$$

Thus the total number of Toffoli gates is

$$\begin{aligned} &2(\text{D}_{M,R,N\beta,\lambda} + \text{DU}_{M,R,N\beta,\lambda}) + 4(\text{STATE}_{M,2n_R+\mu+1} + N(2\beta + 1)) \\ &\leq \min_{\lambda' \in [0, \lambda]} \left(\frac{2M}{1 + \lambda'} + 2\lambda' N\beta + 4N(2\beta + 1) \right) + \mathcal{O}(\sqrt{Rn_M} + \sqrt{M \log(1/\epsilon)}). \end{aligned} \quad (89)$$

Note that converting this block-encoding to a quantum walk using the qubitization procedure [Theorem 1](#) requires an additional reflection REF about the state $|0 \cdots 0\rangle$ on the ancillary register of the block-encoding. This reflection may be implemented using a number of Toffoli gates that is at most equal to the number of qubits comprising the ancillary register. Importantly, this ancillary register excludes any additional clean or dirty qubits that are used in intermediate steps, such as in data-lookup. Thus the cost of REF is subdominant to that of the block-encoding.

VIII. MATRIX SCHATTEN AND ENTRYWISE 1-NORM

Let $h \in \mathbb{C}^{N \times N}$ be any Hermitian matrix. This matrix has eigenvalues $h \cdot U_k = \sigma_k U_k$, where the orthonormal k^{th} eigenvector U_k can be viewed as the k^{th} column of some unitary matrix $U \in \mathbb{C}^{N \times N}$. We now prove that the following inequality is true

$$\frac{1}{N} \|h\|_{\text{EW}} \leq \|h\|_{\text{SC}} \leq \|h\|_{\text{EW}}, \quad (90)$$

where

$$\|h\|_{\text{SC}} \doteq \sum_{k \in [N]} |\sigma_k|, \quad \|h\|_{\text{EW}} \doteq \sum_{j,k \in [N]} |h_{jk}|. \quad (91)$$

Moreover, we show that this inequality is tight. We have not been able to find a proof of this statement in the literature, so our derivation may be of independent interest.

To prove the lower bound, observe that

$$\sum_{k \in [N]} |\sigma_k| \geq \sqrt{\sum_{k \in [N]} |\sigma_k|^2} = \sqrt{\sum_{j,k \in [N]} |h_{jk}|^2} \geq \frac{1}{N} \sum_{j,k \in [N]} |h_{jk}|. \quad (92)$$

The middle equality follows from the definition of the Frobenius norm, and the first and last inequalities follow from the usual vector norm inequality $\sqrt{\sum_{j \in [M]} |x_j|^2} \leq \sum_{j \in [M]} |x_j| \leq \sqrt{M \sum_{j \in [M]} |x_j|^2}$ for any vector x . This is an equality when every entry in h is one, and is hence tight.

To prove the upper bound, observe that

$$\begin{aligned} \sum_{k \in [N]} |\sigma_k| &= \sum_{k \in [N]} |(U_k)^\dagger \cdot h \cdot U_k| = \sum_{k \in [N]} \left| \sum_{i,j \in [N]} U_{ki}^\dagger h_{ij} U_{jk} \right| \leq \sum_{i,j \in [N]} \left(\sum_{k \in [N]} |U_{ki}^\dagger| |U_{jk}| \right) |h_{ij}| \\ &\leq \sum_{i,j \in [N]} |h_{ij}|. \end{aligned} \quad (93)$$

The final inequality follows from applying the Cauchy-Schwartz inequality on the term in round brackets. Using the fact that any row or column of any unitary has unit 2-norm,

$$\sum_{k \in [N]} |U_{ki}^\dagger| |U_{jk}| \leq \sqrt{\sum_{k \in [N]} |U_{ki}^\dagger|^2} \sqrt{\sum_{k \in [N]} |U_{jk}|^2} = 1. \quad (94)$$

This upper bound is also an equality by choosing h to contain only a single non-zero entry that lies on the diagonal, and is hence tight.

IX. M06-L/DEF2-SVP OPTIMIZED CARTESIAN COORDINATES FOR STABLE INTERMEDIATE I

The M06-L/def2-SVP optimized Cartesian coordinates of stable intermediate I given in the Supporting Information of Ref. [1] were erroneous and we obtained the correct ones in a private communication from Dr. Markus Hölscher. We reproduce them here for further reference.

100

H 5.400100000000 -3.818200000000 -1.311700000000

H	4.155000000000	-2.978300000000	-3.299400000000
C	4.393600000000	-3.410200000000	-1.197400000000
C	3.697900000000	-2.939300000000	-2.308200000000
H	4.317900000000	-3.761200000000	0.932900000000
C	3.788500000000	-3.373200000000	0.059400000000
C	2.410900000000	-2.418300000000	-2.164100000000
H	1.899900000000	-2.055300000000	-3.059100000000
H	-1.522700000000	-6.160300000000	-1.987500000000
H	-2.707500000000	-6.642600000000	0.150600000000
H	6.870300000000	1.841700000000	0.070400000000
H	5.886300000000	-0.074000000000	-1.189900000000
C	2.503900000000	-2.857300000000	0.201800000000
C	-1.511200000000	-5.428600000000	-1.176900000000
C	-2.172700000000	-5.699200000000	0.022400000000
C	1.799100000000	-2.357700000000	-0.904400000000
H	-0.296300000000	-4.039200000000	-2.277800000000
C	5.790200000000	1.776700000000	-0.076800000000
C	-0.827200000000	-4.228100000000	-1.339600000000
C	5.240300000000	0.706700000000	-0.781200000000
H	2.028700000000	-2.855300000000	1.184600000000
C	-2.142100000000	-4.766000000000	1.055100000000
H	-2.657200000000	-4.972500000000	1.996200000000
H	5.373500000000	3.615100000000	0.978600000000
C	4.951900000000	2.768800000000	0.431800000000
C	-0.805400000000	-3.275100000000	-0.307900000000
H	0.001800000000	-1.791600000000	-3.029400000000
C	-1.462300000000	-3.558400000000	0.891500000000
C	3.861600000000	0.623600000000	-0.968800000000
H	3.456300000000	-0.237100000000	-1.503900000000
H	1.680200000000	0.186000000000	-2.572700000000
H	-1.451300000000	-2.818200000000	1.696600000000
H	0.111400000000	-0.038800000000	-4.688600000000
P	0.105700000000	-1.704000000000	-0.588100000000
C	3.574200000000	2.692000000000	0.238400000000
C	-0.526000000000	-1.214100000000	-2.256800000000
C	3.009600000000	1.616600000000	-0.465900000000
H	2.932700000000	3.481100000000	0.641600000000
H	-1.563400000000	-1.577000000000	-2.300200000000
H	-1.642400000000	-0.121600000000	-4.426900000000
C	0.891300000000	0.908400000000	-2.309900000000
C	-0.723200000000	0.400500000000	-4.122100000000
H	1.056100000000	1.773900000000	-2.969600000000
C	-0.491700000000	0.285600000000	-2.613500000000
H	-0.817400000000	1.451300000000	-4.432100000000
P	1.181300000000	1.455800000000	-0.562300000000
Ru	-0.047300000000	0.041300000000	0.958600000000

H	1.827000000000	3.646000000000	-2.436100000000
H	-5.061500000000	-2.431900000000	2.138800000000
H	-3.264200000000	-0.743000000000	2.004000000000
C	-4.719600000000	-2.084100000000	1.161400000000
C	-3.716000000000	-1.124500000000	1.083500000000
C	-1.633700000000	1.056800000000	-1.906800000000
C	1.154200000000	4.050900000000	-1.674200000000
H	-2.570100000000	0.942400000000	-2.474500000000
C	0.687500000000	3.231600000000	-0.632200000000
H	0.039700000000	1.450700000000	2.022500000000
H	-6.054700000000	-3.375300000000	0.054400000000
C	-5.277400000000	-2.610600000000	-0.004100000000
H	-1.408400000000	2.135900000000	-1.932200000000
P	-1.937200000000	0.628900000000	-0.136500000000
C	-3.262700000000	-0.655000000000	-0.158400000000
H	1.167400000000	6.016000000000	-2.553900000000
C	0.794000000000	5.393400000000	-1.738000000000
C	-4.842400000000	-2.149000000000	-1.243200000000
C	-3.853900000000	-1.166300000000	-1.320200000000
C	-0.122100000000	3.803300000000	0.353300000000
H	-5.280600000000	-2.545000000000	-2.161700000000
H	-0.484400000000	3.193700000000	1.183100000000
H	-3.557200000000	-0.808300000000	-2.309000000000
C	-0.034300000000	5.944900000000	-0.757900000000
C	-2.891400000000	2.068700000000	0.492900000000
C	-0.485300000000	5.149800000000	0.291700000000
H	-2.541300000000	1.552100000000	2.567000000000
H	-3.463700000000	2.849500000000	-1.453300000000
H	-0.318600000000	6.998000000000	-0.811400000000
C	-3.024300000000	2.250000000000	1.876400000000
C	-3.530900000000	2.968800000000	-0.369700000000
H	-1.127000000000	5.571000000000	1.068900000000
C	-3.765000000000	3.313500000000	2.386400000000
C	-4.267400000000	4.036400000000	0.141900000000
H	-3.859700000000	3.439500000000	3.467100000000
H	-4.755200000000	4.732400000000	-0.543900000000
C	-4.384000000000	4.213900000000	1.519100000000
H	-4.962100000000	5.050200000000	1.917600000000
H	-0.952100000000	-0.951500000000	1.897300000000
C	1.382600000000	-1.559900000000	3.369100000000
C	3.440300000000	-0.516100000000	3.819500000000
C	2.732600000000	-1.853200000000	3.979000000000
H	0.855300000000	-2.435000000000	2.959000000000
H	0.698800000000	-1.064900000000	4.082100000000
H	4.534000000000	-0.585300000000	3.873900000000
H	3.119200000000	0.180400000000	4.609200000000

H	3.250700000000	-2.640200000000	3.408000000000
H	2.664400000000	-2.195000000000	5.019400000000
O	1.665600000000	-0.662300000000	2.280600000000
C	2.957100000000	-0.044500000000	2.462600000000
H	2.840700000000	1.047200000000	2.388100000000
H	3.612800000000	-0.372800000000	1.637900000000
H	-0.485500000000	0.871800000000	2.422700000000

X. PBE/DEF2-TZVP OPTIMIZED CARTESIAN COORDINATES OF INTERMEDIATES AND TRANSITION STATES

A. Stable intermediate I

100

H	5.3467652	-4.0620811	-1.5408059
H	4.0926440	-3.1077082	-3.4724386
C	4.3733646	-3.5936827	-1.3864493
C	3.6714082	-3.0599560	-2.4668243
H	4.3466242	-3.9621961	0.7431586
C	3.8127382	-3.5354622	-0.1077529
C	2.4188585	-2.4692755	-2.2728935
H	1.8982865	-2.0719643	-3.1452685
H	-1.2303386	-6.3183450	-1.9390001
H	-2.3770141	-6.8302644	0.2162593
H	6.8894103	1.9218885	-0.0035308
H	5.9314313	0.0065669	-1.2845387
C	2.5645983	-2.9459478	0.0853854
C	-1.2664022	-5.5702254	-1.1455328
C	-1.9074697	-5.8571319	0.0630226
C	1.8479758	-2.4005269	-0.9928855
H	-0.1392416	-4.1388533	-2.2801310
C	5.8092962	1.8284340	-0.1278109
C	-0.6597761	-4.3310091	-1.3395956
C	5.2727557	0.7583394	-0.8455377
H	2.1307566	-2.9221419	1.0848827
C	-1.9386697	-4.8957205	1.0724767
H	-2.4361609	-5.1112241	2.0195865
H	5.3587395	3.6295988	0.9806459
C	4.9524295	2.7841309	0.4226824
C	-0.6965107	-3.3523507	-0.3302362
H	-0.0341901	-1.8215111	-3.0690435
C	-1.3390064	-3.6491474	0.8753093
C	3.8905920	0.6406711	-1.0111176
H	3.5035862	-0.2172111	-1.5606581
H	1.6854069	0.1946881	-2.6002976

H	-1.3758827	-2.8904869	1.6590155
H	0.1002470	-0.0584394	-4.7135150
P	0.1555732	-1.7405875	-0.6273468
C	3.5724202	2.6731840	0.2513664
C	-0.5320094	-1.2444568	-2.2769909
C	3.0210291	1.6010240	-0.4716906
H	2.9209553	3.4398669	0.6738715
H	-1.5758438	-1.5926867	-2.2691807
H	-1.6572136	-0.1365786	-4.4433076
C	0.8887494	0.9035529	-2.3328536
C	-0.7336832	0.3839739	-4.1478944
H	1.0248231	1.7778900	-2.9853773
C	-0.4950701	0.2645326	-2.6290296
H	-0.8248285	1.4381977	-4.4496939
P	1.1802478	1.4418906	-0.5767848
Ru	-0.0362848	0.0070243	0.9119775
H	1.8212552	3.6119472	-2.4832596
H	-5.1810334	-2.3446956	2.1435413
H	-3.2016593	-0.8755944	1.9833979
C	-4.8598719	-1.9775745	1.1673356
C	-3.7477001	-1.1434336	1.0769211
C	-1.6402163	1.0360418	-1.9181179
C	1.2043586	4.0438832	-1.6928281
H	-2.5718953	0.9180300	-2.4893150
C	0.7332662	3.2400964	-0.6383483
H	-0.0098568	1.4084727	1.9225571
H	-6.4276167	-3.0022283	0.0834920
C	-5.5584608	-2.3460940	0.0148140
H	-1.4088869	2.1127432	-1.9239510
P	-1.9316460	0.5878885	-0.1460388
C	-3.3208409	-0.6412765	-0.1628399
H	1.3004971	6.0156855	-2.5548840
C	0.9255300	5.4088262	-1.7289309
C	-5.1381297	-1.8649201	-1.2242237
C	-4.0347117	-1.0109405	-1.3118186
C	-0.0024344	3.8482106	0.3847007
H	-5.6743639	-2.1451819	-2.1324256
H	-0.3751631	3.2487936	1.2152503
H	-3.7533400	-0.6366137	-2.2967743
C	0.1786679	5.9998088	-0.7051680
C	-2.8846015	2.0320140	0.5076653
C	-0.2785850	5.2188262	0.3545650
H	-2.5050619	1.5265310	2.5789523
H	-3.5109659	2.7932772	-1.4293835
H	-0.0387882	7.0686817	-0.7335780
C	-3.0151135	2.2055321	1.8935469

C	-3.5734918	2.9065438	-0.3467612
H	-0.8581185	5.6709513	1.1612919
C	-3.8039041	3.2316844	2.4142423
C	-4.3560825	3.9389862	0.1746224
H	-3.8959846	3.3477833	3.4954999
H	-4.8804404	4.6123560	-0.5054398
C	-4.4734473	4.1060444	1.5550677
H	-5.0901960	4.9096892	1.9606077
H	-0.9280923	-1.0292973	1.7973158
C	1.3378154	-1.5319181	3.4011766
C	3.2728388	-0.3202031	4.0156118
C	2.6497891	-1.7175315	4.1406225
H	0.8939997	-2.4524575	3.0001828
H	0.5828711	-1.0207579	4.0231085
H	4.3644121	-0.3235517	4.1291005
H	2.8553795	0.3490331	4.7819271
H	3.2715028	-2.4723203	3.6357164
H	2.5036511	-2.0320824	5.1819182
O	1.6798343	-0.6894853	2.2644245
C	2.8450502	0.1293127	2.6183662
H	2.5545055	1.1877945	2.5764244
H	3.6086816	-0.0587448	1.8513541
H	-0.5264219	0.7815522	2.3441392

B. Stable intermediate II

90

H	-3.5339194	-5.8134021	0.7154303
H	-2.8828583	-4.5857087	2.7848281
C	-2.7878389	-5.0187876	0.6707413
C	-2.4249571	-4.3298811	1.8276514
H	-2.4367085	-5.2430098	-1.4508818
C	-2.1745456	-4.6972246	-0.5430550
C	-1.4648308	-3.3145957	1.7730738
H	-1.1972253	-2.8074961	2.7010195
H	4.0447509	-5.0032186	1.5248357
H	4.6257704	-5.4865551	-0.8498353
H	-6.9424288	-1.0572568	-0.8489737
H	-5.6541614	-2.1885011	0.9605540
C	-1.2131616	-3.6888161	-0.5962258
C	3.5324311	-4.4778357	0.7172409
C	3.8577104	-4.7485084	-0.6135181
C	-0.8501479	-2.9745776	0.5597285
H	2.2928246	-3.3649200	2.0694393
C	-5.9424138	-0.7091293	-0.5867670

C	2.5443401	-3.5405037	1.0224599
C	-5.2212192	-1.3414937	0.4256799
H	-0.7092122	-3.4805713	-1.5422166
C	3.1943722	-4.0721958	-1.6392311
H	3.4419659	-4.2786302	-2.6819584
H	-5.9318348	0.8799617	-2.0540790
C	-5.3756389	0.3750716	-1.2625045
C	1.8842706	-2.8451860	-0.0030466
H	0.5482637	-1.8718378	2.8271484
C	2.2180869	-3.1221608	-1.3355503
C	-3.9409031	-0.8959159	0.7676030
H	-3.4025233	-1.4184765	1.5573864
H	-1.7520289	-0.5852893	2.4090356
H	1.7216499	-2.5731918	-2.1386833
H	-0.2276327	-0.3572974	4.5490732
P	0.4870886	-1.7047662	0.3801736
C	-4.0998357	0.8234416	-0.9225842
C	0.8525218	-1.1077287	2.0974671
C	-3.3662972	0.1971043	0.1037136
H	-3.6794455	1.6861233	-1.4444495
H	1.9502640	-1.0454284	2.1616566
H	1.4427245	0.2226901	4.3439378
C	-1.2653987	0.3736318	2.1828482
C	0.3997269	0.3856686	4.0338455
H	-1.7195915	1.1197769	2.8510531
C	0.2529006	0.2656288	2.5028157
H	0.0928914	1.3838068	4.3798787
P	-1.6693102	0.8441027	0.4312741
Ru	0.0415500	0.0787294	-1.0430842
H	-3.4364971	2.3732688	2.2276231
H	5.5508989	-1.1292919	-1.7375133
H	3.1714975	-0.4324962	-1.7053632
C	5.1686562	-0.5511105	-0.8947219
C	3.8293119	-0.1582569	-0.8800472
C	1.0515757	1.4409814	1.8698538
C	-2.9679142	3.0880432	1.5473566
H	1.9394366	1.6412793	2.4854269
C	-2.0549238	2.6476564	0.5712613
H	-0.4369552	1.4561661	-2.0038409
H	7.0572918	-0.5236336	0.1563813
C	6.0113482	-0.2132042	0.1644635
H	0.4333868	2.3509809	1.9064705
P	1.5743010	1.2220596	0.1041735
C	3.3108499	0.5814438	0.1914567
H	-4.0258849	4.7597303	2.3994422
C	-3.3134529	4.4347265	1.6394014

C	5.5093639	0.5318195	1.2339090
C	4.1732011	0.9330985	1.2450332
C	-1.5123513	3.5856436	-0.3140454
H	6.1619527	0.8113919	2.0626371
H	-0.8027279	3.2670739	-1.0783201
H	3.8259940	1.5437210	2.0793896
C	-2.7593723	5.3639604	0.7524551
C	1.9325683	2.9291860	-0.4951383
C	-1.8619483	4.9369995	-0.2252055
H	2.2575338	2.2337655	-2.5225002
H	1.7383905	3.9532013	1.4139813
H	-3.0337675	6.4176549	0.8231227
C	2.2606460	3.0950337	-1.8510831
C	1.9739393	4.0452473	0.3535690
H	-1.4265658	5.6533717	-0.9236661
C	2.6072277	4.3501706	-2.3492191
C	2.3212349	5.3021967	-0.1484847
H	2.8621323	4.4615150	-3.4043972
H	2.3465729	6.1612497	0.5240211
C	2.6353199	5.4591196	-1.4987626
H	2.9081739	6.4412764	-1.8877254
H	1.1990551	-0.5574839	-2.0047565
O	-1.5496481	-1.0274756	-2.4549650
H	0.2386696	1.0535691	-2.4415570
C	-2.5477139	-1.5735677	-2.7519342
O	-3.5175158	-2.1258482	-3.0858970

C. Transition state II-III

90

H	-3.3110113	5.9892207	1.0614647
H	-4.2699731	4.2457791	2.5646655
C	-3.0206823	4.9443578	0.9411378
C	-3.5551641	3.9679033	1.7884389
H	-1.7138037	5.3312324	-0.7361600
C	-2.1264645	4.5776821	-0.0631642
C	-3.1811684	2.6340605	1.6402700
H	-3.6277160	1.8806884	2.2931144
H	-5.6160706	-2.7121710	1.1039665
H	-6.9243089	-1.7456590	-0.7848797
H	2.2922500	6.7135450	-1.2644906
H	1.7977477	4.9663614	-2.9725257
C	-1.7490437	3.2402931	-0.2142156
C	-5.2161958	-1.8742172	0.5304563
C	-5.9476568	-1.3334376	-0.5263815

C	-2.2602892	2.2598538	0.6443485
H	-3.4101655	-1.8109259	1.6817662
C	2.1117394	5.6823443	-0.9566678
C	-3.9621095	-1.3533817	0.8608104
C	1.8365741	4.7034730	-1.9140823
H	-1.0589769	2.9633107	-1.0083301
C	-5.4252112	-0.2587683	-1.2511941
H	-5.9898498	0.1730898	-2.0785599
H	2.3737919	6.0988230	1.1483993
C	2.1569557	5.3382049	0.3964698
C	-3.4314232	-0.2746544	0.1400394
H	-1.9093419	0.6457296	2.8766625
C	-4.1811057	0.2707808	-0.9169211
C	1.5998822	3.3856847	-1.5195481
H	1.3618145	2.6317415	-2.2730301
H	0.1324406	2.1468070	2.1220360
H	-3.7991235	1.1276967	-1.4762929
H	-0.1622500	0.9200354	4.5156734
P	-1.7898612	0.4866969	0.4682011
C	1.9314756	4.0197348	0.7944430
C	-1.3581619	-0.0181335	2.1948070
C	1.6445597	3.0334958	-0.1618108
H	1.9840510	3.7707294	1.8557653
H	-1.7398248	-1.0358147	2.3616180
H	-0.3053609	-0.8547770	4.5168659
C	0.8384432	1.3039855	2.0506034
C	0.2504868	-0.0066745	4.0898762
H	1.6781083	1.5528995	2.7144019
C	0.1467645	0.0036826	2.5516048
H	1.2993952	-0.0924259	4.4116776
P	1.4154808	1.2704176	0.2981193
Ru	-0.0580826	-0.0105605	-1.0282051
H	3.4484813	0.7669848	2.5245745
H	-3.2870024	-4.5938061	-1.2882619
H	-1.8154783	-2.6079569	-1.3493182
C	-2.5166489	-4.4718823	-0.5251153
C	-1.6833561	-3.3513062	-0.5612275
C	0.8531797	-1.2773087	2.0363862
C	3.9135837	0.5869699	1.5546861
H	0.5775641	-2.1172447	2.6901033
C	3.1837715	0.7222675	0.3644458
H	0.9114846	-0.7396226	-2.2942093
H	-3.0277398	-6.2905288	0.5234630
C	-2.3720066	-5.4190782	0.4879301
H	1.9394546	-1.1417143	2.1330924
P	0.5082569	-1.7662838	0.2799070

C	-0.6882511	-3.1688492	0.4063762
H	5.8094743	0.1187158	2.4675051
C	5.2626919	0.2217700	1.5284322
C	-1.3765958	-5.2519381	1.4551523
C	-0.5332464	-4.1429149	1.4097780
C	3.8478677	0.5010974	-0.8521713
H	-1.2477823	-5.9948543	2.2439597
H	3.3167662	0.6211521	-1.7996011
H	0.2634056	-4.0610900	2.1519374
C	5.9063693	-0.0053451	0.3122289
C	2.0092923	-2.6851927	-0.2709110
C	5.1945846	0.1439739	-0.8807738
H	1.1253032	-3.0341700	-2.2209773
H	3.1671390	-2.5809671	1.5682949
H	6.9580223	-0.2951589	0.2922381
C	1.9984905	-3.1903690	-1.5823841
C	3.1239399	-2.9388468	0.5397158
H	5.6875698	-0.0238491	-1.8396120
C	3.0862125	-3.9048771	-2.0797414
C	4.2143493	-3.6557303	0.0388926
H	3.0601414	-4.2877262	-3.1012456
H	5.0784948	-3.8334063	0.6811896
C	4.2035194	-4.1325937	-1.2711213
H	5.0591475	-4.6860065	-1.6611601
H	-1.2075135	-0.8482710	-1.9275095
O	-0.8679910	1.3150199	-2.6888645
H	1.4073377	-0.0947416	-1.9902143
C	-1.4523573	0.2818584	-3.0210830
O	-2.1601399	-0.2683888	-3.8009511

D. Stable intermediate V

101

H	1.8269673	-6.4995226	-1.8331652
H	-0.1987775	-5.8444899	-3.1316653
C	1.3357599	-5.5452970	-1.6361930
C	0.2004959	-5.1775756	-2.3656564
H	2.7207290	-4.9627857	-0.0853206
C	1.8313185	-4.6876922	-0.6553924
C	-0.4354660	-3.9645232	-2.1074060
H	-1.3415289	-3.7201738	-2.6648629
H	-5.4381068	-3.4308995	-1.4499820
H	-5.7231633	-4.1081567	0.9313397
H	6.8126364	-2.2405036	-0.5533612
H	5.0462895	-3.1389195	-2.0682447

C	1.2007010	-3.4643685	-0.4040235
C	-4.6524851	-3.2205525	-0.7223230
C	-4.8130288	-3.5981606	0.6118353
C	0.0608975	-3.0881173	-1.1250500
H	-3.3956802	-2.2873749	-2.1843592
C	5.8318240	-1.7643652	-0.5971816
C	-3.4881512	-2.5699563	-1.1352722
C	4.8442785	-2.2658724	-1.4452872
H	1.6041304	-2.7885258	0.3494945
C	-3.8030790	-3.3164865	1.5343161
H	-3.9218460	-3.6006504	2.5814336
H	6.3275628	-0.2279502	0.8421000
C	5.5595456	-0.6389062	0.1844456
C	-2.4662044	-2.2841338	-0.2159046
H	-1.1415037	-1.6116831	-3.1391415
C	-2.6401863	-2.6642794	1.1234962
C	3.5908833	-1.6518536	-1.5113046
H	2.8440551	-2.0769602	-2.1801291
H	1.3623215	-0.9359586	-2.8199790
H	-1.8736126	-2.4241663	1.8588721
H	-0.1338313	-0.3032581	-4.8952739
P	-0.8563124	-1.5244629	-0.7170093
C	4.3112658	-0.0213328	0.1140267
C	-1.2345476	-0.8090490	-2.3930810
C	3.3046685	-0.5194259	-0.7333012
H	4.1294584	0.8753389	0.7083816
H	-2.2879545	-0.4913255	-2.3861758
H	-1.5963034	0.6712922	-4.6105906
C	1.1412825	0.1082683	-2.5575217
C	-0.5327454	0.5648136	-4.3493954
H	1.7583057	0.7306354	-3.2204188
C	-0.3554164	0.3870354	-2.8286795
H	-0.0043198	1.4621509	-4.7045371
P	1.6863344	0.3895464	-0.8090269
Ru	0.0389462	-0.0005865	0.7252379
H	3.2250833	1.9918618	-2.8187053
H	-5.5616749	-0.0730762	1.5080617
H	-3.0995036	0.0692163	1.4036755
C	-5.0912348	0.5200997	0.7222509
C	-3.6967614	0.5926086	0.6606666
C	-0.8058406	1.7022572	-2.1467946
C	3.1041163	2.5953737	-1.9176497
H	-1.6802305	2.1081867	-2.6727341
C	2.3760418	2.1111900	-0.8156072
H	-6.9628336	1.1363562	-0.1658733
C	-5.8742870	1.1959233	-0.2124547

H	-0.0032940	2.4459640	-2.2507600
P	-1.2230027	1.5568335	-0.3491218
C	-3.0659053	1.3453680	-0.3394307
H	4.2796205	4.2051116	-2.7335698
C	3.7218335	3.8443641	-1.8676434
C	-5.2560505	1.9631166	-1.2035989
C	-3.8653575	2.0450311	-1.2620198
C	2.3018202	2.8984359	0.3427203
H	-5.8584004	2.5116529	-1.9297298
H	1.7439962	2.5460789	1.2092780
H	-3.4174294	2.6879964	-2.0210913
C	3.6439259	4.6211635	-0.7074815
C	-1.1572670	3.2886783	0.2895171
C	2.9387037	4.1425219	0.3957026
H	-2.3118478	2.7421554	2.0422977
H	-0.0363799	4.1968011	-1.3387761
H	4.1381050	5.5932326	-0.6663737
C	-1.8041316	3.5490818	1.5106727
C	-0.5524518	4.3537888	-0.3921529
H	2.8715419	4.7397278	1.3065679
C	-1.8384943	4.8383125	2.0375311
C	-0.5987907	5.6484078	0.1320905
H	-2.3486429	5.0219847	2.9844605
H	-0.1308477	6.4664138	-0.4182261
C	-1.2372162	5.8945216	1.3471326
H	-1.2740729	6.9067416	1.7528829
C	0.6236532	-2.5200666	2.8855962
C	2.4293019	-1.6723168	4.1713895
C	1.6770189	-2.9768655	3.8829715
H	0.3086067	-3.3025469	2.1820304
H	-0.2608002	-2.1002196	3.3881616
H	3.4302248	-1.8336599	4.5922643
H	1.8592748	-1.0454939	4.8739104
H	2.3496344	-3.7192823	3.4274900
H	1.2272891	-3.4258756	4.7779230
O	1.2614393	-1.4553573	2.1062169
C	2.4874088	-1.0259966	2.7960327
H	2.4919838	0.0700512	2.8166982
H	3.3427331	-1.3902960	2.2082809
C	-0.4839753	0.8530861	3.0969704
O	-1.2519694	-0.0067675	2.5614182
O	0.4999295	1.3293584	2.4521989
H	-0.6736869	1.1882045	4.1351206

E. Stable intermediate VIII

92

H	5.3410691	4.6103038	-0.7286968
H	5.6351375	2.6660762	-2.2625989
C	4.6692268	3.7531301	-0.6607933
C	4.8326629	2.6645963	-1.5231454
H	3.5170406	4.5758757	0.9712987
C	3.6517439	3.7331876	0.2910867
C	3.9818701	1.5656267	-1.4308562
H	4.1541688	0.7093404	-2.0863048
H	5.3441144	-3.5263402	-1.2875126
H	6.3265024	-3.4109990	0.9988512
H	-0.2194183	7.1237700	1.5006299
H	0.3818143	6.5065105	-0.8378647
C	2.7938990	2.6325550	0.3767315
C	4.9201146	-2.8513314	-0.5421202
C	5.4694667	-2.7877908	0.7387700
C	2.9447130	1.5387409	-0.4810763
H	3.4202316	-2.1181527	-1.8906689
C	-0.3175908	6.0908944	1.1634668
C	3.8276699	-2.0491872	-0.8814573
C	0.0166225	5.7455689	-0.1461321
H	1.9949747	2.6417497	1.1182516
C	4.9206702	-1.9178771	1.6848405
H	5.3472060	-1.8581592	2.6875602
H	-1.0603318	5.3701172	3.0625313
C	-0.7863201	5.1079734	2.0394093
C	3.2713351	-1.1743183	0.0622773
H	2.1946169	0.0350266	-2.7286776
C	3.8295682	-1.1182642	1.3496498
C	-0.1124367	4.4242007	-0.5823675
H	0.1555086	4.1841315	-1.6115250
H	0.7015766	2.1672788	-1.9844840
H	3.4102245	-0.4384432	2.0936124
H	0.7653964	0.9882288	-4.3831132
P	1.9113448	0.0104144	-0.3093269
C	-0.9160337	3.7893734	1.6059889
C	1.4246694	-0.3701459	-2.0562641
C	-0.5756526	3.4303314	0.2915612
H	-1.3039069	3.0346863	2.2937037
H	1.4373852	-1.4647132	-2.1728465
H	0.3132470	-0.7317237	-4.4733566
C	-0.2371225	1.5929680	-1.9597140
C	0.0395239	0.2389821	-4.0335098

H	-0.9410518	2.0976545	-2.6364120
C	0.0333062	0.1608490	-2.4939166
H	-0.9527088	0.5195701	-4.4176326
P	-0.8962277	1.6899576	-0.2303813
Ru	-0.0238083	0.0640677	1.0843357
H	-2.5842051	3.1984707	-2.1387174
H	2.2239112	-5.1614667	0.6413664
H	1.2762615	-2.8955149	0.9246553
C	1.3794016	-4.8504076	0.0239379
C	0.8463580	-3.5672878	0.1844869
C	-1.1018803	-0.8114226	-2.0894157
C	-3.2491400	2.6641909	-1.4576714
H	-1.1186280	-1.6618118	-2.7870707
C	-2.7300027	1.8238793	-0.4557841
H	-1.4667938	0.0410227	1.9091058
H	1.2550573	-6.7239207	-1.0431248
C	0.8398346	-5.7222469	-0.9197954
H	-2.0642370	-0.2869640	-2.1904927
P	-1.0195287	-1.4892020	-0.3653207
C	-0.2343198	-3.1473190	-0.5990082
H	-5.0079336	3.5173888	-2.3599551
C	-4.6232194	2.8624432	-1.5765175
C	-0.2441571	-5.3130698	-1.7032069
C	-0.7805561	-4.0379677	-1.5410167
C	-3.6189847	1.2110202	0.4344335
H	-0.6801801	-5.9938817	-2.4362601
H	-3.2318789	0.5675248	1.2245666
H	-1.6491382	-3.7494463	-2.1369265
C	-5.5019440	2.2380120	-0.6867936
C	-2.7446225	-2.0357360	-0.0188175
C	-4.9962038	1.4189572	0.3213980
H	-2.2503101	-2.5061510	2.0364853
H	-3.5747692	-1.7216522	-2.0057686
H	-6.5773453	2.4000441	-0.7765359
C	-3.0238833	-2.5230440	1.2670865
C	-3.7517322	-2.0852668	-0.9931031
H	-5.6731647	0.9323251	1.0256158
C	-4.2804323	-3.0393222	1.5770725
C	-5.0128779	-2.5994562	-0.6799775
H	-4.4773207	-3.4147045	2.5825244
H	-5.7884109	-2.6233868	-1.4472268
C	-5.2816081	-3.0765302	0.6026616
H	-6.2665695	-3.4801891	0.8428596
O	0.8694350	-1.3975618	2.5338386
C	0.3062612	-1.6250898	3.6154095
H	0.7705045	-2.2836480	4.3663928

O	-0.8503584	-1.1356522	3.9761388
H	-1.1598523	-0.5655116	3.1644263
H	0.9748962	1.1899218	1.9454773
H	0.1735184	1.2213257	2.3440611

F. Transition state VIII-IX

90

H	-4.6740691	5.2558103	0.7566860
H	-3.6565780	4.3324926	2.8349996
C	-4.1354118	4.3074042	0.7292914
C	-3.5661585	3.7903366	1.8922326
H	-4.4625976	3.9910424	-1.3853212
C	-4.0157646	3.5992936	-0.4700558
C	-2.8873823	2.5684966	1.8623977
H	-2.4691171	2.1869670	2.7946513
H	-5.9128906	-2.6923533	1.2233453
H	-6.4076056	-2.8870920	-1.2100055
H	1.1573864	6.8809743	-1.0129677
H	-0.8506188	5.4569338	-1.4299762
C	-3.3307875	2.3861081	-0.5044693
C	-5.2652676	-2.2056811	0.4921476
C	-5.5429165	-2.3139708	-0.8721107
C	-2.7615192	1.8505448	0.6650799
H	-3.9799328	-1.3760665	2.0008758
C	1.1655870	5.8257319	-0.7358246
C	-4.1653394	-1.4654646	0.9292547
C	0.0437524	5.0287268	-0.9742557
H	-3.2431514	1.8484092	-1.4501893
C	-4.7123334	-1.6855437	-1.8016271
H	-4.9237644	-1.7656228	-2.8692849
H	3.1803520	5.8816053	0.0436688
C	2.2991020	5.2658453	-0.1434690
C	-3.3203178	-0.8399957	0.0003320
H	-2.1425426	0.2094387	2.9427620
C	-3.6018057	-0.9591481	-1.3700645
C	0.0578379	3.6763202	-0.6261028
H	-0.8283114	3.0659516	-0.8063629
H	-0.2237945	2.0407436	2.2035585
H	-2.9507921	-0.4807551	-2.1055095
H	-0.4689263	0.7373564	4.6029011
P	-1.9054598	0.2207814	0.5050528
C	2.3198105	3.9137427	0.2033037
C	-1.4836231	-0.3009075	2.2257558
C	1.1963386	3.1045336	-0.0325657

H	3.2192495	3.4885514	0.6490400
H	-1.7275057	-1.3727420	2.2903341
H	-0.3976348	-1.0403009	4.5706550
C	0.5618104	1.2714340	2.1562441
C	0.0646738	-0.1240085	4.1740517
H	1.3560399	1.6141361	2.8354213
C	0.0029848	-0.1002639	2.6344315
H	1.1056714	-0.0885412	4.5286102
P	1.1937713	1.3136515	0.4186758
Ru	-0.0502612	0.0907209	-0.9359617
H	3.2400038	1.0439519	2.6791411
H	-2.2708536	-4.6301779	-2.2456786
H	-0.9002952	-2.6033156	-1.8754508
C	-1.7962634	-4.4684538	-1.2766370
C	-1.0245996	-3.3266690	-1.0650562
C	0.8745284	-1.2724616	2.1150515
C	3.7308124	0.9132315	1.7139380
H	0.6474571	-2.1747953	2.7003186
C	3.0008941	0.9637346	0.5156672
H	1.1979307	-0.0817098	-2.0463828
H	-2.5683667	-6.2918788	-0.4107251
C	-1.9641008	-5.3980079	-0.2486223
H	1.9333601	-1.0382542	2.2997734
P	0.7143326	-1.6350116	0.3026225
C	-0.4035018	-3.0981142	0.1720287
H	5.6638259	0.6708030	2.6390232
C	5.1129118	0.7071425	1.6975290
C	-1.3517570	-5.1807289	0.9870476
C	-0.5717110	-4.0422139	1.1958857
C	3.6904433	0.8118030	-0.6981318
H	-1.4745639	-5.9043785	1.7944560
H	3.1425629	0.8554028	-1.6419038
H	-0.0857470	-3.9164201	2.1644913
C	5.7854488	0.5561642	0.4846131
C	2.3108267	-2.4370568	-0.1492510
C	5.0698177	0.6126831	-0.7140876
H	1.9134758	-2.2134053	-2.2624267
H	2.9957102	-2.8609007	1.8708624
H	6.8647676	0.3970375	0.4725288
C	2.5912894	-2.6233298	-1.5105191
C	3.1892928	-2.9729186	0.8033170
H	5.5868648	0.4979821	-1.6679094
C	3.7253951	-3.3253232	-1.9144325
C	4.3328686	-3.6650056	0.3975521
H	3.9261437	-3.4656270	-2.9778593
H	5.0130722	-4.0682375	1.1496283

C	4.6030751	-3.8443649	-0.9594408
H	5.4939874	-4.3904368	-1.2732091
O	-0.9132205	0.8654868	-2.6709122
C	0.3095768	0.7863575	-3.1225920
H	0.5452669	0.0469906	-3.9019490
O	1.0473226	1.9109786	-3.3266879
H	0.7127012	2.6178760	-2.7307738

G. Stable intermediate IX

104

H	-6.7995766	-0.3501329	-1.2158299
H	-5.1753779	-0.9590749	-3.0073767
C	-5.7494307	-0.0685308	-1.1249154
C	-4.8414893	-0.4064133	-2.1277195
H	-6.0099582	0.9370106	0.7720970
C	-5.3053977	0.6476996	-0.0097862
C	-3.4980684	-0.0377207	-2.0157358
H	-2.8205216	-0.3190427	-2.8220142
H	-3.2315181	5.5927273	-1.9725616
H	-2.4924030	6.8084725	0.0777993
H	-4.3211783	-5.4897958	-0.9008141
H	-4.5905028	-3.3058516	0.2709790
C	-3.9658356	1.0187301	0.0969376
C	-2.6596967	5.0727789	-1.2020891
C	-2.2471292	5.7533495	-0.0526568
C	-3.0375664	0.6805307	-0.9029689
H	-2.7130496	3.2024809	-2.2540851
C	-3.4898211	-4.7843036	-0.8565248
C	-2.3547852	3.7227087	-1.3636205
C	-3.6390470	-3.5637666	-0.1975612
H	-3.6478379	1.6145266	0.9537025
C	-1.5240554	5.0741083	0.9266362
H	-1.1936406	5.5946199	1.8269241
H	-2.1420149	-6.0571500	-1.9711422
C	-2.2684227	-5.1030952	-1.4567385
C	-1.6182261	3.0276471	-0.3860160
H	-1.4574439	1.1865906	-3.1168537
C	-1.2101190	3.7221361	0.7568958
C	-2.5737994	-2.6606659	-0.1356760
H	-2.7017218	-1.7083980	0.3780825
H	-0.9941388	-1.3447239	-2.8400148
H	-0.6215437	3.2283114	1.5305027
H	-0.2280357	0.0395821	-4.8662646
P	-1.2756409	1.2251309	-0.6716396

C	-1.2005443	-4.2086014	-1.3919092
C	-0.6128586	1.2766046	-2.4182513
C	-1.3442298	-2.9760656	-0.7291134
H	-0.2464680	-4.4802099	-1.8464876
H	-0.2166420	2.2928316	-2.5572826
H	0.9118141	1.3848621	-4.6301559
C	0.0392206	-1.1980355	-2.4947567
C	0.6796760	0.3524804	-4.3289267
H	0.6452415	-1.9024327	-3.0837550
C	0.4805290	0.2535758	-2.8016234
H	1.5082061	-0.2906873	-4.6610048
P	0.0627704	-1.7810041	-0.7282679
Ru	0.0930258	0.0068958	0.7993430
H	2.4742873	-2.4438087	-2.4802423
H	2.9855487	4.7401895	2.5258626
H	2.6625124	2.3446909	2.0250055
C	2.6682402	4.4368614	1.5266525
C	2.4769153	3.0858398	1.2434949
C	1.8347820	0.5919089	-2.1394964
C	2.4861307	-3.0588992	-1.5798602
H	2.2696554	1.4842751	-2.6149850
C	1.4863220	-2.9369876	-0.6046473
H	2.6290528	6.4549888	0.7479404
C	2.4731109	5.3975275	0.5292998
H	2.5495402	-0.2221114	-2.3300301
P	1.8718447	0.8499631	-0.2966950
C	2.0839300	2.6675862	-0.0408503
H	4.2892360	-4.0661169	-2.1980894
C	3.5229412	-3.9828688	-1.4259395
C	2.0903948	4.9949559	-0.7493951
C	1.8975109	3.6394096	-1.0325173
C	1.5496737	-3.7572998	0.5369440
H	1.9421909	5.7356658	-1.5368044
H	0.7886846	-3.6667854	1.3108696
H	1.6076595	3.3583150	-2.0455412
C	3.5741800	-4.7951918	-0.2936153
C	3.5876016	0.2876868	0.0868466
C	2.5849085	-4.6787563	0.6869250
H	4.4825058	1.9480644	-0.9984736
H	3.0102813	-1.4404467	1.2339408
H	4.3807546	-5.5206835	-0.1761200
C	4.6637632	1.0289478	-0.4376464
C	3.8482108	-0.8730074	0.8261054
H	2.6168757	-5.3127650	1.5745904
C	5.9757214	0.6073355	-0.2287307
C	5.1677117	-1.2833586	1.0395582

H	6.8018130	1.1906840	-0.6388095
H	5.3600896	-2.1849733	1.6237376
C	6.2309044	-0.5497987	0.5136163
H	7.2594827	-0.8719464	0.6849303
O	1.0670624	-1.2835636	2.0778444
C	1.5871606	-0.8290624	3.2992178
H	1.9242493	-1.6992758	3.8944679
H	2.4705860	-0.1665927	3.1772942
H	-0.1490045	1.4846206	1.6989277
H	0.4885841	1.0944823	2.1179673
H	0.8475740	-0.2803425	3.9228606
O	-1.7466699	-0.6275675	2.2837152
C	-1.7317061	-1.8827200	3.0229225
C	-2.2224936	0.3401404	3.2524878
C	-3.0380220	-1.8690967	3.8225342
H	-1.6541370	-2.6937791	2.2919727
H	-0.8446431	-1.9038831	3.6731363
C	-3.3722768	-0.3612382	3.9797136
H	-1.3999265	0.5896606	3.9475022
H	-2.5124323	1.2461145	2.7073037
H	-2.9148452	-2.3747266	4.7888091
H	-3.8360056	-2.3876118	3.2749787
H	-3.4298618	-0.0474345	5.0299026
H	-4.3342064	-0.1240359	3.5066121

H. Stable intermediate XVIII

90

H	-2.5470040	6.3737910	-0.0663331
H	-2.8123688	5.2837003	2.1590310
C	-2.3575811	5.3050645	0.0461674
C	-2.5053953	4.6951169	1.2928448
H	-1.8557613	5.0087803	-2.0352058
C	-1.9710474	4.5402664	-1.0564995
C	-2.2738967	3.3255410	1.4375671
H	-2.4225212	2.8750703	2.4198606
H	-6.4658186	-0.4517580	1.3317265
H	-7.1063609	-0.4963390	-1.0755395
H	2.6557529	6.2942052	-1.4687730
H	2.6184172	5.8584372	0.9834332
C	-1.7294505	3.1746660	-0.9123259
C	-5.7147847	-0.2699971	0.5610415
C	-6.0732010	-0.2947159	-0.7877950
C	-1.8803888	2.5510336	0.3364899
H	-4.1455477	0.0191627	1.9948402

C	2.3956306	5.3032142	-1.0935693
C	-4.3952745	-0.0058546	0.9334925
C	2.3751741	5.0591297	0.2813670
H	-1.4301507	2.5835298	-1.7811090
C	-5.1048465	-0.0547732	-1.7657306
H	-5.3774960	-0.0715606	-2.8223592
H	2.1024472	4.4592222	-3.0617405
C	2.0867078	4.2748854	-1.9863009
C	-3.4181977	0.2319862	-0.0454710
H	-2.0467422	0.9808698	2.7867311
C	-3.7839051	0.2069953	-1.4010590
C	2.0524934	3.7902287	0.7651273
H	2.0614547	3.6161788	1.8424160
H	0.2799551	2.1595239	2.2435168
H	-3.0318347	0.3759459	-2.1729904
H	-0.4329712	1.0976984	4.5735037
P	-1.6937413	0.7161533	0.3812452
C	1.7531024	3.0089158	-1.5045840
C	-1.5279993	0.2401619	2.1618835
C	1.7341262	2.7546438	-0.1254665
H	1.5072438	2.2099149	-2.2089384
H	-2.0783239	-0.7063544	2.2815788
H	-0.8311301	-0.6372895	4.6187758
C	0.8360055	1.2104261	2.1943488
C	-0.1214917	0.1031833	4.2204333
H	1.6924210	1.3170373	2.8744149
C	-0.0796827	0.0562400	2.6813970
H	0.8692688	-0.1126510	4.6478115
P	1.4151070	1.0356322	0.4486581
Ru	-0.0120573	-0.0641878	-0.9092097
H	3.3997536	0.3976754	2.7128807
H	-3.9488523	-3.7342434	-1.3914406
H	-2.0900837	-2.0952718	-1.3008549
C	-3.2197666	-3.7905063	-0.5815364
C	-2.1728248	-2.8665122	-0.5318431
C	0.4819087	-1.3320907	2.2709993
C	3.8678869	0.2287837	1.7421868
H	0.0202657	-2.1082765	2.8983765
C	3.1569307	0.4221504	0.5485563
H	-4.1575089	-5.4876614	0.3702908
C	-3.3363978	-4.7698197	0.4048525
H	1.5622408	-1.3565187	2.4750974
P	0.2047409	-1.7607250	0.4927662
C	-1.2317972	-2.9166010	0.5050001
H	5.7458365	-0.3063248	2.6569492
C	5.2073851	-0.1709298	1.7172452

C	-2.3945911	-4.8347603	1.4358905
C	-1.3456095	-3.9175421	1.4847999
C	3.8216208	0.2062141	-0.6715346
H	-2.4733336	-5.6066754	2.2032278
H	3.2927936	0.3596796	-1.6134471
H	-0.6056583	-4.0041204	2.2830725
C	5.8566025	-0.3811118	0.5004738
C	1.5535622	-2.9109735	-0.0092705
C	5.1576602	-0.1900365	-0.6944923
H	0.3720305	-3.5806934	-1.7031940
H	2.9739559	-2.5290542	1.5906045
H	6.9048341	-0.6835812	0.4825197
C	1.3385830	-3.6429203	-1.1953357
C	2.7672232	-3.0758877	0.6711517
H	5.6572457	-0.3448820	-1.6522310
C	2.3197484	-4.5014654	-1.6923373
C	3.7421841	-3.9473198	0.1775979
H	2.1314131	-5.0683171	-2.6056658
H	4.6776283	-4.0699228	0.7260186
C	3.5274686	-4.6540340	-1.0055431
H	4.2921683	-5.3327582	-1.3861909
O	-0.9205047	-0.1437941	-2.7216529
C	0.0671504	-0.6760065	-3.4936715
H	-0.1305676	-1.7179961	-3.8145929
O	1.2946578	-0.6984889	-2.6269831
H	1.5840222	-1.6252772	-2.4886499
H	0.3195803	-0.0480147	-4.3664138

-
- [1] S. Wesselbaum, V. Moha, M. Meuresch, S. Brosinski, K. M. Thenert, J. Kothe, T. vom Stein, U. Englert, M. Hölscher, J. Klankermayer, and W. Leitner, *Chem. Sci.* **6**, 693 (2015).
- [2] M. Hölscher, Private communication (Oct. 25 2019).
- [3] R. Ahlrichs, M. Bär, M. Häser, H. Horn, and C. Kölmel, *Chem. Phys. Lett.* **162**, 165 (1989).
- [4] J. P. Perdew, K. Burke, and M. Ernzerhof, *Phys. Rev. Lett.* **77**, 3865 (1996).
- [5] J. P. Perdew, M. Ernzerhof, and K. Burke, *J. Chem. Phys.* **105**, 9982 (1996).
- [6] F. Weigend and R. Ahlrichs, *Phys. Chem. Chem. Phys.* **7**, 3297 (2005).
- [7] A. C. Vaucher and M. Reiher, *J. Chem. Theory Comput.* **13**, 1219 (2017).
- [8] B. O. Roos, P. R. Taylor, and P. E. M. Siegbahn, *Chem. Phys.* **48**, 157 (1980).
- [9] H.-J. Werner and P. J. Knowles, *J. Chem. Phys.* **82**, 5053 (1985).
- [10] P. J. Knowles and H.-J. Werner, *Chem. Phys. Lett.* **115**, 259 (1985).
- [11] K. Ruedenberg, M. W. Schmidt, M. M. Gilbert, and S. T. Elbert, *Chem. Phys.* **71**, 41 (1982).
- [12] P.-O. Widmark, P.-Å. Malmqvist, and B. O. Roos, *Theoret. Chim. Acta* **77**, 291 (1990).
- [13] B. O. Roos, R. Lindh, P.-Å. Malmqvist, V. Veryazov, and P.-O. Widmark, *J. Phys. Chem. A* **108**, 2851 (2004).
- [14] B. O. Roos, R. Lindh, P.-Å. Malmqvist, V. Veryazov, and P.-O. Widmark, *J. Phys. Chem. A* **109**, 6575 (2005).
- [15] I. Fdez. Galván, M. Vacher, A. Alavi, C. Angeli, F. Aquilante, J. Autschbach, J. J. Bao, S. I. Bokarev, N. A. Bogdanov, R. K. Carlson, L. F. Chibotaru, J. Creutzberg, N. Dattani, M. G. Delcey, S. S. Dong, A. Dreuw, L. Freitag, L. M. Frutos, L. Gagliardi, F. Gendron, A. Giussani, L. González, G. Grell, M. Guo, C. E. Hoyer, M. Johansson, S. Keller, S. Knecht, G. Kovačević, E. Källman, G. Li Manni, M. Lundberg, Y. Ma, S. Mai, J. P. Malhado, P. Å. Malmqvist, P. Marquetand, S. A. Mewes, J. Norell, M. Olivucci, M. Oppel, Q. M. Phung, K. Pierloot, F. Plasser, M. Reiher, A. M. Sand, I. Schapiro, P. Sharma, C. J. Stein, L. K. Sørensen, D. G. Truhlar, M. Ugandi, L. Ungur, A. Valentini, S. Vancoillie, V. Veryazov, O. Weser, T. A. Wesolowski, P.-O. Widmark, S. Wouters, A. Zech, J. P. Zobel, and R. Lindh, *J. Chem. Theory Comput.* **15**, 11 (2019).
- [16] R. Olivares-Amaya, W. Hu, N. Nakatani, S. Sharma, J. Yang, and G. K.-L. Chan, *J. Chem. Phys.* **142**, 034102 (2015).
- [17] J. Pipek and P. G. Mezey, *J. Chem. Phys.* **90**, 4916 (1989).
- [18] S. Keller, K. Boguslawski, T. Janowski, M. Reiher, and P. Pulay, *J. Chem. Phys.* **142**, 244104 (2015).
- [19] C. J. Stein and M. Reiher, *J. Chem. Theory Comput.* **12**, 1760 (2016).
- [20] C. J. Stein and M. Reiher, *J. Comput. Chem.* **40**, 2216 (2019).
- [21] K. Boguslawski, K. H. Marti, and M. Reiher, *J. Chem. Phys.* **134**, 224101 (2011).
- [22] C. J. Stein and M. Reiher, *Mol. Phys.* **115**, 2110 (2017).
- [23] M. Reiher, N. Wiebe, K. M. Svore, D. Wecker, and M. Troyer, *PNAS* **114**, 7555 (2017).
- [24] M. Motta, E. Ye, J. R. McClean, Z. Li, A. J. Minnich, R. Babbush, and G. K.-L. Chan, *arXiv preprint arXiv:1808.02625* (2018).
- [25] G. H. Low, N. P. Bauman, C. E. Granade, B. Peng, N. Wiebe, E. J. Bylaska, D. Wecker, S. Krishnamoorthy, M. Roetteler, K. Kowalski, *et al.*, *arXiv preprint arXiv:1904.01131* (2019).
- [26] D. W. Berry, C. Gidney, M. Motta, J. R. McClean, and R. Babbush, *arXiv preprint*

- arXiv:1902.02134 (2019).
- [27] B. Peng and K. Kowalski, *J. Chem. Theory Comput.* **13**, 4179 (2017).
 - [28] I. D. Kivlichan, C. Gidney, D. W. Berry, N. Wiebe, J. McClean, W. Sun, Z. Jiang, N. Rubin, A. Fowler, A. Aspuru-Guzik, *et al.*, arXiv preprint arXiv:1902.10673 (2019).
 - [29] D. Wecker, M. B. Hastings, N. Wiebe, B. K. Clark, C. Nayak, and M. Troyer, *Phys. Rev. A* **92**, 062318 (2015).
 - [30] R. Babbush, C. Gidney, D. W. Berry, N. Wiebe, J. McClean, A. Paler, A. Fowler, and H. Neven, *Phys. Rev. X* **8**, 041015 (2018).
 - [31] G. H. Low, V. Kliuchnikov, and L. Schaeffer, arXiv preprint arXiv:1812.00954 (2018).
 - [32] V. V. Shende, S. S. Bullock, and I. L. Markov, *IEEE Transactions on Computer-Aided Design of Integrated Circuits and Systems* **25**, 1000 (2006).
 - [33] G. H. Low and I. L. Chuang, *Quantum* **3**, 163 (2019).
 - [34] C. Gidney, *Quantum* **2**, 74 (2018).
 - [35] S. A. Cuccaro, T. G. Draper, S. A. Kutin, and D. P. Moulton, arXiv preprint quant-ph/0410184 (2004).